RAY ANALYSIS OF ELECTROMAGNETIC SCATTERING FROM SEMI-INFINITE PERIODIC ARRAY OF DIPOLES IN FREE SPACE

A THESIS SUBMITTED TO
THE GRADUATE SCHOOL OF NATURAL AND APPLIED SCIENCES
OF
MIDDLE EAST TECHNICAL UNIVERSITY

BY

ÖZGÜR MURAT POLAT

IN PARTIAL FULFILLMENT OF THE REQUIREMENTS
FOR
THE DEGREE OF MASTER OF SCIENCE
IN
ELECTRICAL AND ELECTRONICS ENGINEERING

APRIL 2007

Approval of the Graduate School of Natural and Applied Sciences

_____

Prof. Dr. Canan Özgen

Director

I certify that this thesis satisfies all the requirements as a thesis for the degree of Master of Science.

_____

Prof. Dr. İsmet Erkmen

Head of Department

This is to certify that we have read this thesis and that in our opinion it is fully adequate, in scope and quality, as a thesis for the degree of Master of Science.

_____

Assoc. Prof. Dr. Özlem Aydın Çivi

Supervisor

Examining Committee Members

Prof. Dr. Gülbin Dural (METU, EE) _____

Assoc. Prof. Dr. Özlem Aydın Çivi (METU, EE) _____

Assoc. Prof. Dr. S. Sencer Koç (METU, EE) _____

Assoc. Prof. Dr. Vakur B. Ertürk (Bilkent Unv., EE) _____

Asst. Prof. Dr. Lale Alatan (METU, EE) _____

I hereby declare that all information in this document has been obtained and presented in accordance with academic rules and ethical conduct. I also declare that, as required by these rules and conduct, I have fully cited and referenced all material and results that are not original to this work.

Name, Last name : Özgür Murat, POLAT

Signature :

ABSTRACT

RAY ANALYSIS OF ELECTROMAGNETIC SCATTERING FROM SEMI-INFINITE PERIODIC ARRAY OF DIPOLES IN FREE SPACE

Polat, Özgür Murat
M.S., Department of Electrical and Electronics Engineering
Supervisor: Assoc. Prof. Dr. Özlem Aydın Çivi

April 2007, 119 pages

Electromagnetic wave scattering from a semi-infinite array of dipoles in free space is described by using asymptotic high frequency methods. An electric field integral expression is obtained and solved with asymptotic high frequency methods. An asymptotic field expression is obtained for a finite × infinite array of dipoles in free space. The analytical closed form expression for the array guided surface wave launching coefficient is obtained via a combination of an asymptotic high frequency analysis of a related reciprocal problem and Lorentz reciprocity integral formulation for the semi-infinite planar dipole array in which modified Kirchhoff approximation is used. The accuracy and the validity of the asymptotic analytical solutions are compared with the numerical solutions available in the literature before.

Keywords : Surface Waves, Antenna Arrays, Asymptotic High Frequency Methods, Periodic Structures

ÖZ

SERBEST UZAYDA BULUNAN YARI SONSUZ PERİYODİK DÜZLEMSEL DİPOL DİZİSİNDEN ELEKTROMANYETİK DALGA SAÇILIMININ IŞIN ANALİZİ

Polat, Özgür Murat
Yüksek Lisans, Elektrik Elektronik Mühendisliği Bölümü
Tez Yöneticisi: Doç. Dr. Özlem Aydın Çivi

Nisan 2007, 119 sayfa

Serbest uzayda bulunan yarı sonsuz periyodik düzlemsel dipol dizisinden elektromanyetik dalga saçılımı asimptotik yüksek frekans yöntemleri ile açıklanmıştır. Elektrik alan integral ifadeleri elde edilip, yüksek frekans yöntemleri ile çözülmüştür. Dipol elementlerinden oluşan sonlu × sonsuz bir dizinin elektromanyetik alan ifadeleri asimptotik yöntemlerle elde edilmiştir. Dizi kılavuzlu yüzey dalgalarının kapalı form uyarım katsayısı, asimptotik teknikler ile karşılıklılık ilkesine dayalı, değiştirilmiş Kirchhoff yaklaşımının uygulandığı ilgili bir problemin çözümü ve Lorentz karşılıklılık integral formülasyonun uygulanması ile elde edilmiştir. Asimptotik çözümlerin doğruluğu ve geçerliliği literatürde mevcut olan çalışmalarla karşılaştırılmıştır.

Anahtar Kelimeler : Yüzey Dalgaları, Anten Dizileri, Asimptotik Yüksek Frekans Yöntemleri, Periyodik Yapılar

To My Family

ACKNOWLEDGMENTS

I wish to express my deepest gratitude to my supervisor Assoc. Prof. Dr. Özlem Aydın Çivi for her guidance, advice, criticism, encouragements and insight throughout the research.

It is a very big pleasure for me to thank to my family, without their valuable support, all this work would not be possible.

I also thank to my colleagues in TÜBİTAK-UEKAE for their friendship.

TABLE OF CONTENTS

LIST OF FIGURES

FIGURES

LIST OF ABBREVIATIONS

AGSW:	Array Guided Surface Wave
FW:	Floquet Wave
SW:	Surface Wave
FSS:	Frequency Selective Surface
EM:	Electromagnetic
VdW:	Van der Waerden
SDP:	Steepest Descent Path
HF:	High Frequency
MoM:	Method of Moments
UTD:	Uniform Theory of Diffraction

CHAPTER 1

INTRODUCTION

There are many important structures whose characteristics are periodic in space. Examples are three-dimensional lattice structures for crystals, artificial dielectric consisting of periodically placed conducting pieces, Yagi antennas that have periodically spaced elements, corrugated surfaces and waveguides with periodic loadings. Considering antenna theory, periodic arrays are employed for a variety of applications, most importantly as phased array antennas which produce highly directional beams and frequency selective surfaces (FSSs) which have a desired frequency filtering response [1-5].

In the early studies of the periodic surfaces, the analysis of the infinite planar structures have been used. The reflection and transmission coefficients of the passive array system, or self-impedance of an active antenna array are determined as a function of scan angle and/or frequency [1], [6].

However, the real problem geometry is always finite, and infinite array approach does not predict the truncation effects. Because of this reason, the studies are concentrated on finite array analysis. The truncated array problems can be solved with numerical techniques [1], [2], [7-13] or can be solved with analytical high frequency techniques [14-15]. Also, the truncated array problems can be solved by using hybrid numerical-analytical techniques [15].

Typically, for a large (in terms of wavelength) truncated array, the currents on the interior elements are very close to those predicted in the infinite array case, namely Floquet currents. Only those elements near the edge of the array exhibit some perturbation due to the mutual coupling effects [14-15], [20-21]. In a large finite array, when an interior element looks around itself, it senses the structure as if it is infinite; because it sees same number of elements in all directions and at same distance to itself. However, an element near the edge of an array does not see same number of elements with same distance to itself in all directions. Due to this mutual coupling difference, the interior element currents and near edge element currents are different in a large finite array.

The most rigorous analysis tools for large finite array antennas are numerical methods such as Method of Moments (MoM), which however becomes computationally inefficient for large-size arrays. Therefore, the attention has recently been given to the efficient representation of the Green's function of the periodic large array. The Floquet wave representation of infinite array has been modified to take into account truncation of array by using asymptotic high frequency techniques [14-15]. Asymptotic high frequency analysis for describing the fields of a large finite array [15] shows that the field at an observation point that is sufficiently far from the array truncation boundaries can be represented as a superposition of fields of a few rays arising from interior points, points at edges and corners.

It has been shown that at lower frequencies, there can also exist array guided surface waves which are guided by the metallic dipole elements of the array. This type of surface wave is guided by the metallic array itself as opposed to the dielectric slab-guided waves encountered in the context of periodic arrays [1], [6], [18], [19-22]. For lossless elements, along the array surface, these surface waves propagate unattenuated and are evanescent normal to the array face [1], [7-9], [16-18]. These types of surface waves have been studied and given in literature previously in [24-29]. In a one dimensional Yagi Uda array, these types of surface

waves are excited when the spacing between the elements and the element lengths are smaller than a half wavelength. Perturbations in the currents in one dimensional finite truncated array of dipoles have been observed by [16].

The array guided surface waves are important, because most antenna array and frequency selective surface (FSS) designs keep the array element spacings small enough to avoid grating lobes. When these interelement spacings are kept small enough, actually the existence conditions of the array guided surface waves are forced. The existence, the launching and the reflection coefficients of the array guided surface waves have been determined in [1], [7-9] via a numerical Method of Moments (MoM) approach for solving the pertinent canonical array problem configurations.

Recently, on finite × finite planar dipole arrays in free space or on infinite grounded slab, array guided surface waves (AGSWs) have been studied in [18]; the effects of AGSWs on the currents and scattering patterns of finite dipole array with/without grounded dielectric substrate has been investigated. In [18] it has been shown that the array guided surface waves have important effects on the scattered fields especially near end-fire directions.

1.1. Problem Statement

In order to predict the behaviour of large finite arrays, the infinite structure approach is not very satisfactory. Therefore, the Floquet wave representation needs to be modified when dealing with a geometrical discontinuity such as edges, corners in planar arrays. In the present study, the electric field expressions for finite array are obtained by asymptotic high frequency techniques.

Furthermore, in the present study, the array guided surface wave launching coefficient is obtained analytically, in essentially closed form, via a combination of an asymptotic high frequency analysis and the reciprocity integral [23] formulation

for the plane wave scattering by a planar semi-infinite array of dipoles in free space, together with a modified Kirchhoff approximation [17].

Chapter 2 provides a solution strategy for the analysis of EM radiation/scattering from an infinite array of dipoles in free space and gives the scan impedance concept. Also, in Chapter 2, a solution strategy for the analysis of EM radiation/scattering from a semi-infinite array of dipoles in free space with analytical high frequency techniques is provided. A spectral domain expression of the Green's function is used and the obtained expression is solved with analytical high frequency techniques in closed form. The validity and the accuracy of the expressions in near field are investigated for several cases. Then, for a finite × infinite array of dipoles in free space a far field formula is obtained by using spectral domain expressions; and the results are compared with array theory. Asymptotic field expressions for semi-infinite array of dipoles on infinite grounded dielectric slab are provided.

In Chapter 3, existence conditions of array guided surface waves are revisited and propagation constants of the surface waves are found by setting the infinite array scan impedance to zero. Then, the distant line source excited semi-infinite array problem is solved analytically for surface waves. A reciprocal problem is constructed to find the excitation coefficient of the edge excited surface wave due to diffraction. This analytically found excitation coefficient is compared by numerical solutions provided in [9].

CHAPTER 2

PLANAR INFINITE OR SEMI-INFINITE ARRAY OF DIPOLES IN FREE SPACE

The starting point in the analysis of periodic structures is Floquet's theorem [1], [23], [30]. By using Floquet's theorem, the currents on the elements of an array of infinite extent can be described. If an infinite structure is truncated on one dimension, this theorem can not be used in that dimension in order to fully describe the currents on the elements.

Analytical high frequency techniques can be used for the analysis of radiation and scattering from a large finite array antennas. In [14] uniform asymptotic high frequency ray solutions have been developed for this type of problem. Then, a hybrid method, which combines the asymptotic high frequency based UTD ray concept with the numerical MoM approach has been developed in [15] to provide a relatively efficient analysis of electromagnetic radiation/scattering from an electrically large, planar, periodic, finite array.

In this chapter, Floquet's theorem and a solution technique for infinite planar dipole array in free space is provided. Also, for an infinite dipole array the scan impedance (self impedance) concept is discussed. Then, a procedure of an analytical solution technique for the fields of a semi-infinite planar periodic array of dipoles in free space is given. A comparison of fields obtained by element-by-element method and asymptotic methods are provided for different array parameters.

An $e^{+j\omega t}$ time convention for the fields is assumed and suppressed in this thesis, where $\omega = 2\pi f$, f is the wave frequency, t denotes the time.

2.1. Plane Wave Incidence on a Periodic Structure

The problem of reflection and transmission of a plane wave incident on a periodic structure is an important problem. In antenna engineering, plane wave incidence on frequency selective surfaces (FSSs) and array antennas are two examples of this type of problem.

In order to demonstrate the solution approach, an example is given below. A periodic structure is located at z = 0 plane, and a plane wave is incident on this surface from the direction defined by (θ_p, φ_p).

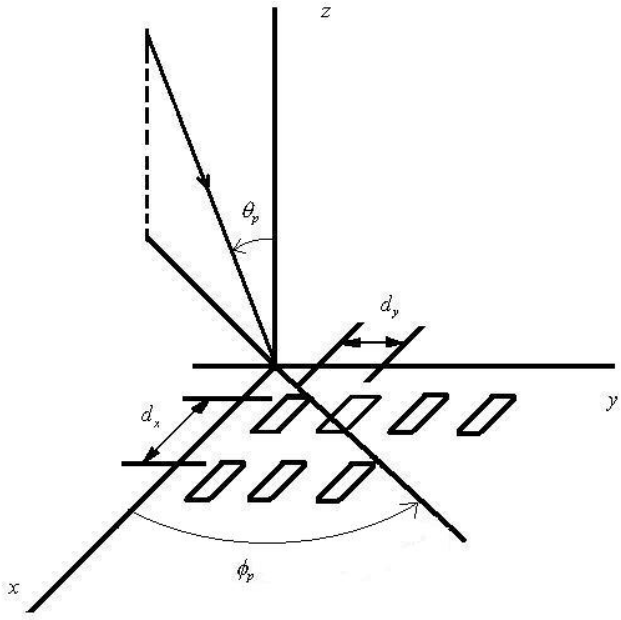

Figure 2.1. Plane wave incident on a periodic structure at z = 0 plane (Adopted from [30])

In Figure 2.1, the structure is assumed to be infinite; therefore, Floquet's theorem (Appendix B) can be used to describe the reflected wave from this surface. Interelement spacings d_x and d_y are actually spatial periods of this periodic structure. The incident wave whether it is an electric field or magnetic field can be written as:

$$U_i = A_i e^{-j\gamma_x x - j\gamma_y y + j\gamma_z z} \tag{2.1}$$

Where the direction cosines are given as,

$$\begin{aligned} \gamma_x &= k \sin\theta_p \cos\phi_p \\ \gamma_y &= k \sin\theta_p \sin\phi_p \\ \gamma_z &= k \cos\theta_p \end{aligned} \tag{2.2}$$

The free space wavenumber is k = 2 π / λ, where λ is wavelength. The reflected wave is written in terms of space harmonics in the x and y directions. Considering the wave equation the reflected wave can be written as

$$U_r = \sum_{p=-\infty}^{\infty} \sum_{q=-\infty}^{\infty} B_{pq} e^{-jk_{xp}x - jk_{yq}y - jk_{zpq}z} \tag{2.3}$$

In Equation (2.4), Floquet wavenumbers are given as,

$$\begin{aligned} k_{xp} &= \gamma_x + \frac{2\pi p}{d_x} \quad ; \quad p = 0, \pm 1, \pm 2, \ldots \\ k_{yq} &= \gamma_y + \frac{2\pi q}{d_y} \quad ; \quad q = 0, \pm 1, \pm 2, \ldots \end{aligned} \tag{2.4}$$

Where k_{zpq} is defined as,

$$k_{zpq} = \sqrt{k^2 - k_{xp}^2 - k_{yq}^2} \tag{2.5}$$

B_{pq} can be determined by applying boundary conditions. The propagation constant of each mode in the z direction is given in (2.5). This propagation constant, depending on the angle of incidence and (p, q) set, can be real or imaginary. If k_{zpq} is real, the wave propagates away from the surface carrying real power and is called as "grating mode". If k_{zpq} is purely imaginary, the wave does not carry real power away from the surface and is called as "evanescent".

2.2. Infinite × Infinite Array of Dipoles in Free Space

In this part, fields of an infinite array of infinitesimal dipoles in free space are derived. In order to apply Floquet's theorem, the currents on the array elements must have the equal magnitude, progressive phase characteristic as would be induced by an incident plane wave. In a scattering problem the phases of currents are matched to the incident field phase. In a radiation problem elements are excited such that between elements a linear phase is kept, while they have equal magnitude. Floquet's theorem holds for the fields radiated by the array currents as well as for the currents themselves.

In Figure 2.2, an infinite array of infinitesimal y-directed dipoles on z = 0 plane is illustrated. The dipole elements have unit current amplitude. The interelement period is d_x and d_y in the x and y directions respectively. The dipoles are linearly phased with γ_x and γ_y denoting interelement phasings along the x and y coordinates, respectively. The dipole currents can be represented as

$$\overline{J}_{nm}(\overline{r}\,') = \hat{y}\delta(x' - nd_x)\delta(y' - md_y)\delta(z')e^{-j\gamma_x nd_x}e^{-j\gamma_y md_y} \qquad (2.6)$$

where (nd_x, md_y) is the position of the $(n,m)^{th}$ dipole.

Interelement phasings are represented as

$$\gamma_x = k \sin\theta_0 \cos\phi_0$$
$$\gamma_y = k \sin\theta_0 \sin\phi_0$$
$$(\theta_0, \phi_0) : \textit{scan direction} \ (\textit{radiation problem}), \qquad (2.7)$$
$$\textit{incident field direction} \ (\textit{scattering problem})$$
$$k = \frac{2\pi}{\lambda}$$

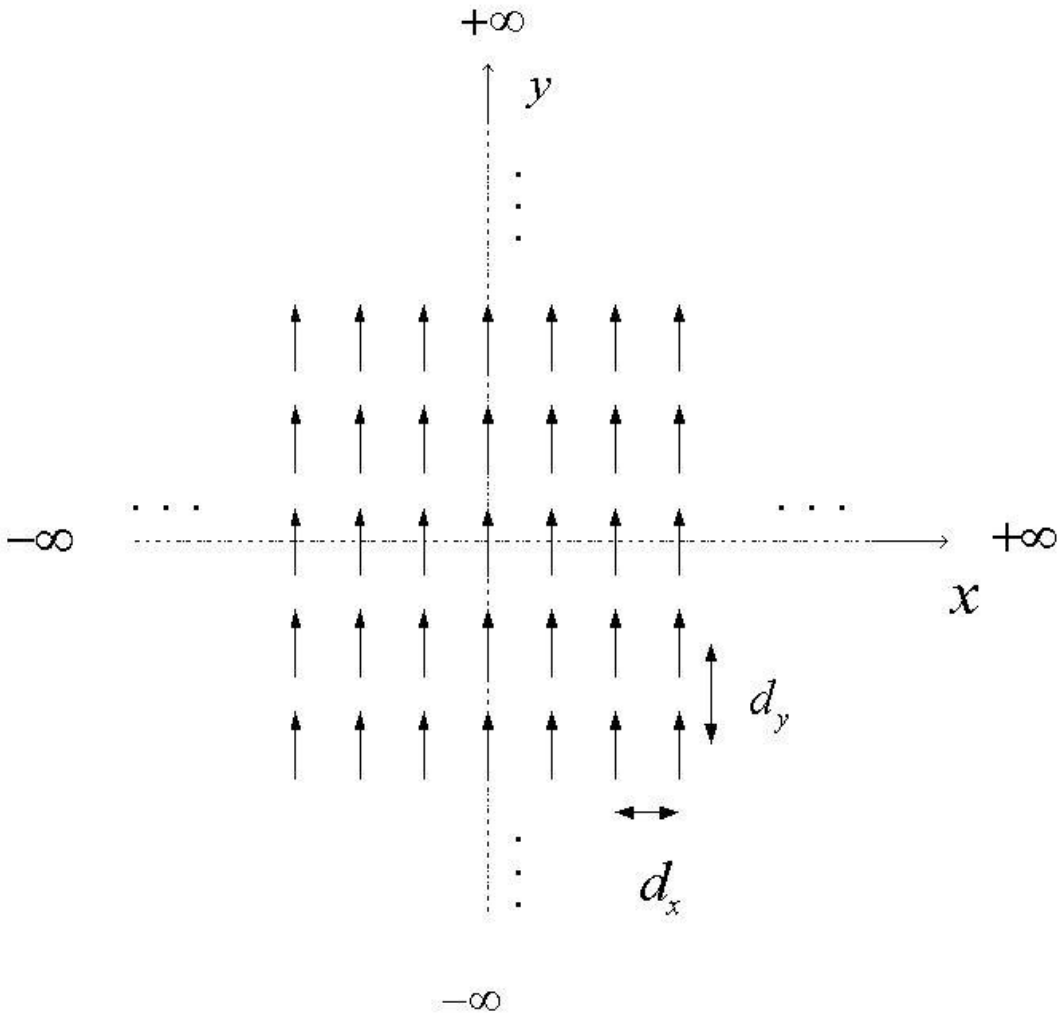

Figure 2.2. Infinite array of infinitesimal dipoles at z = 0 plane.

In (2.7) k is free-space wavenumber. The electromagnetic vector field at any observation point (x, y, z) can be derived from magnetic vector potential. Without loss of generality, observations can be restricted on z > 0 plane. From symmetry, the results can be extended to z < 0.

The magnetic vector potential can be expressed as,

$$\bar{A}(\bar{r}) = \sum_{n=-\infty}^{\infty} \sum_{m=-\infty}^{\infty} \int_{x'} \int_{y'} \int_{z'} dx'dy'dz' \; \bar{J}(\bar{r}') \; g(\bar{r}, \bar{r}')$$

$$\bar{r} = (x, y, z) \text{ ; observation point} \tag{2.8}$$

$$\bar{r}' = (x', y', z') \text{ ; source point}$$

where free-space scalar Green's function,

$$g(\bar{r}, \bar{r}') = \frac{e^{-jk\left|\bar{r} - nd_x\hat{x} - md_y\hat{y}\right|}}{4\pi\left|\bar{r} - nd_x\hat{x} - md_y\hat{y}\right|} \tag{2.9}$$

For Green's function the spectral wavenumber Fourier representation can be employed [31],

$$g(\bar{r}, \bar{r}') = \frac{1}{8\pi^2 j} \int_{-\infty}^{\infty} \int_{-\infty}^{\infty} \frac{e^{-j[k_x(x-x')+k_y(y-y')+k_z z)]}}{k_z} \; dk_x dk_y$$
$$\text{where } k_z = \sqrt{k^2 - k_x^2 - k_y^2} \text{ and } (x', y') = (nd_x, md_y) \tag{2.10}$$

Equation (2.10) is valid for z > 0 and (nd_x, md_y) is the source position. The branches of the square root in (2.10) must be chosen to represent waves which propagate or evanesce away from the array, when k_z is real or imaginary, respectively.

Substituting (2.10) into magnetic vector potential expression given in (2.8) and after taking the integral operators outside the summations and with some algebra following A_y expression is obtained:

$$A_y = \frac{1}{8\pi^2 j} \int_{-\infty}^{\infty} \int_{-\infty}^{\infty} \sum_{n=-\infty}^{\infty} \sum_{m=-\infty}^{\infty} e^{j(k_x-\gamma_x)nd_x} e^{j(k_y-\gamma_y)md_y} \times \frac{e^{-jk_x x} e^{-jk_y y} e^{-jk_z z}}{k_z} dk_x dk_y \qquad (2.11)$$

Since the elements of the array y-directed only, the magnetic vector potential can be written as in (2.11). However, arbitrary orientation of dipole elements can be dealt also using dyadic form of spectral Green's function.

In (2.11) the spatial summations are slowly convergent; however, Poisson sum formulas can be used to increase the efficiency of convergence [32]:

$$\begin{aligned} \sum_{n=-\infty}^{\infty} e^{j(k_x-\gamma_x)\frac{d_x}{2\pi}.2\pi n} &= \frac{2\pi}{d_x} \sum_{p=-\infty}^{\infty} \delta(k_x - \gamma_x - \frac{2\pi p}{d_x}) \\ \sum_{m=-\infty}^{\infty} e^{j(k_y-\gamma_y)\frac{d_y}{2\pi}.2\pi m} &= \frac{2\pi}{d_y} \sum_{q=-\infty}^{\infty} \delta(k_y - \gamma_y - \frac{2\pi q}{d_y}) \end{aligned} \qquad (2.12)$$

Using the bilateral Poisson sum formulas in (2.12), the integrations in (2.11) reduces to (p, q) series evaluated at spectral k_{xp} and k_{yq} points. The Floquet wave (FW) wavenumbers can be written as

$$\begin{aligned} k_{xp} &= \gamma_x + \frac{2\pi p}{d_x} \quad ; \quad p = 0, \pm 1, \pm 2, ... \\ k_{yq} &= \gamma_y + \frac{2\pi q}{d_y} \quad ; \quad q = 0, \pm 1, \pm 2, ... \end{aligned} \qquad (2.13)$$

Then, the magnetic vector potential can be written as

$$A_y = \bar{A}.\hat{y} = \frac{1}{2j\, d_x\, d_y} \sum_{p=-\infty}^{\infty} \sum_{q=-\infty}^{\infty} \frac{e^{-jk_{xp}x} e^{-jk_{yq}y} e^{-jk_{zpq}z}}{k_{zpq}} \qquad (2.14)$$

The vector electric field generated by the dipole array is obtained from the vector potential in (2.14) via

$$\bar{E} = -j\omega\mu\bar{A} + \frac{1}{j\omega\varepsilon}\nabla\nabla.\bar{A} \tag{2.15}$$

Then, the electric field can be written as

$$\begin{aligned}\bar{E}(\bar{r}) = \left(\frac{1}{\omega\varepsilon}\right)\frac{1}{2d_x d_y}\sum_p\sum_q\left\{\hat{x}(k_{xp}k_{yq}) + \hat{y}(k_{yq}^2 - k^2) + \hat{z}(k_{zpq}k_{yq})\right\} \\ \times\left[\frac{e^{-jk_{xp}x}e^{-jk_{yq}y}e^{-jk_{zpq}z}}{k_{zpq}}\right]\end{aligned} \tag{2.16}$$

The term (1 / ωε) can be expressed as Z / k, where Z is the intrinsic impedance of the ambient medium. Also, by introducing a spectral vector as in (2.17), electric field expression can be expressed as in Equation (2.18).

$$\bar{G}(k_x, k_y, k_z) = \frac{Z}{k}\left\{\hat{x}(k_{xp}k_{yq}) + \hat{y}(k_{yq}^2 - k^2) + \hat{z}(k_{zpq}k_{yq})\right\} \tag{2.17}$$

$$\bar{E}_{pq}(\bar{r}) = \sum_p\sum_q\frac{1}{2d_x d_y}\,\bar{G}(k_{xp}, k_{yq}, k_{zpq})\frac{e^{-jk_{xp}x}e^{-jk_{yq}y}e^{-jk_{zpq}z}}{k_{zpq}} \tag{2.18}$$

The equation is the spectral domain Green's function for a planar array of Hertzian elements. Each term of the plane wave expansion is indexed by an order pair (p, q). Each of (p, q) term is called a "mode".

The spectral domain expansion has certain advantages over a spatial domain representation, one of which is the relatively rapid convergence of summation. The propagation constant in the z- direction k_z is real for only a finite number of modes. This means that except for a small values of z, the terms decay away exponentially in magnitude as |p| and |q| increase. The (0, 0) mode is called "fundamental" or "dominant" mode, corresponding the maxima of the radiation pattern.

Modes for which k_z is real, other than the fundamental mode, are propagating plane waves and correspond to the grating lobes of the finite array. These contribute a component to far zone field which is comparable to that of the fundamental mode. The interelement spacings are designed to be less than one-half wavelength to avoid grating lobes in general.

Modes for which k_z is imaginary are evanescent modes and do not contribute to the far zone pattern. However, they are important in calculating the array impedance, because the array impedance determines the array currents.

2.3. Finite Length Dipoles and Thin Wire Approximation

In practical problems to model the dipole elements, finite length thin wire dipole elements can be used. In the next section scan impedance formula is derived from the thin wire element fields. Therefore, the formulation of fields according to thin wire elements is given.

For an (n, m)th dipole element having a finite length L in y-direction with a current distribution function f(y), the source term can be written as

$$\overline{J}_{nm}(\overline{r}\,') = \hat{y} f(y' - md_y)\delta(x' - nd_x)\delta(z') e^{-j\gamma_x nd_x} e^{-j\gamma_y md_y} \qquad (2.19)$$

Applying the formulation steps given in previous section and after some algebra, following expression is obtained for A_y.

$$A_y = \frac{1}{8\pi^2 j} \int_{-\infty}^{\infty}\int_{-\infty}^{\infty} \sum_{n=-\infty}^{\infty}\sum_{m=-\infty}^{\infty} e^{j(k_x-\gamma_x)nd_x} e^{-j\gamma_y md_y} \times \left(\int_{y'=mdy-L/2}^{mdy+L/2} f(y' - md_y) e^{jk_y y'} dy' \right) \left[\frac{e^{-jk_x x} e^{-jk_y y} e^{-jk_z z}}{k_z} \right] dk_x dk_y \qquad (2.20)$$

The spatial integration in Equation (2.20) can be written as

$$\int_{y'=mdy-L/2}^{mdy+L/2} f(y'-md_y)e^{jk_y y'}dy' = \tilde{f}(k_y)e^{jk_y md_y} \tag{2.21}$$

In (2.21) the shifted version of the Fourier transform of f(y) is appearing. Then, the field for such a current distribution can be expressed as

$$\begin{aligned}\bar{E}_{pq}(\bar{r}) = \sum_p \sum_q \frac{1}{2d_x d_y}\tilde{f}(k_{yq})\ \bar{G}(k_{xp}, k_{yq}, k_{zpq}) \\ \times \left[\frac{e^{-jk_{xp}x}e^{-jk_{yq}y}e^{-jk_{zpq}z}}{k_{zpq}}\right]\end{aligned} \tag{2.22}$$

In practice, wires are cylindrical, but thin. If the radius of the wire is much smaller than the wavelength, the current distribution on the axis of the wire element can be represented with a sinusoidal profile. The sinusoidal basis functions closely models the actual current on a wire. Also, sinusoidal current distributions give the advantage of having closed form field expressions.

The Fourier transform of a sinusoidal current distribution can be expressed as

$$\begin{aligned}\tilde{f}(k_y) &= \frac{1}{\sin(k\frac{L}{2})}\int_{-L/2}^{L/2}\sin\left[k(\frac{L}{2}-|y'|)\right]e^{jk_y y'}dy' \\ &= \frac{2}{\sin(k\frac{L}{2})}\left[\cos(k_y\ L/2)-\cos(k\ L/2)\right]\end{aligned} \tag{2.23}$$

This Fourier transform in (2.23) is associated with the far-field pattern of a thin wire dipole whose current is sinusoidal.

2.4. Infinite Array Scan Impedance

Here a result for the scan impedance of the planar array of straight wire elements is given. When the array is transmitting, this is the impedance looking into the

terminals, often referred to as scan impedance. The scan impedance is the impedance of an element as a function of scan angles, with all elements excited by the proper amplitude and phase. In a scattering problem, the self-impedance is equal to the voltage induced by the incident field divided by the resulting terminal current. In general, these two definitions are numerically the same only when one mode is used to expand the current [1], [2], [3]. In either case, the self-impedance is the same for all elements in the planar array since the currents follow the same linear phase progression as the impressed or induced voltages.

In Appendix C, an information on calculating the scan impedance is given.

In [1], a result for self impedance by using one sinusoidal mode to model the current on the elements, is given as

$$Z_{11} = \frac{2Z}{k^2 d_x d_y \sin^2(kL/2)} \sum_{p=-\infty}^{\infty} \sum_{q=-\infty}^{\infty} \frac{e^{-jkr_z a}}{r_z} \frac{\left[\cos(kL/2) - \cos(kr_y L/2)\right]^2}{1 - r_y^2} \quad (2.24)$$

where

$$\begin{aligned} r_x &= s_x + \frac{p\lambda}{d_x} \\ r_y &= s_y + \frac{q\lambda}{d_y} \\ r_z &= \begin{cases} \sqrt{1 - r_x^2 - r_y^2} & ;\ r_x^2 + r_y^2 < 1 \\ -j\sqrt{-1 + r_x^2 + r_y^2} & ;\ r_x^2 + r_y^2 > 1 \end{cases} \end{aligned} \quad (2.25)$$

and

$$\hat{s} = \hat{x}s_x + \hat{y}s_y \pm \hat{z}\sqrt{1 - s_x^2 - s_y^2} \quad (2.26)$$

is the direction toward which the array is scanning. Z is the intrinsic impedance of the ambient medium.

2.5. Analytical Approach for the Fields of a Semi-Infinite Planar Dipole Array with Hertzian Elements

The theory of periodic structures can not be applied directly to solve the finite array problems. Because, by truncation of an infinite array actually the periodicity is broken and the Floquet wave basis is not complete.

All of the GTD or UTD asymptotic ray solutions are based on the Kirchhoff approximation. Kirchhoff approximation assumes that the aperture field distribution over the finite array is the same as that for the corresponding infinite array. When a truncated Kirchhoff integral is evaluated asymptotically for high frequencies, it provides a ray description for the truncation effects of the structure. Edge and corner diffracted rays are found by evaluating field integral by high frequency techniques provided that the observation point is not too close to the array edges and corners. Kirchhoff approximation can not provide accurate results for the input impedance of the array elements close to the edges or corners of the array.

Asymptotic evaluation of the field integrals of the aperture current assuming Kirchhoff approximation gives rise to Floquet waves truncated by the discontinuities plus a modulated Floquet type diffracted waves by the discontinuities.

The problem of radiation from the phased array of dipoles is intimately related to the problem of plane wave scattering from an array of dipoles provided that the incident plane wave parameters are matched to the interelement phasing of radiating array. In this section a procedure for a radiation problem is discussed.

In order to evaluate the array fields, the magnetic vector potential is expressed in terms of spectral wavenumber Fourier representation of Green's function. If the array elements are on the dielectric media, then Green's function for this type of problem has to be derived and used [18], [20-22]. In this type of problem due to dielectric structures there are surface wave modes, and they have to be dealt.

Then, the spatial summation terms are converted to relatively faster spectral series by Poisson summation formulas [32]. In finite or semi-infinite summations one encounters with geometric series inside the spectral integrals; then geometric series inside the integral can be evaluated in closed form.

After obtaining an expression for magnetic vector potential, the electric field expression can be derived. The electric field expression can be solved by high frequency asymptotic techniques [31]. In this study, semi-infinite array is considered.

2.6. Asymptotic Field Expressions of a Semi-Infinite Planar Dipole Array with Hertzian Elements

In Figure 2.3, a semi-infinite array of infinitesimal y-directed dipoles on z = 0 plane is illustrated. The dipole elements have unit current amplitude. The interelement period is d_x and d_y in the x and y directions respectively. The dipoles are linearly phased to scan the beam (θ_0, ϕ_0). The dipole currents can be represented as

$$\overline{J}_{nm}(\overline{r}\,') = \hat{y}\delta(x' - nd_x)\delta(y' - md_y)\delta(z')e^{-j\gamma_x nd_x}e^{-j\gamma_y md_y} \tag{2.27}$$

where (nd_x, md_y) is the position of the $(n,m)^{th}$ dipole and

$$\begin{aligned} \gamma_x &= k\sin\theta_0\cos\phi_0 \\ \gamma_y &= k\sin\theta_0\sin\phi_0 \end{aligned} \tag{2.28}$$

The electromagnetic vector field at any observation point (x, y, z) can be derived from magnetic vector potential. Without loss of generality, observations can be restricted on z > 0 plane. From symmetry, the results can be extended to z < 0.

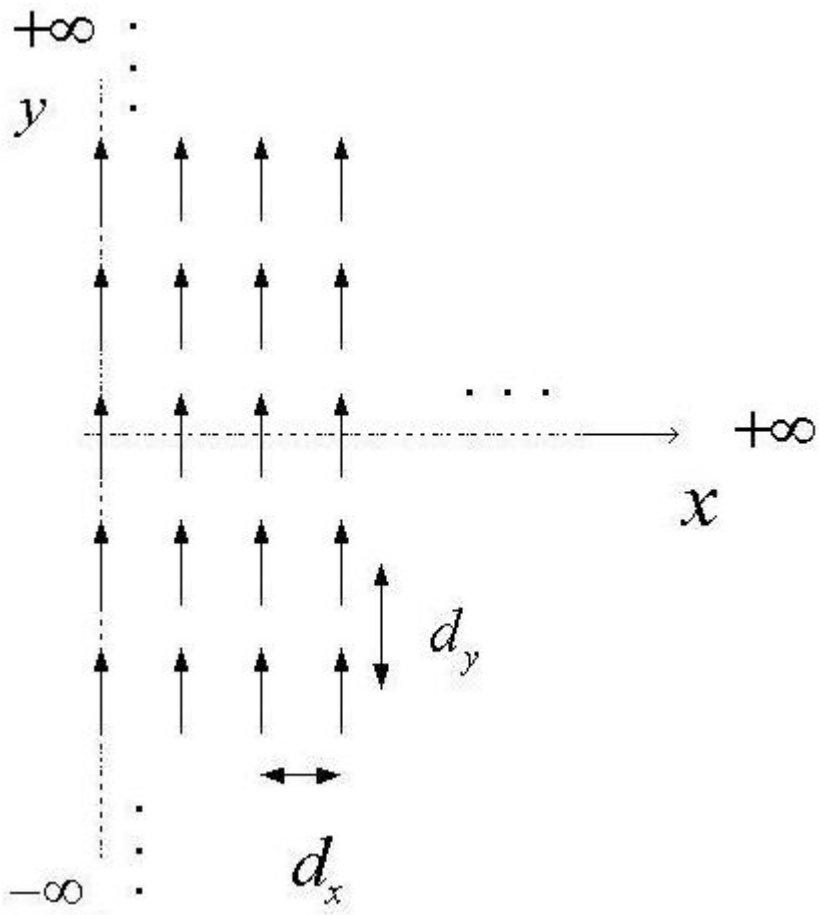

Figure 2.3. Semi-infinite array of infinitesimal dipoles at z = 0 plane, occupying the region x > 0.

The magnetic vector potential can be expressed as,

$$\bar{A}(\bar{r}) = \sum_{n=0}^{\infty} \sum_{m=-\infty}^{\infty} \int_{x'} \int_{y'} \int_{z'} dx'dy'dz' \; \bar{J}(\bar{r}') \; g(\bar{r}, \bar{r}') \tag{2.29}$$

In (2.29), (x, y, z) represents the observation point coordinates, whereas (x', y', z') represents the source point coordinates (nd_x, md_y, 0) and free-space Green's function is given as

$$g(\bar{r},\bar{r}') = \frac{e^{-jk\left|\bar{r}-nd_x\hat{x}-md_y\hat{y}\right|}}{4\pi\left|\bar{r}-nd_x\hat{x}-md_y\hat{y}\right|} \tag{2.30}$$

For Green's function the spectral wavenumber Fourier representation can be employed [31],

$$\begin{aligned} g(\bar{r},\bar{r}') &= \frac{1}{8\pi^2 j}\int_{-\infty}^{\infty}\int_{-\infty}^{\infty}\frac{e^{-j[k_x(x-x')+k_y(y-y')+k_z z)]}}{k_z}\,dk_x dk_y ; z>0 \\ k_z &= \sqrt{k^2-k_x^2-k_y^2} \end{aligned} \tag{2.31}$$

On the top Riemann sheet of the complex k_x plane, the branch of k_z is chosen as [31].

$$\begin{aligned} &\mathrm{Im}\{k_z\}<0 \quad ; \; for \; k^2-k_y^2<k_x^2 \\ &\mathrm{Re}\{k_z\}>0 \quad ; \; for \; k^2-k_y^2>k_x^2 \end{aligned} \tag{2.32}$$

Substituting (2.31) into magnetic vector potential expression and after taking the integral operators outside the summations and with some algebra (2.33) can be obtained.

$$A_y = \frac{1}{8\pi^2 j}\sum_{m=-\infty}^{\infty}\int_{-\infty}^{\infty}dk_y\int_{-\infty}^{\infty}dk_x\sum_{n=0}^{\infty}e^{j(k_x-\gamma_x)nd_x}e^{j(k_y-\gamma_y)md_y}\frac{e^{-jk_x x}e^{-jk_y y}e^{-jk_z z}}{k_z} \tag{2.33}$$

Since the elements of the array y-directed only, the magnetic vector potential can be written as in (2.33). However, arbitrary orientation of dipole elements can be dealt also using dyadic form of spectral Green's function.

Since the exponential term depending on the n index is less than unity along the integration path, the series inside the integral can be evaluated in closed form. After the evaluation of geometric series inside the integral, A_y becomes

$$A_y = \frac{1}{8\pi^2 j}\sum_{m=-\infty}^{\infty}\int_{-\infty}^{\infty} dk_y \int_{-\infty}^{\infty} dk_x \frac{1}{1-e^{jd_x(k_x-\gamma_x)}}\, \mathrm{e}^{j(k_y-\gamma_y)md_y}\, \frac{e^{-jk_x x}e^{-jk_y y}e^{-jk_z z}}{k_z} \qquad (2.34)$$

The Floquet wavenumbers along the x-direction is defined by the real poles located at

$$k_{xp} = \gamma_x + \frac{2\pi p}{d_x} \quad ; \text{p=0}, \pm 1, ... \qquad (2.35)$$

Using the bilateral Poisson sum formula [32], the infinite series can be converted to train of impulses, and due to the property of the impulse function dk_y integration is eliminated and the following A_y expression is obtained.

$$A_y = \frac{1}{4\pi j d_y}\sum_{q=-\infty}^{\infty}\int_{-\infty}^{\infty} dk_x \frac{1}{1-e^{jd_x(k_x-\gamma_x)}}\frac{e^{-jk_x x}e^{-jk_{yq} y}e^{-jk_{zq} z}}{k_{zq}} \qquad (2.36)$$

where

$$k_{zq} = \sqrt{k^2 - k_x^2 - k_{yq}^2} \qquad (2.37)$$

The electric field generated by this array can be obtained from the vector potential as

$$\bar{E}(\bar{r}) = \frac{Z}{4\pi k d_y}\sum_{q=-\infty}^{\infty}\int_{-\infty}^{\infty} dk_x \frac{\left\{\hat{x}(k_x k_{yq}) + \hat{y}(k_{yq}^2 - k^2) + \hat{z}(k_{zq} k_{yq})\right\}}{1-e^{jd_x(k_x-\gamma_x)}} \times \frac{e^{-jk_x x}e^{-jk_{yq} y}e^{-jk_{zq} z}}{k_{zq}} \qquad (2.38)$$

The asymptotic evaluation of the Equation (2.38) can be performed by steepest descent methods given in Appendix A. Due to the residues of the poles and saddle point condition, after evaluation of the integral (p, q) indexed Floquet wave series

and corresponding q indexed diffracted fields from the edge of the array are obtained.

In order to simplify the integrand, the change of variables from the Cartesian (k_x, k_{zq}) to the cylindrical polar ($k_{\rho q}$, α) coordinates in the spectral domain is introduced.

$$\begin{aligned} k_x &= k_{\rho q}\cos(\alpha) \\ k_{zq} &= k_{\rho q}\sin(\alpha) \end{aligned} \tag{2.39}$$

where $\alpha = \alpha_r + j\alpha_i = \mathrm{Re}\{\alpha\} + j\,\mathrm{Im}\{\alpha\}$ and $k_{\rho q}$ is defined as

$$k_{\rho q} = \sqrt{k^2 - k_{yq}^2} \tag{2.40}$$

After steepest descent transformation, the physical coordinates (x, y, z) are represented in terms of the polar coordinates (ρ, φ, y) as

$$\begin{aligned} x &= \rho\cos(\phi) \\ z &= \rho\sin(\phi) \end{aligned} \tag{2.41}$$

where $\phi \in (0, \pi)$.

By using the transformations given in (2.39) and (2.41), (2.38) can be expressed as

$$\bar{E}(\bar{r}) = \frac{1}{4\pi d_y}\sum_{q=-\infty}^{\infty}\int_{C_\alpha}\bar{D}_q(\alpha)e^{-jk_{\rho q}\rho\cos(\alpha-\phi)}e^{-jk_{yq}y}d\alpha \tag{2.42}$$

where

$$\begin{aligned} \bar{D}_q(\alpha) &= \frac{\bar{G}(k_{\rho q}\cos\alpha, k_{yq}, k_{\rho q}\sin\alpha)}{1 - e^{jd_x(k_{\rho q}\cos\alpha - \gamma_x)}} \\ \bar{G}(k_x, k_y, k_z) &= \frac{Z}{k}\left(\hat{x}k_x k_y + \hat{y}(k_y^2 - k^2) + \hat{z}k_z k_y\right) \end{aligned} \tag{2.43}$$

The integration path C_α in the complex α-plane corresponds to the real axis in the k_x-plane. The poles of the function $D_q(\alpha)$ are defined as

$$\alpha_{pq} = \cos^{-1}\left(\frac{k_{xp}}{k_{\rho q}}\right) = \cos^{-1}\left(\frac{\gamma_x + \frac{2\pi p}{d_x}}{k_{\rho q}}\right) \tag{2.44}$$

where $k_{\rho q}$ may assume real or imaginary values. Also, k_{zpq} can be defined as

$$k_{zpq} = \sqrt{k^2 - k_{xp}^2 - k_{yq}^2} = k_{\rho q}\sin(\alpha_{pq}) \tag{2.45}$$

Poles with $k_{xp}^2 + k_{yq}^2 < k^2$ are associated with propagating Floquet waves (real k_{zpq}), while all other poles are associated with evanescent Floquet waves (imaginary k_{zpq}). For propagating Floquet waves α_{pq} is real.

To evaluate the integral in (2.42) in the high-frequency range, the integration contour is deformed into the steepest descent path (SDP) through its pertinent saddle point in the phase function. After path deformation the integral can be written as the sum of the saddle point contribution and the residue contribution which comes from the residues of the intercepted poles during path deformation.

$$\int_C f(\alpha)e^{\Omega g(\alpha)}d\alpha \to \int_{SDP} f(\alpha)e^{\Omega g(\alpha)}d\alpha + 2\pi j\sum(\textit{residue of poles}) \tag{2.46}$$

The fast phase function g(α), and the relatively slow amplitude function f(α) can be written as

$$f(\alpha) = \frac{\bar{G}(k_{\rho q}\cos\alpha, k_{yq}, k_{\rho q}\sin\alpha)}{1 - e^{jd_x(k_{\rho q}\cos\alpha - \gamma_x)}}\exp\{-jk_{yq}y\}$$
$$g(\alpha) = -j\cos(\alpha - \phi), \qquad \Omega = k_{\rho q}\rho \tag{2.47}$$

In order to apply Van der Waerden method given in the Appendix A, the saddle point α_s and the second derivative of phase function and distance parameter s_i in the complex α plane can be evaluated as

$$\begin{aligned}
&g(\alpha) = -j\cos(\alpha-\phi)\\
&g'(\alpha) = j\sin(\alpha-\phi)\\
&g'(\alpha_s) = j\sin(\alpha_s-\phi) = 0 \Rightarrow \alpha_s = \phi\\
&g''(\alpha) = j\cos(\alpha-\phi) \Rightarrow g''(\alpha_s) = j\\
&s_i^2 = g(\alpha_s) - g(\alpha_{pq}) = -j + j\cos(\alpha_{pq}-\phi) = -2j\sin^2(\frac{\alpha_{pq}-\phi}{2})\\
&s_i = \sqrt{-2j}\sin(\frac{\alpha_{pq}-\phi}{2})
\end{aligned} \tag{2.48}$$

The residue of the intercepted poles can be written as

$$\begin{aligned}
&r_i = \lim_{\alpha\to\alpha_i} f(\alpha)(\alpha-\alpha_i) \Rightarrow\\
&r_i = \lim_{\alpha\to\alpha_{pq}} f(\alpha) = \frac{\bar{G}(k_{\rho q}\cos\alpha, k_{yq}, k_{\rho q}\sin\alpha)}{1-e^{jd_x(k_{\rho q}\cos\alpha-\gamma_x)}} e^{-jk_{yq}y}(\alpha-\alpha_i)
\end{aligned} \tag{2.49}$$

After applying the L'opital rule to (2.49) one can obtain the residue contribution as

$$r_i = \frac{\bar{G}(k_{xp}, k_{yq}, k_{zpq})}{jd_x k_{zpq}} e^{-jk_{yq}y} \tag{2.50}$$

Then, after path deformation the residue contribution to the Equation in (2.46) is

$$\begin{aligned}
pole\ contribution = \frac{1}{4\pi d_y} 2\pi j \sum_{p,q} \frac{\bar{G}(k_{xp}, k_{yq}, k_{zpq})}{jd_x k_{zpq}} e^{-jk_{yq}y}\\
\times e^{k_{\rho q}\rho\cos(\alpha_{pq}-\phi)} U(\phi_{pq}^{SB}-\phi)
\end{aligned} \tag{2.51}$$

where U(.) represents the unit step function and

$$\bar{E}_{pq}^{FW}(\bar{r}) = \frac{1}{2d_x d_y k_{zpq}} \bar{G}(k_{xp}, k_{yq}, k_{zpq}) e^{-j(k_{xp}x + k_{yq}y + k_{zpq}z)} \tag{2.52}$$

The SDP, for $k_{\rho q}$ real or imaginary, can be found by decomposing the argument of the exponential term in (2.42) into its imaginary and real parts as

$$\begin{aligned} -jk_{\rho q}\rho\cos(\alpha-\phi) = -jk_{\rho q}\rho(&\cos(\alpha_r-\phi)\cosh\alpha_i \\ &+j\sin(\alpha_r-\phi)\sinh\alpha_i) \end{aligned} \tag{2.53}$$

The SDP is the locus of points for which the imaginary part of the phase function is equal to that at the saddle point $\alpha = \phi$.

$$\begin{aligned} &\mathrm{Im}\{-jk_{\rho q}\rho(\cos(\alpha_r-\phi)\cosh\alpha_i + j\sin(\alpha_r-\phi)\sinh\alpha_i)\} \\ &= \mathrm{Im}\{-jk_{\rho q}\rho\} \\ &= \begin{cases} k_{\rho q}\rho \ , \ for\ k_{\rho q}\ real \\ 0 \ , \ for\ k_{\rho q}\ imaginary \end{cases} \end{aligned} \tag{2.54}$$

The SDP can be written as

$$\begin{aligned} &\cos(\alpha_r-\phi)\cosh\alpha_i = 1 \quad ; for\ k_{\rho q}\ real \\ &\sin(\alpha_r-\phi) = 0 \quad ; for\ k_{\rho q}\ imaginary \end{aligned} \tag{2.55}$$

The shadow boundary angle ϕ_{pq}^{SB} is found by imposing that the SDP passes through the pole at $\alpha = \alpha_{pq}$, thus,

$$\begin{aligned} &\cos(\mathrm{Re}\{\alpha_{pq}\}-\phi_{pq}^{SB})\cosh(\mathrm{Im}\{\alpha_{pq}\}) = 1 \quad ; for\ k_{\rho q}\ real \\ &\sin(\mathrm{Re}\{\alpha_{pq}\}-\phi_{pq}^{SB}) = 0 \quad ; for\ k_{\rho q}\ imaginary \end{aligned} \tag{2.56}$$

Then the shadow boundary angles, considering (2.44) and the property of hyperbolic functions can be defined as

$$\phi_{pq}^{SB} = \alpha_{pq} = \cos^{-1}(\frac{k_{xp}}{k_{\rho q}}),\ \textit{for real } k_{zpq}$$

$$\phi_{pq}^{SB} = \cos^{-1}(\frac{k_{\rho q}}{k_{xp}}),\ \textit{for imaginary } k_{zpq} \textit{ and real } k_{\rho q} \tag{2.57}$$

$$\phi_{pq}^{SB} = \pi/2,\ \textit{for imaginary } k_{zpq} \textit{ and imaginary } k_{\rho q}$$

The saddle point contribution to (2.42) is

$$I_s(\Omega) = e^{-jk_{\rho q}\rho}\sqrt{\frac{\pi}{k_{\rho q}\rho}}\{\frac{\bar{G}(k_{\rho q}\cos\phi, k_{yq}, k_{\rho q}\sin\phi)}{1-e^{jd_x(k_{\rho q}\cos\phi-\gamma_x)}}e^{-jk_{yq}y}\sqrt{2j}$$
$$+\sum_i \frac{\bar{G}(k_{xp}, k_{yq}, k_{zpq})}{jd_x k_{zpq}\sqrt{-2j}\sin(\frac{\alpha_{pq}-\phi}{2})}e^{-jk_{yq}y}[1-F(\delta_{pq}^2)]\} \tag{2.58}$$

where F is the Fresnel transition function and the index "i" represents the number of poles extracted. The argument of the Fresnel transition function can be expressed as

$$\delta_{pq}^2 = j\Omega s_i^2 = jk_{\rho q}\rho s_i^2 = \sqrt{2k_{\rho q}\rho}\sin(\frac{\alpha_{pq}-\phi}{2}) \tag{2.59}$$

When the argument of Fresnel transition function is much greater than one, then F→1. The expression (2.58) describes the field diffracted from the edge of the array.

The electric field radiated by semi-infinite array can be asymptotically expressed as

$$\bar{E}(\bar{r}) = \sum_{p,q}\bar{E}_{pq}^{FW}(\bar{r})U(\phi_{pq}^{SB}-\phi) + \frac{1}{4\pi d_y}\sum_q I_s(\Omega) \tag{2.60}$$

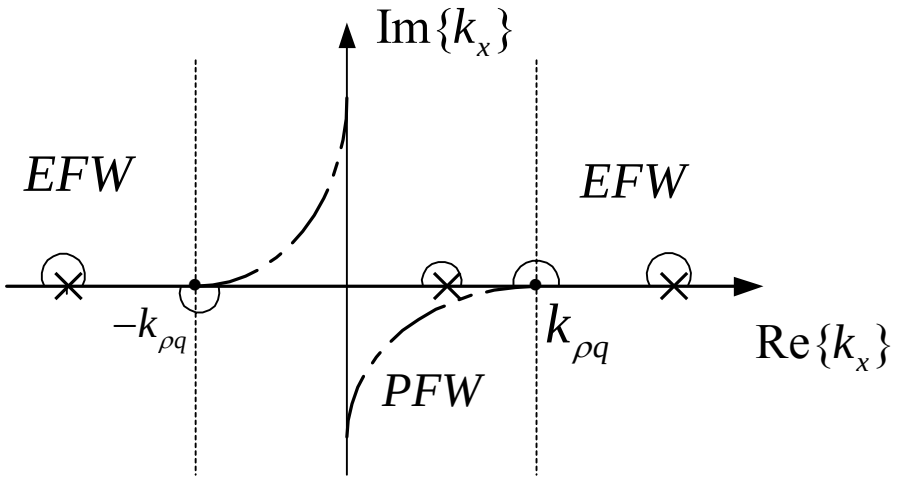

Figure 2.4. Topology of k_x plane for the Equation (2.42). Branch points occur at $k_x = +k_{\rho q}$ and $k_x = -k_{\rho q}$, with $k_{\rho q} = \sqrt{k^2 - k_{yq}^2}$. PFW: Propagating Floquet Waves, EFW: Evanescent Floquet Waves.

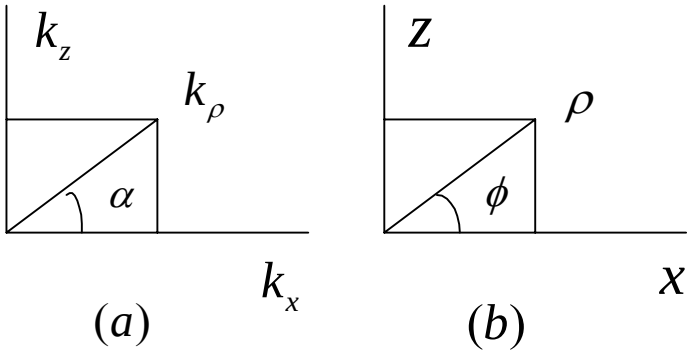

Figure 2.5. The change of variables: (a) for steepest descent transformation, (b) for coordinate transformation.

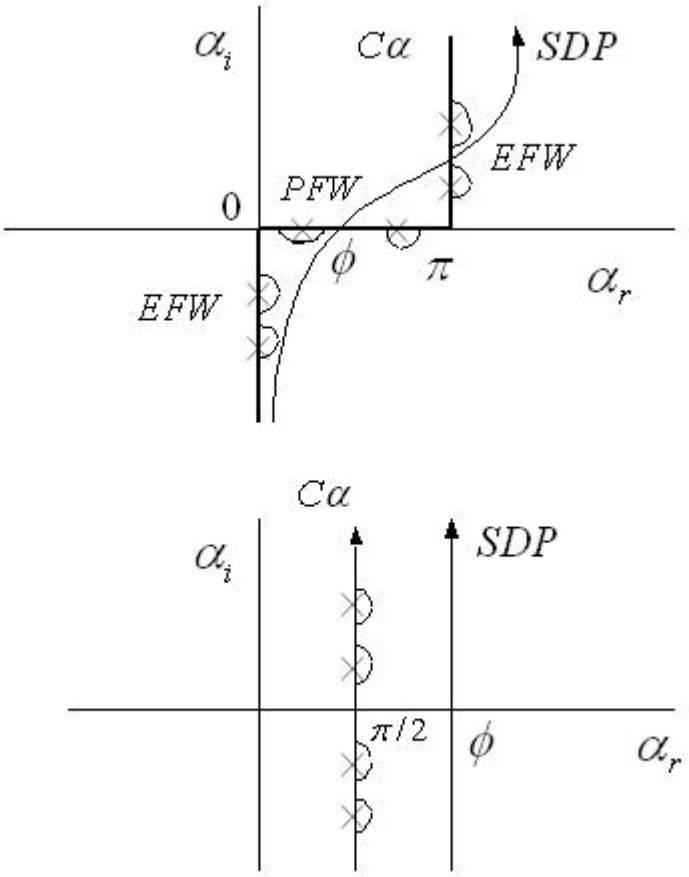

Figure 2.6. Complex α plane, for Floquet problem, after change of variables for cylindrical polar coordinates for $k_{\rho q}$ real and $k_{\rho q}$ imaginary respectively. SDP: Steepest Descent Path.

The ray interpretation of the Floquet wave and diffracted wave solutions is based on the wavenumber vectors defined in (2.61) and (2.62).

$$\bar{k}_{pq}^{FW} = \hat{x}k_{xp} + \hat{y}k_{yq} + \hat{z}k_{zpq} \tag{2.61}$$

$$\bar{k}_{q}^{d} = k_{\rho q}\cos(\phi)\hat{x} + k_{yq}\hat{y} + k_{\rho q}\sin(\phi)\hat{z} \tag{2.62}$$

The vector defined in (2.61) is the wave vector perpendicular to the phasefront of the propagating Floquet waves. For a propagating Floquet wave (PFW), this vector

is real and identifies the ray direction of the (p,q)th PFW. For an evanescent FW, z component of this vector is purely imaginary. The EFW's propagate at grazing with ray (phase propagation) vector

$$\mathrm{Re}\{\bar{k}_{pq}^{EFW}\} = \hat{x}k_{xp} + \hat{y}k_{yq} \tag{2.63}$$

keeping a phase speed less then the speed of light and showing an exponential decay along the z direction with attenuation vector

$$\mathrm{Im}\{\bar{k}_{pq}^{EFW}\} = \hat{z}k_{zpq} \tag{2.64}$$

The diffracted field phase term is generated by the saddle point condition for the steepest descent path integral and can be written as

$$\begin{aligned} &\bar{k}_q^d.\bar{r} = \rho k_{\rho q} + yk_{yq} \\ &\bar{r} = \hat{x}\rho\cos(\phi) + \hat{y}y + \hat{z}\rho\sin(\phi) \end{aligned} \tag{2.65}$$

Because the $\bar{k}_q^d$ in the (ρ,ϕ,y) coordinate system is independent of ϕ, the phase term $\bar{k}_q^d.\bar{r}$ is the same for all points (ρ,y) on a ray cone with a semi-angle

$$\gamma_q = \cos^{-1}(\frac{k_{yq}}{k}) \tag{2.66}$$

The diffracted fields can be categorized as propagating and radially evanescent waves contributions depending on whether $k_{\rho q}$ is real or imaginary respectively. In Figure 2.7 an illustration of the wave mechanism for a semi-infinite array is given.

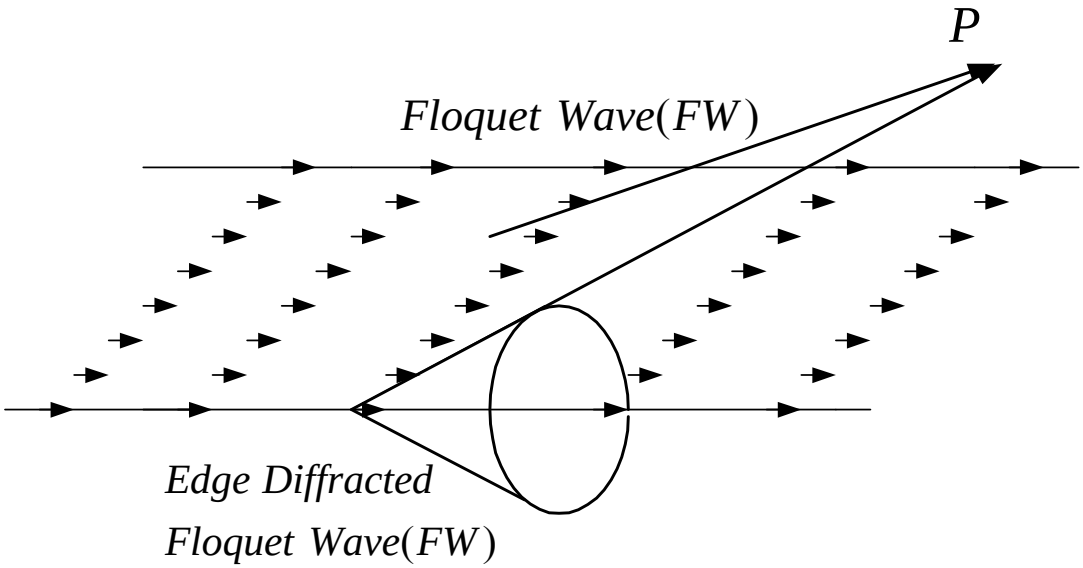

Figure 2.7. Floquet wave and edge diffracted wave contributions for a semi-infinite array.

2.7. A Parametric Study of Asymptotic Solution

In order to test the accuracy and effectiveness of the asymptotic solutions obtained, numerical calculations have been carried out. A reference solution is constructed via the element-by-element summation of the individual dipole contributions.

All field evaluations are referenced to one of the y-oriented edges (y-axis in this study), because the finite array is intended to simulate the semi-infinite array of dipoles. The dimensions of the array should be chosen so that the contributions from the other edges and corners small enough to be negligible.

The array plane and the observation point definition are illustrated in the Figures 2.8 and 2.9.

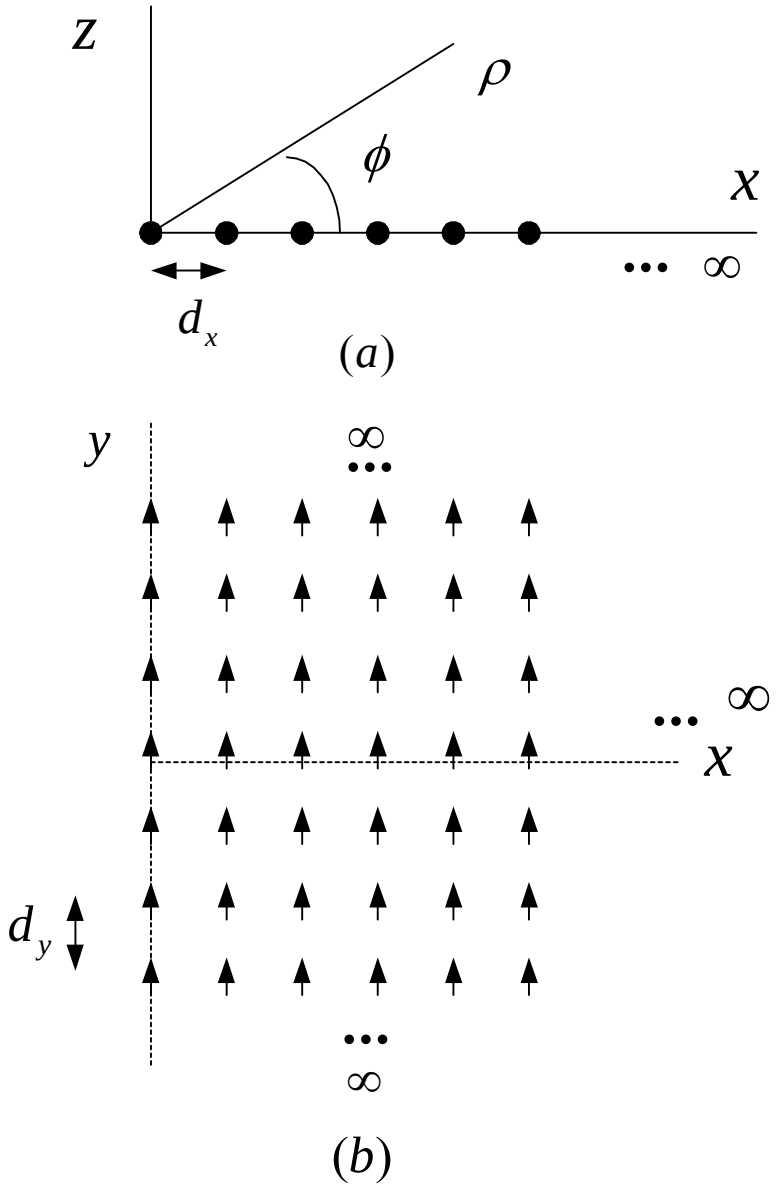

Figure 2.8. Semi-infinite array of dipoles in free space: (a) Side view (b) Top view

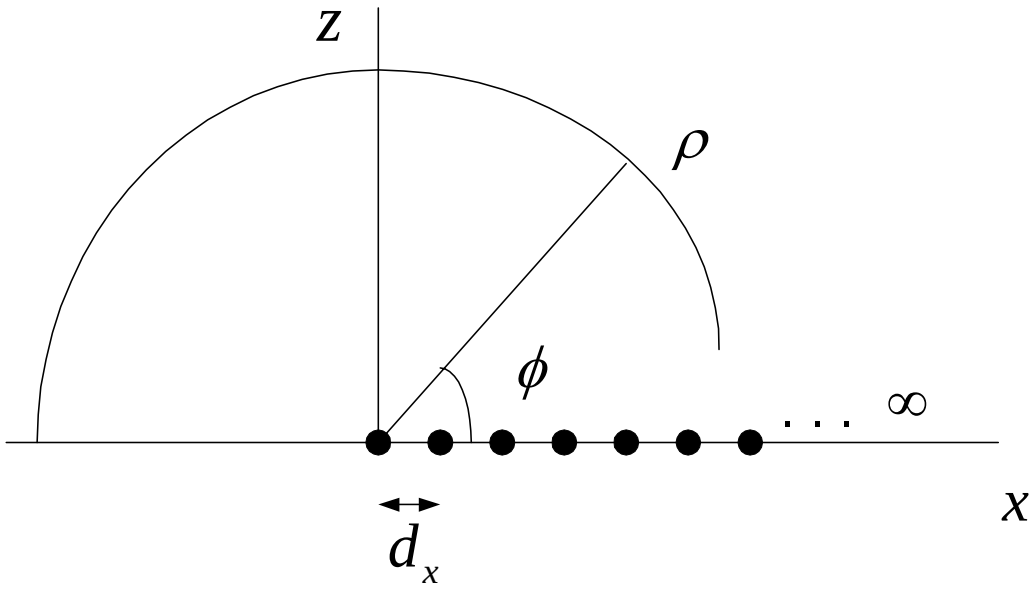

Figure 2.9. The observation plane is xz-plane. The observations are taken at a distance ρ from the edge of the array.

In Figure 2.10, the near-field scan is at ρ = 2λ from the edge of the array, beam is rotated to 60 degrees and the periodicity is dx = 1.4λ, dy = 0.5λ. The reference solution for the number of elements in the x-direction Nx = 1000 and for the number of elements in the y-direction Ny = 3000 is compared with asymptotic solution. For the asymptotic solution code the elapsed computer time is 2.6540 seconds. For reference solution the elapsed time is 277.8100 seconds. Therefore, the asymptotic solution is very fast in comparison to the reference solution. The propagating Floquet modes are (-2,0), (-1,0), (0,0) with shadow boundaries 158, 102, 60 degrees respectively and all the other Floquet modes are evanescent for this case. The region of the existence of each (p,q) mode is $\phi < \phi_{pq}^{SB}$. The FW field is discontinuous at each shadow boundary and the corresponding diffracted fields compensate for the discontinuities so as to provide a continuous total radiated field.

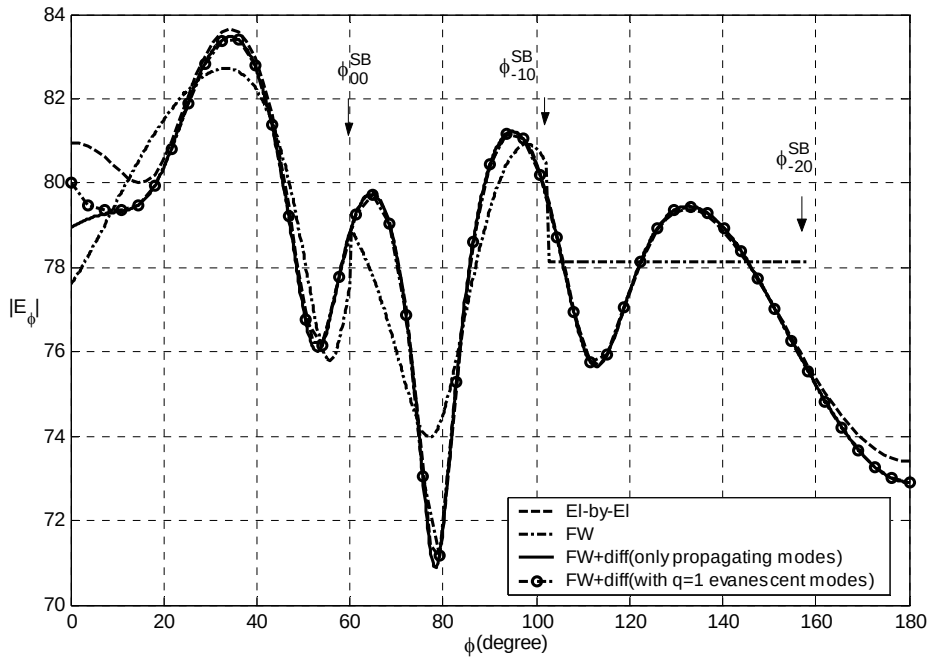

Figure 2.10. The amplitude of ϕ component of the electric field for the near-field scan at $\rho = 2\lambda$ from the edge of the array, beam angle 60 degrees and the periodicity $dx = 1.4\lambda$, $dy = 0.5\lambda$.

In Figure 2.10, Floquet waves and corresponding diffracted fields are plotted for propagating modes. Also, together with propagating modes, the evanescent modes corresponding to q = 1 index are included in the asymptotic solution and the results are compared. When evanescent modes are included, the asymptotic solution behaves similar to reference solution much. Asymptotic solution agrees very well with the reference solution except at grazing angles.

In Figure 2.11, the near-field scan is at $\rho = 2\lambda$ from the edge of the array, beam is rotated to 60 degrees and the periodicity is $dx = 0.5\lambda$, $dy = 1.1\lambda$. For this case only the (0,0) mode is propagating with a shadow boundary 60 degrees and all other modes are evanescent. The next mode is an evanescent (-1,0) mode with a shadow

boundary 131 degrees. In the asymptotic solution one propagating and one evanescent mode is included. Asymptotic solution agrees with reference solution.

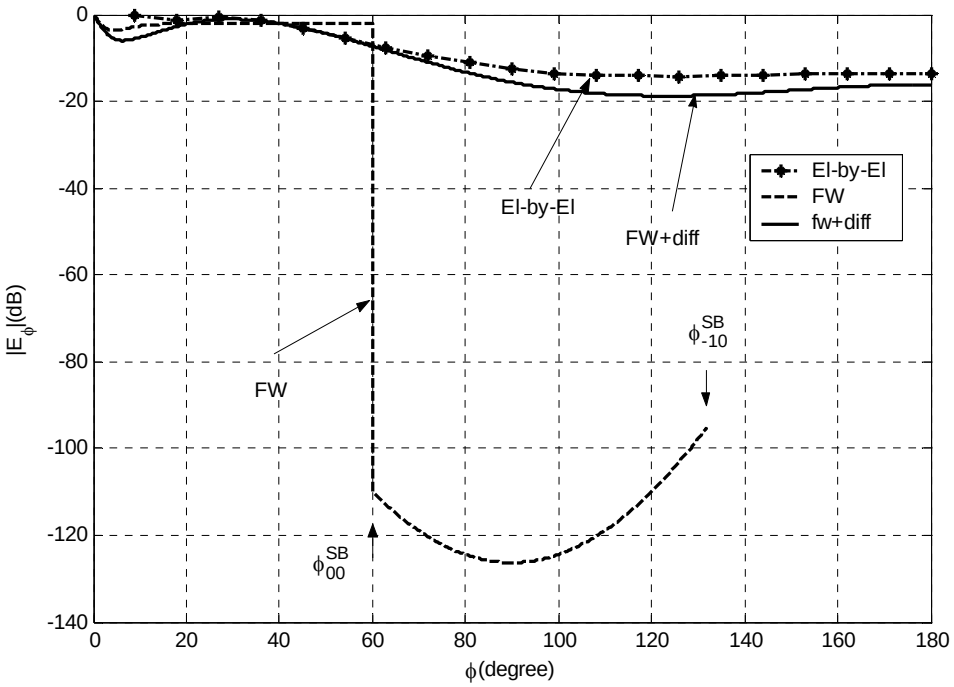

Figure 2.11. The amplitude of ϕ component of the electric field for the near-field scan at $\rho = 2\lambda$ from the edge of the array, beam angle 60 degrees and the periodicity $dx = 0.5\lambda$, $dy = 1.1\lambda$.

In Figure 2.12, the near-field scan is at $\rho = 2\lambda$ from the edge of the array, beam is rotated to 60 degrees and the periodicity is dx = 0.9 cm, dy = 1.6 cm and f = 10 GHz. For this case, (0,0) mode is the only propagating mode and all other modes are evanescent. In Figure 2.12, reference element-by-element solutions for Nx = 100 and Nx = 1000 elements in the x-direction are compared. When the number of elements in the x-direction is increased, the asymptotic solution and the reference

solution are in a good agreement, since the asymptotic solution is a semi-infinite array solution.

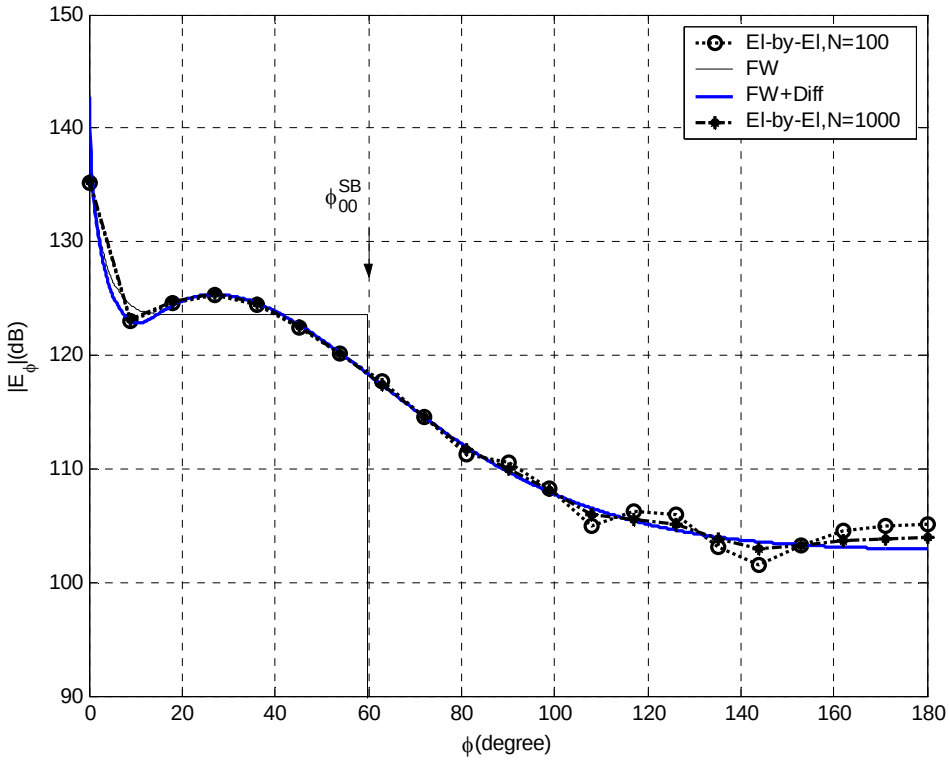

Figure 2.12. The amplitude of ϕ component of the electric field for the near-field scan at $\rho = 2\lambda$ from the edge of the array, beam angle 60 degrees and the periodicity dx = 0.9 cm, dy = 1.6 cm and f = 10 GHz.

In the Figures 2.13 – 2.16, the near field scan for dx = 0.9 cm, dy = 1.6 cm, beam angle 60 degrees, f = 10 GHz with ρ variation are examined. For the cases $\rho > 0.2\lambda$ the asymptotic solution and the reference solution which is based on the element-by-element summation agree well. However, for $\rho < 0.2\lambda$ the asymptotic solution

and the reference solution does not agree; because, in the asymptotic solution it is assumed that ρ is a large parameter.

In the Figure 2.13, ρ = 0.1λ case is demonstrated. The discontinuities of FW are due to the propagating (0,0) mode with a shadow boundary 60^0 and due to evanescent modes (0,-1) and (0,1) modes with shadow boundaries 90^0.

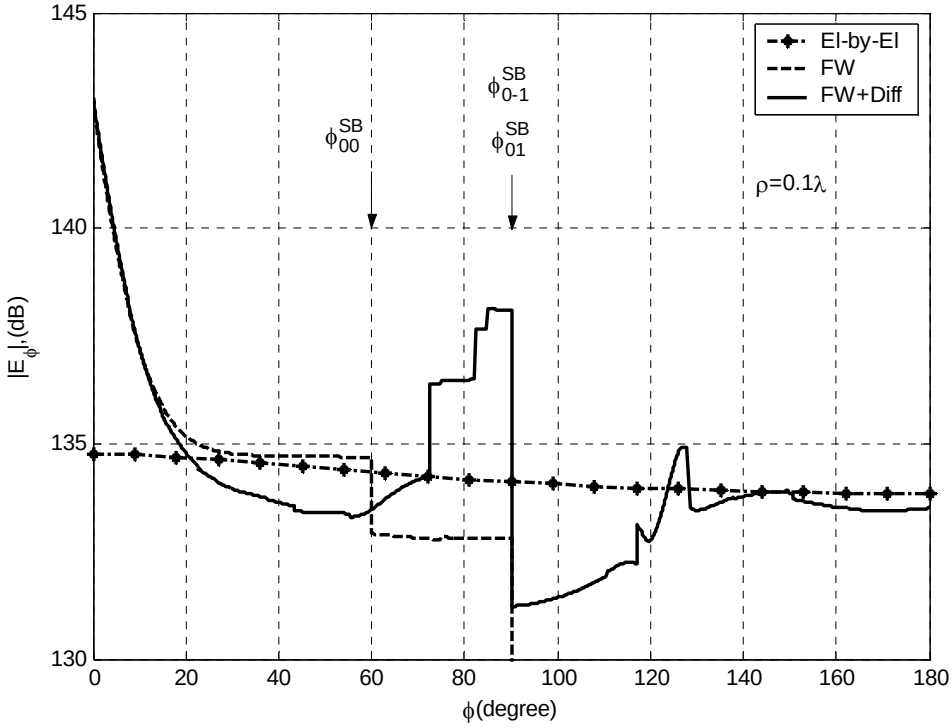

Figure 2.13. The amplitude of ϕ component of the electric field for the near-field scan at ρ = 0.1λ from the edge of the array, beam angle 60 degrees and the periodicity dx = 0.9 cm, dy = 1.6 cm and f = 10 GHz.

In the Figure 2.14, $\rho = 0.2\lambda$ case is demonstrated. The discontinuities of FW are due to the propagating (0,0) mode with a shadow boundary 60^0 and due to evanescent modes (0,-1) and (0,1) modes with shadow boundaries 90^0.

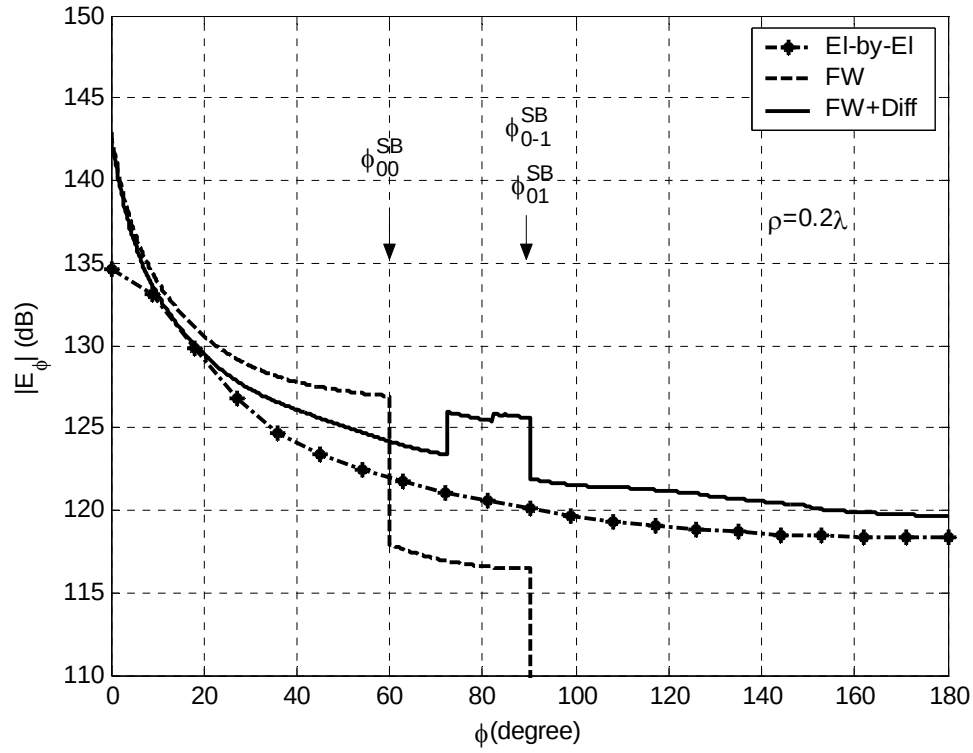

Figure 2.14. The amplitude of ϕ component of the electric field for the near-field scan at $\rho = 0.2\lambda$ from the edge of the array, beam angle 60 degrees and the periodicity dx = 0.9 cm, dy = 1.6 cm and f = 10 GHz.

In the Figure 2.15, $\rho = 0.5\lambda$ case is demonstrated. For this case $\rho > 0.2\lambda$ and the asymptotic solution is in a good agreement with the reference solution.

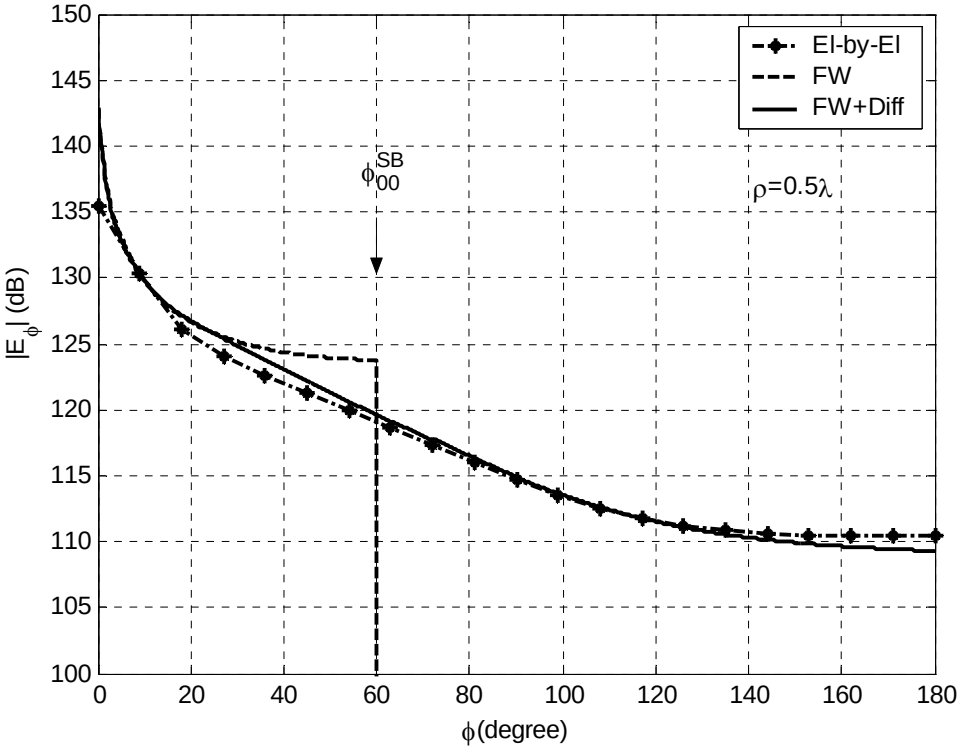

Figure 2.15. The amplitude of ϕ component of the electric field for the near-field scan at ρ = 0.5λ from the edge of the array, beam angle 60 degrees and the periodicity dx = 0.9 cm, dy = 1.6 cm and f = 10 GHz.

In the Figure 2.16, ρ = 1λ case is demonstrated. For this case, again ρ > 0.2λ and the asymptotic solution is in a good agreement with the reference solution.

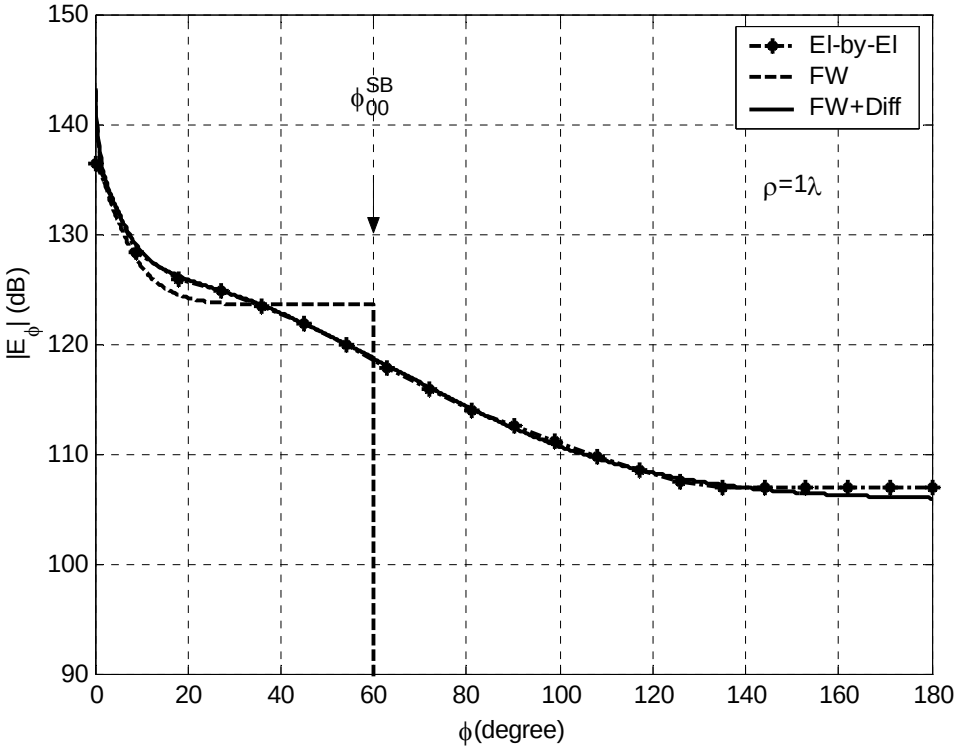

Figure 2.16. The amplitude of ϕ component of the electric field for the near-field scan at ρ = 1λ from the edge of the array, beam angle 60 degrees and the periodicity dx = 0.9 cm, dy = 1.6 cm and f = 10 GHz.

In the Figures 2.17 – 2.21, the near field scan for dx = 0.9 cm, dy = 1.6 cm, f = 10 GHz, ρ = 2λ, for the beam angle variation is examined. The results for 5, 45, 90 and 135 degrees are in a good agreement; however, when the angle approaches to 180 degrees the asymptotic solution and reference solution are not in a good agreement.

In the Figure 2.17, the plot for 5 degrees is given. FW shadow boundary appears at 5 degrees. The reference solution and asymptotic solution is in a good agreement.

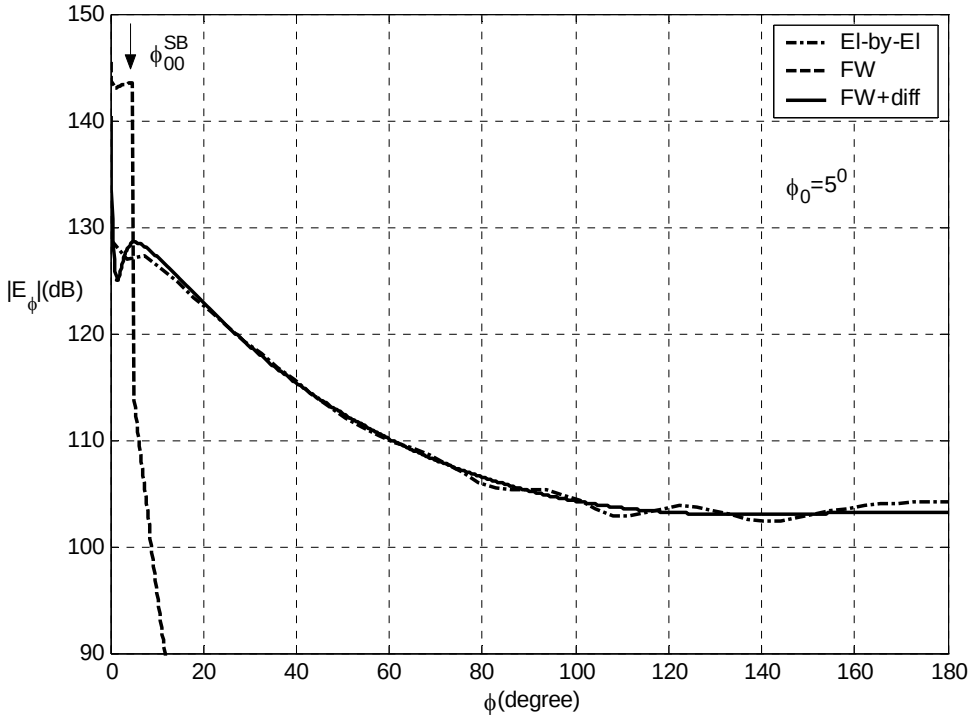

Figure 2.17. The amplitude of ϕ component of the electric field for the near-field scan at $\rho = 2\lambda$ from the edge of the array, beam angle 5 degrees and the periodicity dx = 0.9 cm, dy = 1.6 cm and f = 10 GHz.

In the Figure 2.18, the plot for 45 degrees is given. FW shadow boundary appears at 45 degrees. The reference solution and asymptotic solution is in a good agreement.

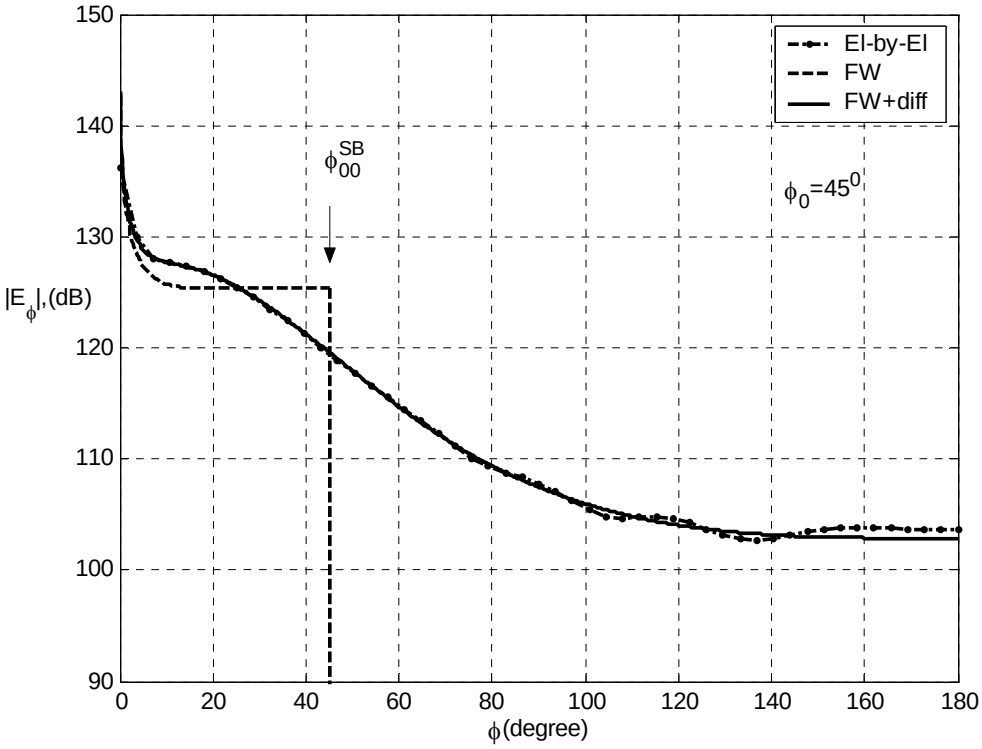

Figure 2.18. The amplitude of ϕ component of the electric field for the near-field scan at $\rho = 2\lambda$ from the edge of the array, beam angle 45 degrees and the periodicity dx = 0.9 cm, dy = 1.6 cm and f = 10 GHz.

In the Figure 2.19, the plot for 90 degrees is given. FW shadow boundary appears at 90 degrees. The reference solution and asymptotic solution is in a good agreement.

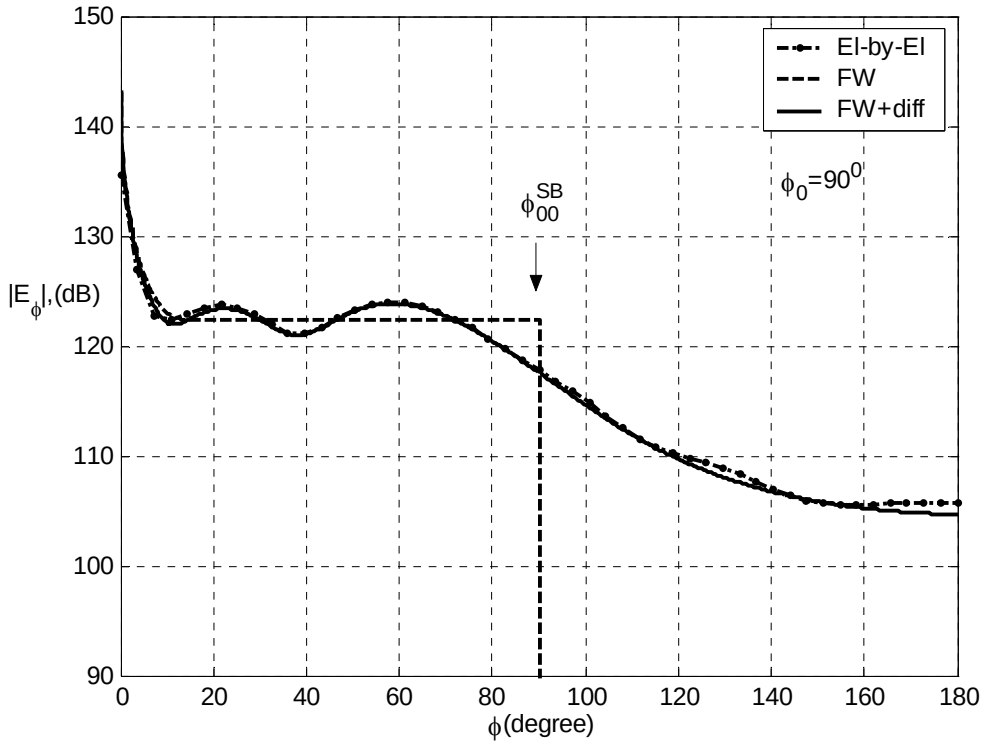

Figure 2.19. The amplitude of ϕ component of the electric field for the near-field scan at $\rho = 2\lambda$ from the edge of the array, beam angle 90 degrees and the periodicity dx = 0.9 cm, dy = 1.6 cm and f = 10 GHz.

In the Figure 2.20, the plot for 135 degrees is given. FW shadow boundary appears at 135 degrees. The reference solution and asymptotic solution is in a good agreement.

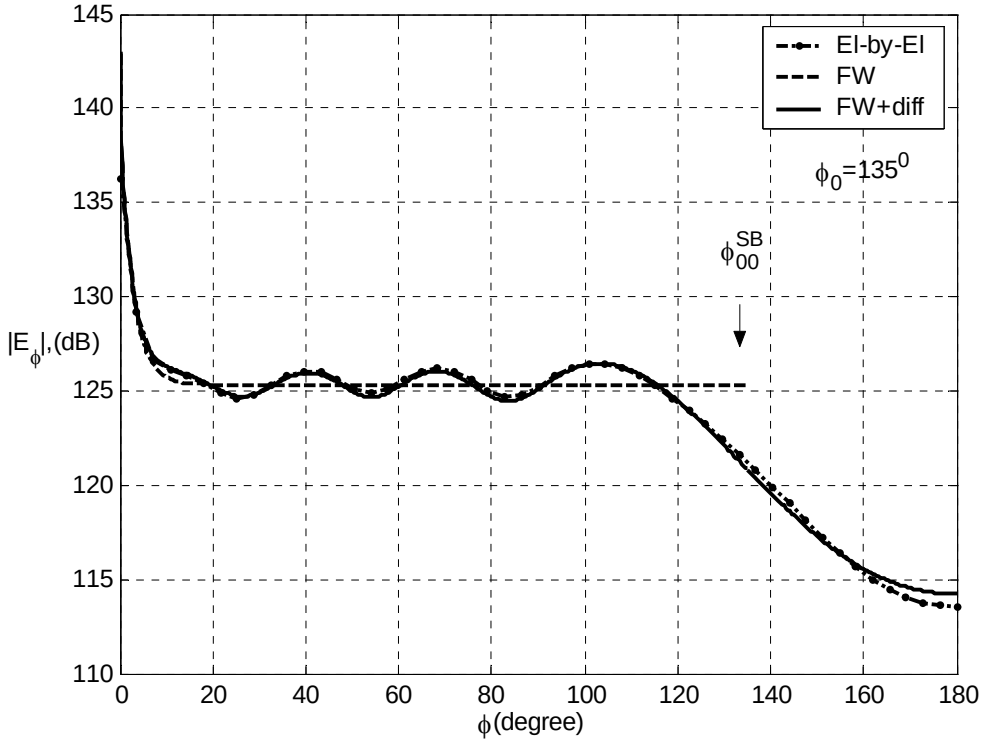

Figure 2.20. The amplitude of ϕ component of the electric field for the near-field scan at $\rho = 2\lambda$ from the edge of the array, beam angle 135 degrees and the periodicity dx = 0.9 cm, dy = 1.6 cm and f = 10 GHz.

In the Figure 2.21, the plot for 175 degrees is given. FW shadow boundary appears at 175 degrees. The reference solution and asymptotic solution is not in a good agreement. Thus, it can be concluded that the asymptotic solution does not predict scattering fields correctly when the incident field comes from grazing.

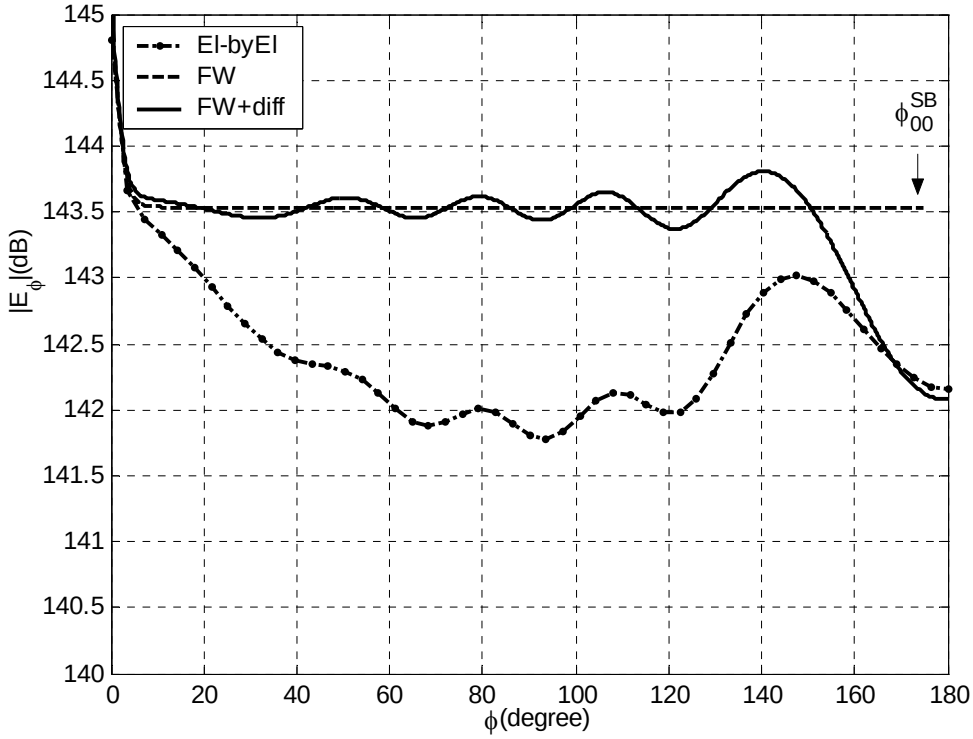

Figure 2.21. The amplitude of ϕ component of the electric field for the near-field scan at $\rho = 2\lambda$ from the edge of the array, beam angle 175 degrees and the periodicity dx = 0.9 cm, dy = 1.6 cm and f = 10 GHz.

2.8. A Far-Field Interpretation for a Strip Array of Dipoles in Free Space

In classical antenna array theory, the far field of an array of same elements can be found by using the pattern multiplication rule. According to the pattern multiplication, the total far-field of an array is the product of the array factor and the field of a single element at the origin of the defined coordinate system for the array.

Consider a strip array of dipoles in free space, infinite in the y-direction but finite in the x-direction. The interelement spacings are d_x and d_y and the length of the finite dimension of the array is L. The array can be considered as an array of columns as

shown in Figure 2.23; i.e., the array can be considered as an array of arrays. The observation point is taken on the xz-plane.

The total far-field potential expression for such an array can be written as

$$A_y = (Array\ Factor) \times (Element\ Factor) \tag{2.67}$$

The array factor of Floquet excited array for the coordinate system in Figure 2.23 and the observation point on xz-plane can be expressed as

$$AF = \sum_{n=0}^{N-1} a_n e^{jk_\rho \hat{\rho}.\vec{r}'} \tag{2.68}$$

where the excitation a_n can be expressed as

$$a_n = I(n)e^{-j\gamma_x n d_x} = I_0 e^{-j\gamma_x n d_x}; n = 0,1,...,N-1 \tag{2.69}$$

Also, a relation between spectral vectors can be written as

$$k_\rho = \sqrt{k_x^2 + k_z^2} = \sqrt{k^2 - k_y^2} \tag{2.70}$$

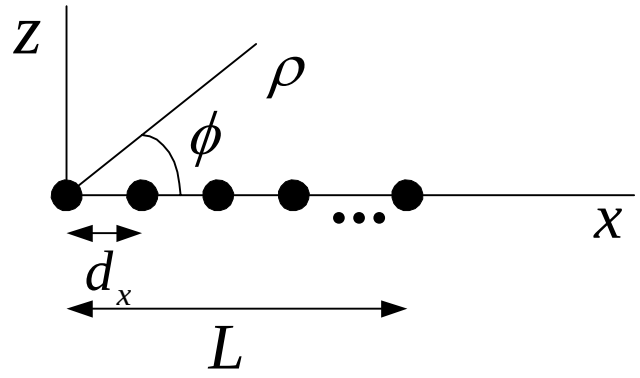

Figure 2.22. Side view of a strip array of dipoles. The number of dipole elements on the x axis is N, and for n = 0, 1, 2,…N-1 indexing, L = (N-1)d_x.

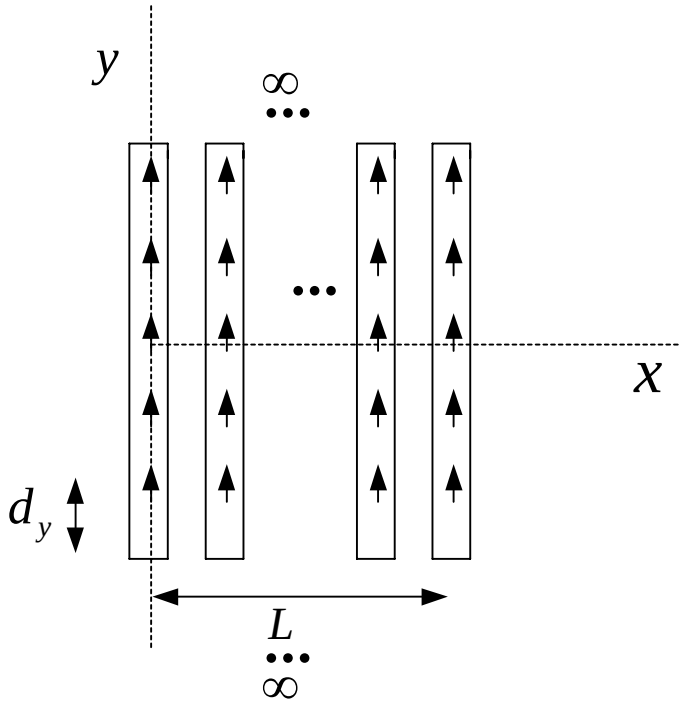

Figure 2.23. Top view of the strip array. The array is infinite on y-dimension but finite in x-dimension.

and coordinate variables and unit vectors are defined as

$$\rho = \sqrt{x^2 + z^2}$$
$$\hat{\rho} = \frac{x\hat{x} + z\hat{z}}{\sqrt{x^2 + z^2}} = \frac{x\hat{x} + z\hat{z}}{\rho} : unit\ vector \tag{2.71}$$

The source point is written as

$$\bar{r}' = nd_x\hat{x} \tag{2.72}$$

The array factor expression can be expressed as

$$AF = \sum_{n=0}^{N-1} I_0 e^{j(k_\rho \cos(\phi)-\gamma_x)nd_x} = \frac{1-e^{jN(k_\rho \cos(\phi)-\gamma_x)d_x}}{1-e^{j(k_\rho \cos(\phi)-\gamma_x)d_x}} : \ if \ I_0 = 1 \tag{2.73}$$

The element factor (EF) can be expressed as

$$EF = \sum_{m=-\infty}^{\infty} \int_{x'}\int_{y'}\int_{z'} \delta(x')\delta(y'-md_y)\delta(z')e^{-j\gamma_y md_y} \frac{e^{-jkR}}{4\pi R} dx'dy'dz' \tag{2.74}$$

For Green's function, two dimensional spectral form can be used as

$$\frac{e^{-jkR}}{4\pi R} = \frac{1}{8\pi j} \int_{-\infty}^{\infty} H_0^{(2)}(k_\rho \rho) e^{-jk_y(y-y')} dk_y \tag{2.75}$$

where

$$R = \sqrt{x^2 + z^2 + (y-y')^2} = \sqrt{\rho^2 + (y-y')^2} \tag{2.76}$$

Inserting the spectral form of the Green's function and evaluating the spatial integrals, EF expression can be written as

$$EF = \frac{1}{8\pi j} \sum_{m=-\infty}^{\infty} e^{-j\gamma_y md_y} \int_{-\infty}^{\infty} H_0^{(2)}(k_\rho \rho) e^{-jk_y(y-md_y)} dk_y \tag{2.77}$$

After some rearranging EF expression is

$$EF = \frac{1}{8\pi j} \sum_{m=-\infty}^{\infty} \int_{-\infty}^{\infty} H_0^{(2)}(k_\rho \rho) e^{-jk_y y} e^{j(k_y-\gamma_y)md_y} dk_y \tag{2.78}$$

The total far field expression for the magnetic vector potential is the product of the array factor and the element factor and can be expressed as

$$A_y^{far-field} = (AF)\times(EF)$$
$$= \frac{1}{8\pi j}\int_{-\infty}^{\infty}\sum_{m=-\infty}^{\infty} H_0^{(2)}(k_\rho\rho)e^{-jk_y y}\frac{1-e^{jN(k_\rho\cos(\phi)-\gamma_x)d_x}}{1-e^{j(k_\rho\cos(\phi)-\gamma_x)d_x}}e^{j(k_y-\gamma_y)md_y}dk_y \quad (2.79)$$

Then, by using bilateral Poisson summation formula, the potential expression can be written as

$$A_y^{far-field} = \frac{1}{4jd_y}\sum_q H_0^{(2)}(k_{\rho q}\rho)e^{-jk_{yq}y}\frac{1-e^{jN(k_{\rho q}\cos(\phi)-\gamma_x)d_x}}{1-e^{j(k_{\rho q}\cos(\phi)-\gamma_x)d_x}} \quad (2.80)$$

where

$$k_{\rho q} = \sqrt{k^2 - k_{yq}^2} \quad (2.81)$$

After introducing the approximation of the Hankel function for large argument as

$$H_0^{(2)}(x) = \sqrt{\frac{2j}{\pi x}}e^{-jx};\quad for\quad x \gg 1 \quad (2.82)$$

The far field expression for the magnetic vector potential can be obtained as

$$A_y^{far-field}(\rho,\phi,y) = \frac{1}{4\pi jd_y}\sum_q \sqrt{\frac{2\pi j}{k_{\rho q}\rho}}e^{-jk_{\rho q}\rho}e^{-jk_{yq}y}\frac{1-e^{jN(k_{\rho q}\cos(\phi)-\gamma_x)d_x}}{1-e^{j(k_{\rho q}\cos(\phi)-\gamma_x)d_x}} \quad (2.83)$$

The electric field expression can be evaluated with multiplying magnetic vector potential by a polarization vector which is defined as

$$\bar{G}(k_{\rho q}\cos\phi, k_{yq}, k_{\rho q}\sin\phi) = \frac{Z}{k}[\hat{x}(k_{\rho q}\cos\phi k_{yq}) + \hat{y}(k_{yq}^2 - k^2) + \hat{z}(k_{\rho q}\sin\phi k_{yq})] \quad (2.84)$$

where Z is the free space impedance.

Then, the total far field for this strip array of dipoles in free space can be written as

$$\bar{E}^{farfield}(\rho,\phi,y)=\frac{\sqrt{2\pi j}}{4\pi d_y}\sum_q \frac{e^{-jk_{\rho q}\rho}}{k_{\rho q}\rho}e^{-jk_{yq}y} \times \bar{G}(k_{\rho q}\cos\phi,k_{yq},k_{\rho q}\sin\phi)\frac{1-e^{jN(k_{\rho q}\cos(\phi)-\gamma_x)d_x}}{1-e^{j(k_{\rho q}\cos(\phi)-\gamma_x)d_x}} \tag{2.85}$$

On the other hand, the fields for a strip array of dipoles in free space can be evaluated by obtaining a spectral integral and using the saddle point techniques for the evaluation of the integral.

The magnetic vector potential for the strip array which is shown in Figure 2.23 and Figure 2.24 can be expressed as

$$\bar{A}(\bar{r})=\sum_{n=0}^{N-1}\sum_{m=-\infty}^{\infty}\int_{x'}\int_{y'}\int_{z'}dx'dy'dz'\ \bar{J}(\bar{r}')\ g(\bar{r},\bar{r}') \tag{2.86}$$

The only difference between the semi-infinite array and the strip array is that the spatial "n summation" in semi-infinite array is taken over zero to infinity, but for strip array it is taken over zero to N-1, where N is the number of dipole elements in x-direction. Therefore, when the geometric series are evaluated as described in Section 2.6, one can obtain the result for the "n summation" for a strip array as

$$\sum_{n=0}^{N-1}e^{j(k_\rho\cos(\phi)-\gamma_x)nd_x}=\frac{1-e^{jN(k_\rho\cos(\phi)-\gamma_x)d_x}}{1-e^{j(k_\rho\cos(\phi)-\gamma_x)d_x}} \tag{2.87}$$

Following the same steps as in Section 2.6, the saddle point evaluation of the spectral electric field integral in a non-uniform manner (Pauli-Clemmow regularization [31]) results in the following diffracted field expression for a strip array.

$$A_q^d(\rho,\phi,y)=\frac{e^{-jk_{\rho q}\rho}e^{-jk_{yq}y}}{2d_y\sqrt{2\pi j\rho k_{\rho q}}}\frac{1-e^{jN(k_{\rho q}\cos(\phi)-\gamma_x)d_x}}{1-e^{j(k_{\rho q}\cos(\phi)-\gamma_x)d_x}}F(\delta_{pq}^2) \tag{2.88}$$

where F is the Fresnel transition function and its argument is defined in Section 2.6. The total field can be expressed as

$$total\ field = \sum_{q} A_q^d \tag{2.89}$$

Far from the edge of the array the argument of the Fresnel transition function is much greater than one; then, one can obtain an expression for the diffracted field considering (2.88) as

$$\begin{aligned} A_q^d(\rho,\phi,y) &= \sum_{q} \frac{e^{-jk_{\rho q}\rho} e^{-jk_{yq}y}}{2d_y\sqrt{2\pi j\rho k_{\rho q}}} \frac{1-e^{jN(k_{\rho q}\cos(\phi)-\gamma_x)d_x}}{1-e^{j(k_{\rho q}\cos(\phi)-\gamma_x)d_x}} \\ for\ \delta_{pq}^2 &\gg 1\ ,\ F(\delta_{pq}^2)\to 1 \\ \rho &\geq \frac{2L^2}{\lambda},\quad L=(N-1)d_x \end{aligned} \tag{2.90}$$

The expression in Equation (2.83) which is derived with classical array theory is the same as the Equation (2.90) which is obtained by asymptotics performed through the Pauli-Clemmow regularization. The same equivalence exists for the electric field expressions.

From the expression (2.90), the far-field pattern of a strip array can be interpreted by the superposition of the non-uniform diffracted rays from the two parallel edges. The far-field pattern is provided by the combination of the diffracted fields from the two edges.

In Figure 2.24, the far field pattern for an array for dx = 1.4λ, dy = 0.5λ, N = 30, f = 10 GHz, the beam angle 60^0 is plotted at the xz-plane. For this case, the far field pattern is provided by three propagating modes with shadow boundaries 60, 102.37 and 158.21 degrees.

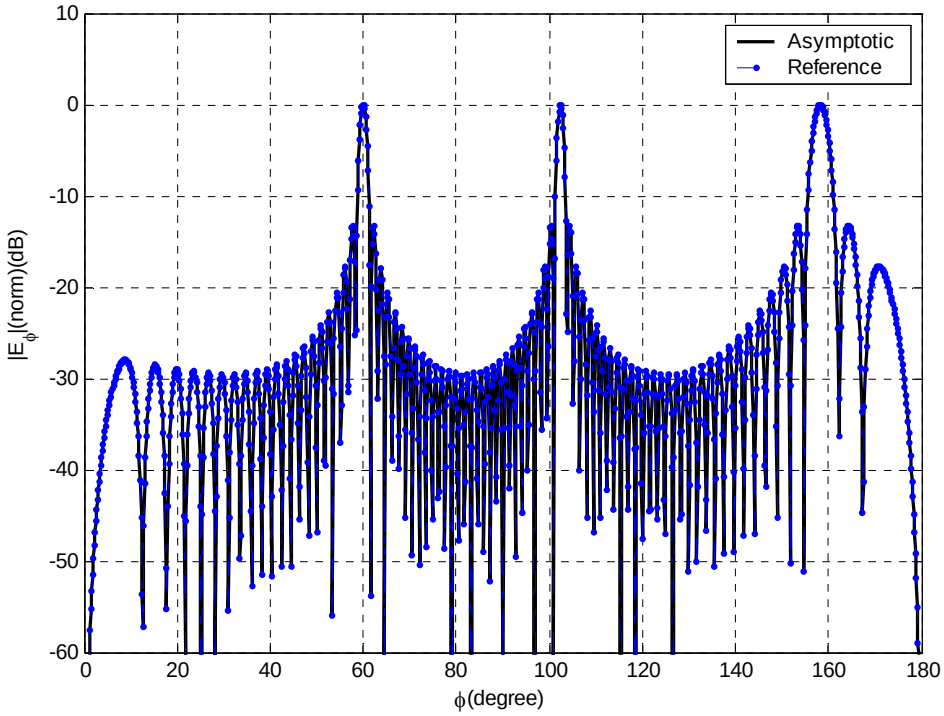

Figure 2.24. The far field pattern of the array : N = 30, dx = 1.4λ, dy = 0.5λ, f = 10 GHz, the beam angle is 60^0, and the observation is performed on xz-plane. The pattern is normalized to the maximum value of the pattern.

In the Figures 2.25-2.29, for an array with N = 30, dx = 0.9 cm, dy = 1.6 cm, f = 10 GHz, the far-field patterns of the array are plotted for changing the beam angle. For this case, there is only one propagating mode corresponding to the fundamental mode of the array.

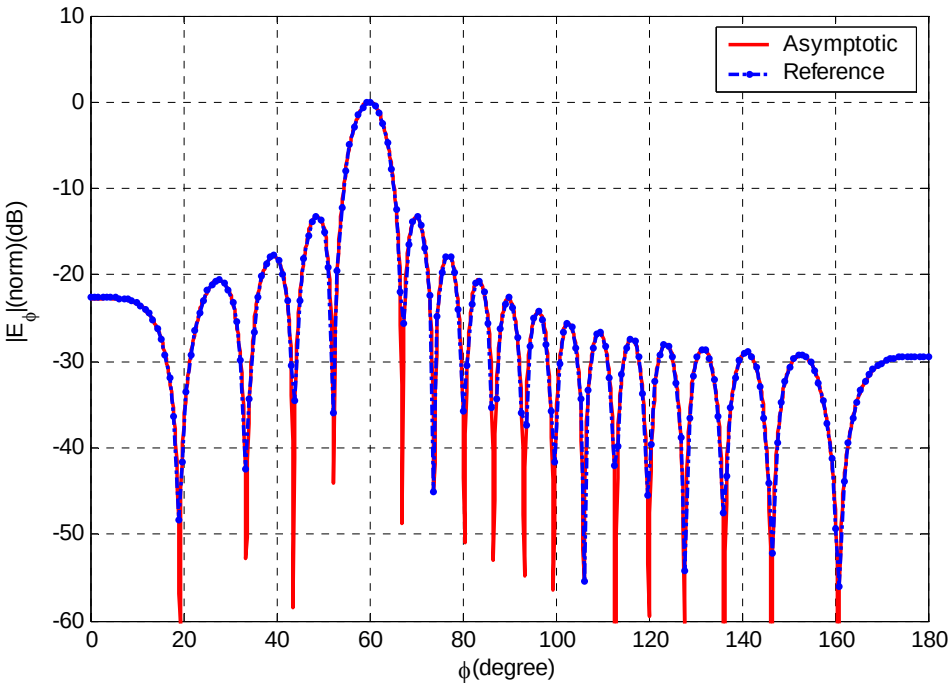

Figure 2.25. The far field pattern of the array : N = 30, dx = 0.9 cm, dy = 1.6 cm, f = 10 GHz, the beam angle is 60^0, and the observation is performed on xz-plane. The pattern is normalized to the maximum value of the pattern.

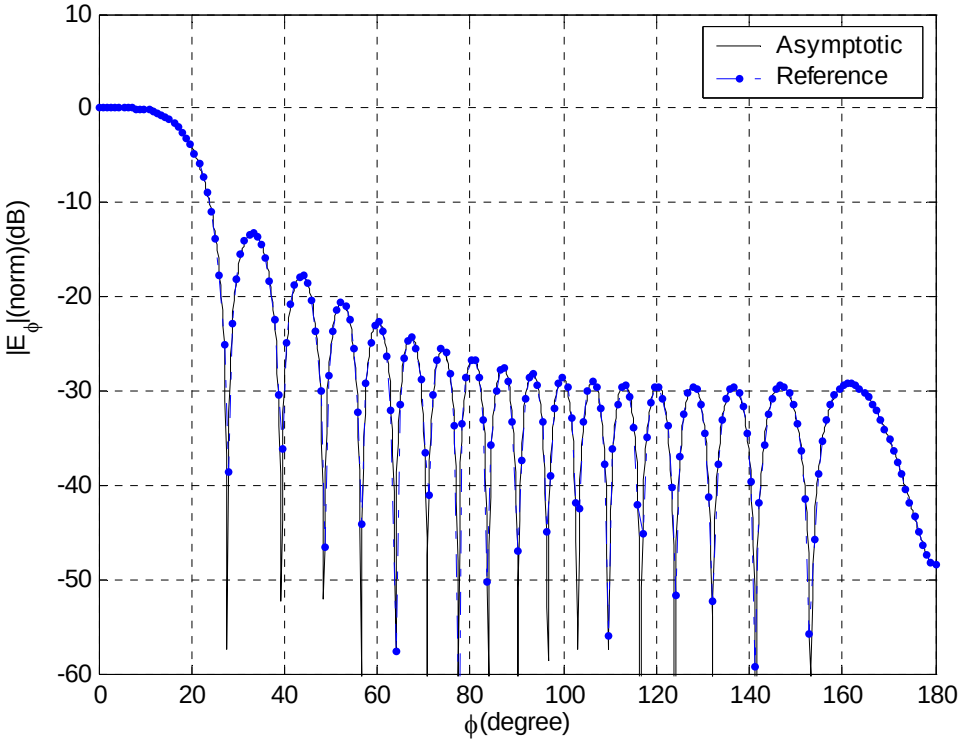

Figure 2.26. The far field pattern of the array : N = 30, dx = 0.9 cm, dy = 1.6 cm, f = 10 GHz, the beam angle is 5^0, and the observation is performed on xz-plane. The pattern is normalized to the maximum value of the pattern.

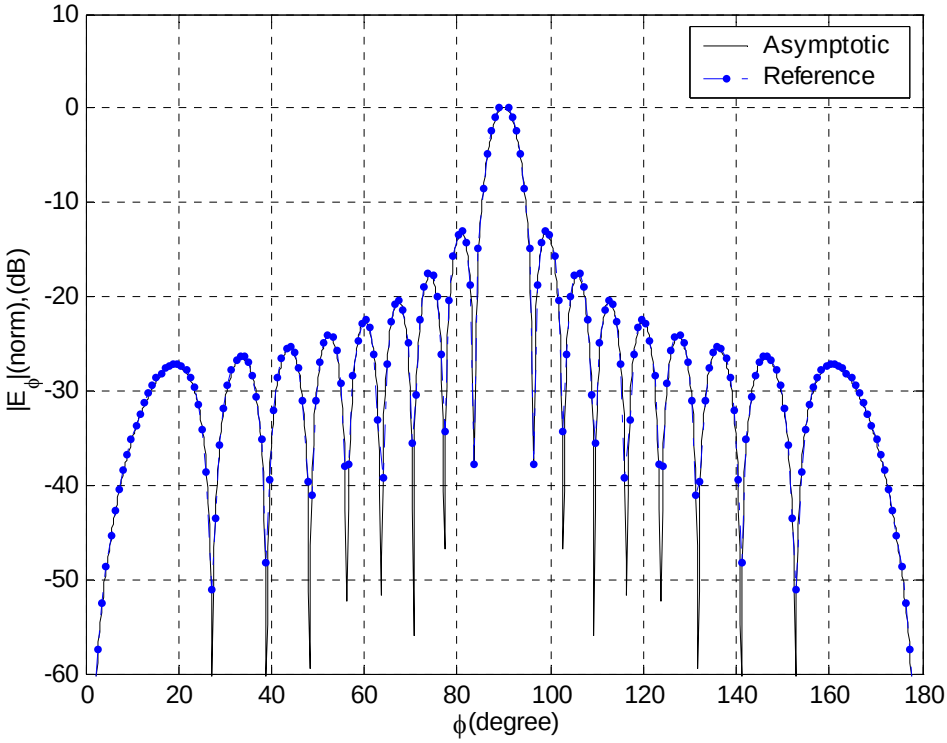

Figure 2.27. The far field pattern of the array : N = 30, dx = 0.9 cm, dy = 1.6 cm, f = 10 GHz, the beam angle is 90^0, and the observation is performed on xz-plane. The pattern is normalized to the maximum value of the pattern.

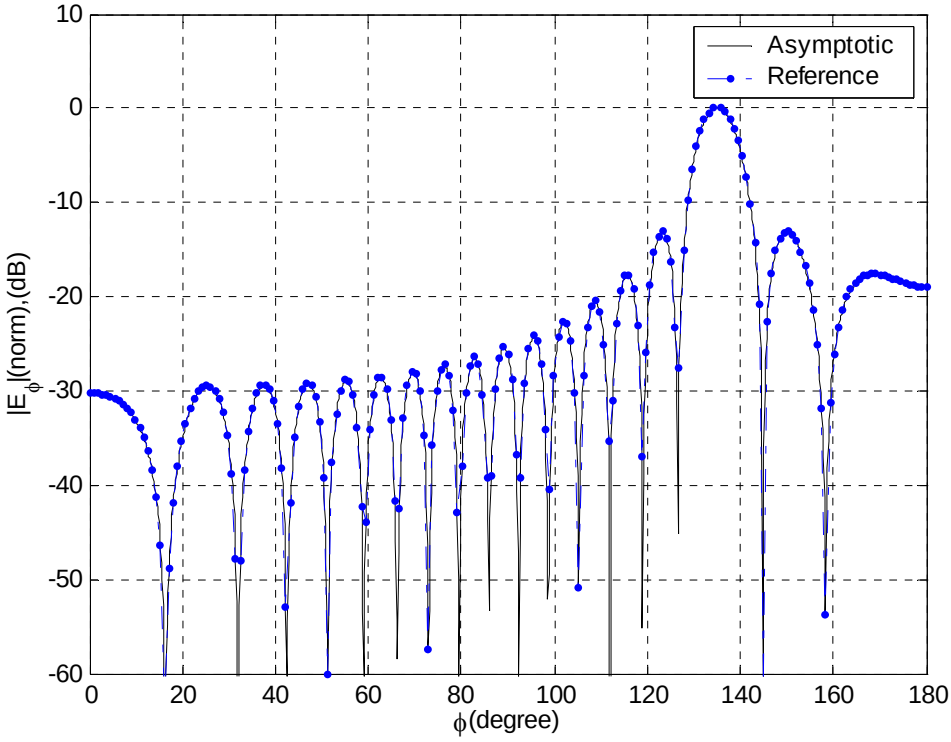

Figure 2.28. The far field pattern of the array : N = 30, dx = 0.9 cm, dy = 1.6 cm, f = 10 GHz, the beam angle is 135^0, and the observation is performed on xz-plane. The pattern is normalized to the maximum value of the pattern.

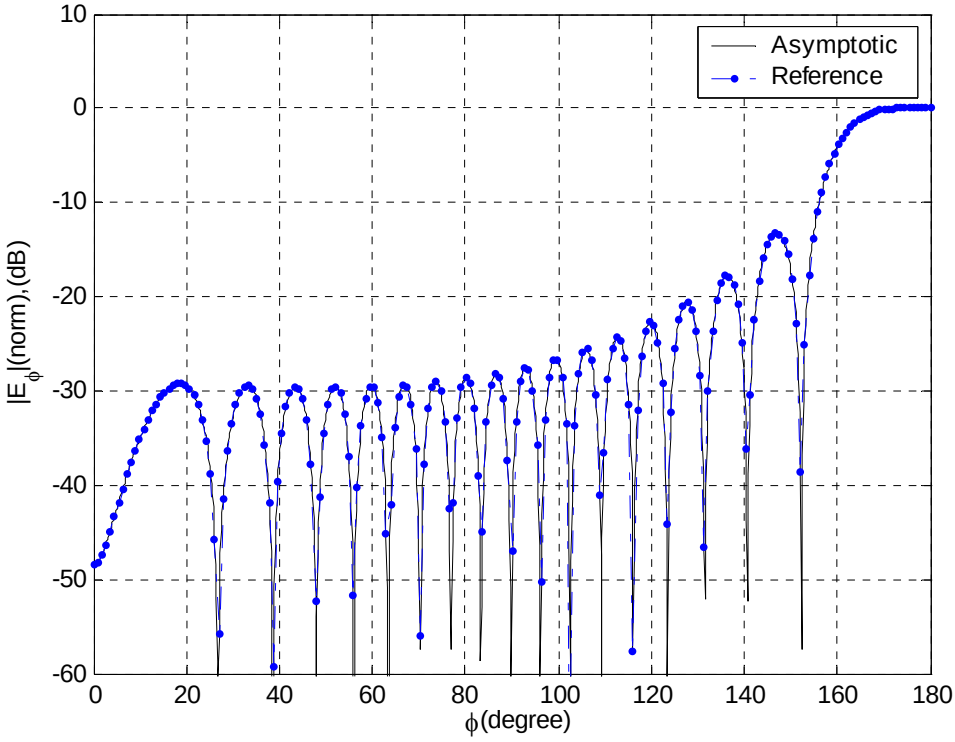

Figure 2.29. The far field pattern of the array : N = 30, dx = 0.9 cm, dy = 1.6 cm, f = 10 GHz, the beam angle is 175^0, and the observation is performed on xz-plane. The pattern is normalized to the maximum value of the pattern.

The lobe angles for the array can be found by evaluating the maxima of the array pattern. Considering the array factor of the array, the main lobe and the grating lobe angles can be calculated as

$$\begin{aligned} &\phi = \cos^{-1}\left(\cos\phi_0 + \frac{m\lambda}{dx}\right) \\ &\phi_0 : \textit{Beam angle} \\ &\left.\begin{aligned} &m = 0 : \textit{main lobe} \\ &m = \pm 1, \pm 2, \pm 3, \ldots : \textit{Grating lobes} \end{aligned}\right\} \phi \in (0, \pi) : \textit{visible region} \end{aligned} \tag{2.91}$$

For example, for the array with the parameters N = 30, dx = 0.9 cm, dy = 1.6 cm, f = 10 GHz, beam angle 45^0, the main lobe is located at 45^0. There is not any grating lobe for this case, since the solution of the (2.91) does not give any real solution other than the main lobe. However, for the array with parameters dx = 1.4λ, dy = 0.5λ, f = 10 GHz, and the scan angle 60^0 the solution of (2.91) gives three real solutions in visible region, which are 60, 102,158 degrees. 102 and 158 degrees are grating lobes of the array.

On the other hand, considering the Equation (2.90) for the Floquet excited array, the array pattern has maxima at

$$\begin{aligned} &Nd_x(k_{\rho q}\cos(\phi)-\gamma_x)=2\pi p \\ &\text{maxima; } \phi=\alpha_{pq},\ with\ \alpha_{pq}: real \end{aligned} \tag{2.92}$$

Therefore, the pattern maxima points correspond to the shadow boundaries of the Floquet waves; i.e. propagating Floquet waves whose diffracted components are forming the array pattern in the far-field region.

2.9. Asymptotic Field Expressions for Semi-Infinite Array of Dipoles on Infinite Grounded Dielectric Slab

A uniform high-frequency solution can be constructed for the electromagnetic fields for a semi-infinite array of dipoles placed on an infinite grounded dielectric slab by using the same techniques as discussed in the previous sections.

The high frequency solution is constructed such that it includes truncated Floquet waves and their corresponding diffracted waves due to the edge of the array and Floquet edge excited surface/leaky waves. The diffracted waves contain discontinuities which compensate for the disappearance of surface/leaky waves and truncated Floquet waves at their pertinent shadow boundaries.

The geometry of the structure is illustrated in Figure 2.30. The thickness of the dielectric slab is d, and the relative permittivity is denoted by ε_r. A semi-infinite array of phased elementary dipoles is placed on the interface of an infinite grounded dielectric slab. All the definitions are the same as the semi-infinite array of dipoles in free space whose solutions are given before. The coordinate system for the solution of this problem is again a cylindrical (ρ, γ, y) coordinate system.

Due to a single $\hat{p}$ oriented dipole placed at the origin of the reference system, the electric field at an observation point $P \equiv (x, y, z)$ can be expressed by plane wave spectral representation ([10], [20-21]) as

$$\bar{\bar{E}}_0(P) = \frac{1}{(2\pi)^2} \int_{-\infty}^{\infty} \int_{-\infty}^{\infty} \bar{\bar{G}}_E(\bar{k}).\hat{p} e^{-j\bar{k}.\bar{r}} dk_x dk_y \tag{2.93}$$

where the vectors and spectral variables are defined as

$$\begin{aligned} &\bar{r} = \hat{x}x + \hat{y}y + \hat{z}z \\ &\bar{k} = \hat{x}k_x + \hat{y}k_y + \hat{z}k_z \\ &k_\rho = \sqrt{k_x^2 + k_y^2} \\ &k_z = \sqrt{k^2 - k_\rho^2}, \ \ \mathrm{Im}\{k_z\} < 0 \ \textit{on the top Riemann sheet} \end{aligned} \tag{2.94}$$

The spectral dyadic Green's function of a single dipole may be expressed as

$$\bar{\bar{G}}_E(\bar{k}) = G_E^{TM}(k_z)\bar{\bar{X}}_E^{TM}(k_x, k_y) + G_E^{TE}(k_z)\bar{\bar{X}}_E^{TE}(k_x, k_y) \tag{2.95}$$

where

$$G_E^{TM}(k_z) = j\frac{Z_0}{k}\frac{k_{z0}k_{z1}\sin(k_{z1}d)}{\varepsilon_r k_{z0}\cos(k_{z1}d) + jk_{z1}\sin(k_{z1}d)} \tag{2.96}$$

$$G_E^{TE}(k_z) = jZ_0 k\frac{\sin(k_{z1}d)}{k_{z1}\cos(k_{z1}d) + jk_{z0}\sin(k_{z1}d)} \tag{2.97}$$

$$\overline{\overline{X}}_E^{TM}(k_x,k_y)=\hat{x}\hat{x}\left(\frac{-k_x^2}{k_x^2+k_y^2}\right)+(\hat{x}\hat{y}+\hat{y}\hat{x})\left(\frac{-k_xk_y}{k_x^2+k_y^2}\right)+\hat{y}\hat{y}\left(\frac{-k_y^2}{k_x^2+k_y^2}\right)+\hat{z}\hat{x}\left(\frac{k_x}{k_{z0}}\right)+\hat{z}\hat{y}\left(\frac{k_y}{k_{z0}}\right) \tag{2.98}$$

$$\overline{\overline{X}}_E^{TE}(k_x,k_y)=\hat{x}\hat{x}\left(\frac{-k_y^2}{k_x^2+k_y^2}\right)+(\hat{x}\hat{y}+\hat{y}\hat{x})\left(\frac{k_xk_y}{k_x^2+k_y^2}\right)+\hat{y}\hat{y}\left(\frac{-k_x^2}{k_x^2+k_y^2}\right) \tag{2.99}$$

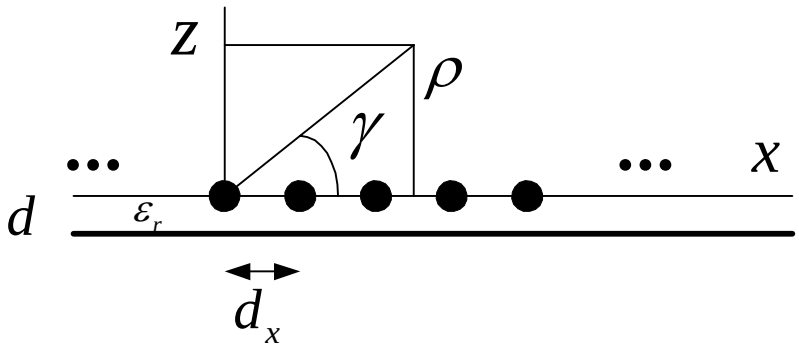

Figure 2.30. A semi-infinite array of phased elementary dipoles is placed on the interface of an infinite grounded dielectric slab.

Between the wavenumbers the following relations can be written.

$$\begin{aligned} k&=\frac{2\pi}{\lambda}=\omega\sqrt{\mu_0\varepsilon_0}\\ k_1&=\omega\sqrt{\mu_0\varepsilon_r\varepsilon_0}\\ k_z^2&=k_{z0}^2=k^2-k_x^2-k_y^2\\ k_{z1}^2&=k_1^2-k_x^2-k_y^2 \end{aligned} \tag{2.100}$$

When H- Field is considered, one can write

$$\bar{H}_0(P) = \frac{1}{(2\pi)^2} \int_{-\infty}^{\infty} \int_{-\infty}^{\infty} \overline{\overline{G}}_H(\bar{k}).\hat{p}e^{-j\bar{k}.\bar{r}} dk_x dk_y \tag{2.101}$$

where

$$\overline{\overline{G}}_H(\bar{k}) = G_H^{TM}(k_z)\overline{\overline{X}}_H^{TM}(k_x, k_y) + G_H^{TE}(k_z)\overline{\overline{X}}_H^{TE}(k_x, k_y) \tag{2.102}$$

with

$$G_H^{TM}(k_z) = -j\frac{k_{z1}\sin(k_{z1}d)}{\varepsilon_r k_{z0}\cos(k_{z1}d) + jk_{z1}\sin(k_{z1}d)} \tag{2.103}$$

$$G_H^{TE}(k_z) = -jk\frac{\sin(k_{z1}d)}{k_{z1}\cos(k_{z1}d) + jk_{z0}\sin(k_{z1}d)} \tag{2.104}$$

$$\begin{aligned}\overline{\overline{X}}_H^{TM}(k_x, k_y) = {} & \hat{x}\hat{x}\left(\frac{-k_x k_y}{k_x^2 + k_y^2}\right) + \hat{x}\hat{y}\left(\frac{-k_y^2}{k_x^2 + k_y^2}\right) + \hat{y}\hat{y}\left(\frac{k_x k_y}{k_x^2 + k_y^2}\right) \\ & + \hat{y}\hat{x}\left(\frac{k_x^2}{k_x^2 + k_y^2}\right)\end{aligned} \tag{2.105}$$

$$\begin{aligned}\overline{\overline{X}}_H^{TM}(k_x, k_y) = {} & \hat{x}\hat{x}\left(\frac{k_x k_y}{k_x^2 + k_y^2}\right) + \hat{x}\hat{y}\left(\frac{-k_x^2}{k_x^2 + k_y^2}\right) + \hat{y}\hat{x}\left(\frac{k_y^2}{k_x^2 + k_y^2}\right) + \hat{y}\hat{y}\left(\frac{-k_x k_y}{k_x^2 + k_y^2}\right) \\ & + \hat{z}\hat{x}\left(\frac{-k_y}{k_{z0}}\right) + \hat{z}\hat{y}\left(\frac{k_x}{k_{z0}}\right)\end{aligned} \tag{2.106}$$

In order to obtain array Green's function, we consider the spatial summation over the individual element Green's functions, linearly phased with reference at the origin.

$$\bar{E}(P) = \sum_{n=0}^{\infty} \sum_{m=-\infty}^{\infty} \bar{E}_0(x - ndx, y - mdy, z)e^{-j\gamma_x n d_x} e^{-j\gamma_y m d_y} \tag{2.107}$$

By using the spectral form this equation can be written as

$$\bar{E}(P)=\frac{1}{(2\pi)^2}\int_{-\infty}^{\infty}\int_{-\infty}^{\infty}\overline{\overline{G}}_E(\bar{k}).\hat{p}e^{-j\bar{k}.\bar{r}}\sum_{n=0}^{\infty}e^{j(k_x-\gamma_x)nd_x}\sum_{m=-\infty}^{\infty}e^{j(k_y-\gamma_y)md_y}dk_xdk_y \tag{2.108}$$

The spatial "n" sum can be evaluated in closed from by using geometric series. The spatial "m" sum can be converted to a impulse train by using Poisson sum formula as explained before.

$$B(k_x)=\sum_{n=0}^{\infty}e^{j(k_x-\gamma_x)nd_x}=\frac{1}{1-e^{j(k_x-\gamma_x)d_x}} \tag{2.109}$$

$$\begin{aligned}&\sum_{m=-\infty}^{\infty}e^{j(k_y-\gamma_y)md_y}=\frac{2\pi}{d_y}\sum_{q=-\infty}^{\infty}\delta(k_y-k_{yq})\\&k_{yq}=\gamma_y+\frac{2\pi q}{d_y}\ ;\ q=0,\pm1,\pm2,...(FW\ numbers\ along\ y\ domain)\end{aligned} \tag{2.110}$$

Then the electric field expression can be written as

$$\begin{aligned}&\bar{E}(P)=\frac{1}{2\pi d_y}\sum_{q}\int_{-\infty}^{\infty}B(k_x)\overline{\overline{G}}_E(\bar{k}_q).\hat{p}e^{-j\bar{k}_q.\bar{r}}dk_x\\&\bar{k}_q=\hat{x}k_x+\hat{y}k_{yq}+\hat{z}\sqrt{k^2-k_x^2-k_{yq}^2}\end{aligned} \tag{2.111}$$

The "q" sum of the above equation represents the FW expansion of the field along the infinite periodic y-domain.

In order to pass into an angular spectrum to perform the integration, one can introduce a change of variables as illustrated in Figure 2.31.

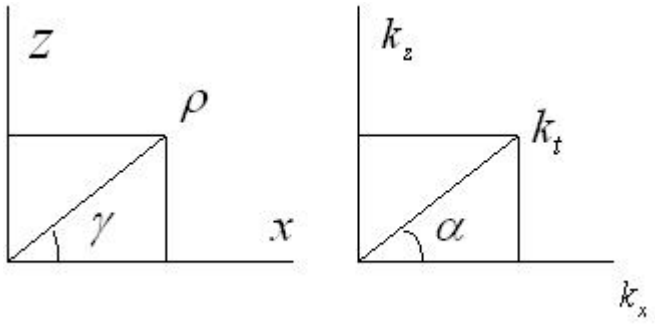

Figure 2.31. A coordinate transformation in order to obtain an angular variable integral to be solved with steepest descent methods.

Then one can write

$$k_{tq} = \sqrt{k^2 - k_{yq}^2} \tag{2.112}$$

The poles of $B(k_x)$ are located on the real k_x axis at

$$k_{xp} = \gamma_x + \frac{2\pi p}{d_x};\ \ p = 0, \pm 1, ... \tag{2.113}$$

which defines Floquet wavenumbers along x-axis.

When k_{tq} is real, the integrand in (2.111) exhibits branch points at $k_x = k_{tq}$ and at $k_x = -k_{tq}$. The residue contributions of the integrand associated with those FW poles located on the proper Riemann sheet ($\mathrm{Im}\{k_{zq}\} < 0$) inside or outside the interval $(-k_{tq}, k_{tq})$ represent the propagating or evanescent Floquet waves respectively.

The spectral dyadic Green's function $\overline{\overline{G}}_E(\bar{k}_q)$ may exhibit real and complex poles k_{zi} corresponding to real and complex solutions of the dispersion equations as

$$\left.\begin{aligned}\frac{1}{G_E^{TM}(k_{zi})}=0\\ \frac{1}{G_E^{TE}(k_{zi})}=0\end{aligned}\right\} i=0,\pm1,\pm2,... \tag{2.114}$$

The residues of these poles correspond to the dielectric slab surface and leaky waves. Leaky wave poles correspond to solution of the dispersion equations with complex k_{zi}, and they are always located on the bottom Riemann sheet of the complex k_x plane.

In order to obtain a formal steepest descent type integral, one can apply change of variables as in Figure 2.31. Then one can write

$$\begin{aligned}&\left.\begin{aligned}x&=\rho_t\cos\gamma\\ z&=\rho_t\sin\gamma\end{aligned}\right\}\gamma\in(0,\pi)\\ &k_x=k_{tq}\cos\alpha\\ &k_z=k_{tq}\sin\alpha\end{aligned} \tag{2.115}$$

Then, the spectral integral can be expressed as

$$\begin{aligned}&\bar{E}(P)=\sum_q \exp\{-jk_{yq}y\}\int_{C_\alpha} B_q(\alpha)\bar{D}_q(\alpha)e^{-jk_{tq}\rho_t\cos(\alpha-\gamma)}d\alpha\\ &B(k_x)=B(k_{tq}\cos\alpha)=B_q(\alpha)\\ &\bar{D}_q(\alpha)=\frac{k_{tq}\sin\alpha}{2\pi d_y}\overline{\overline{G}}_q(\alpha).\hat{p}\\ &\overline{\overline{G}}_q(\alpha)=\overline{\overline{G}}(\bar{k}_\alpha)\\ &\bar{k}_\alpha=\hat{x}k_{tq}\cos\alpha+\hat{y}k_{yq}+\hat{z}k_{tq}\sin\alpha\end{aligned} \tag{2.116}$$

The integration path C_α corresponds to the real axis in the k_x plane.

The Floquet wave poles of the function $B_q(\alpha)$ occur at $\alpha_{pq}^{FW}=\cos^{-1}(k_{xp}/k_{tq})$, and the surface and leaky wave poles occur at $\alpha_{iq}^{SW/LW}=\sin^{-1}(k_{zi}/k_{tq})$.

The total asymptotic field can be expressed as

$$\bar{E}(P) = \sum_p \sum_q \bar{E}_{pq}^{FW} U(\gamma_{pq}^{FW} - \gamma) + \sum_i \sum_q \bar{E}_{iq}^{SW/LW} U(\gamma_{iq}^{SW/LW} - \gamma) + \sum_q \bar{E}_q^d \tag{2.117}$$

The steepest descent path integration gives

$$\bar{E}_q^d = \exp\{-jk_{yq}y\} \int_{SDP} B_q(\alpha)\bar{D}_q(\alpha) e^{-jk_{tq}\rho_t \cos(\alpha-\gamma)} d\alpha \tag{2.118}$$

When one considers the functions and variables as

$$\begin{aligned} \Omega &= k_{tq}\rho_t \\ f(\alpha) &= B_q(\alpha)\bar{D}_q(\alpha) \\ g(\alpha) &= -j\cos(\alpha-\gamma) \end{aligned} \tag{2.119}$$

Then, the formal steepest descent integral of the form

$$\int_{SDP} f(\alpha) e^{\Omega g(\alpha)} d\alpha \tag{2.120}$$

can be formed and solved.

By using the Van der Waerden method as explained in the previous chapters, the following expressions can be derived.

The residue contribution of the Floquet wave poles can be expressed as

$$\bar{E}_{pq}^{FW} = 2\pi j \sum_p \sum_q \frac{\bar{D}_q(\alpha_{pq}^{FW})}{jk_{tq}d_x \sin\alpha_{pq}^{FW}} e^{-j(k_{xp}x + k_{yq}y + k_{zpq}z)} U(\gamma_{pq}^{FW} - \gamma) \tag{2.121}$$

The shadow boundaries have the same expressions for the free space case.

From the first derivative of the phase function, the saddle point is $\alpha_s = \gamma$. Then, the saddle point contribution can be written as

$$I_s(\Omega) \approx e^{-jk_t\rho_t}\sqrt{\frac{\pi}{k_t\rho_t}}(B_q(\gamma)\bar{D}_q(\gamma)\sqrt{2j} + \sum_w \frac{\bar{D}_q(\alpha_{wq}^{GW})[1-F(\delta^2)]}{jk_{tq}d_x \sin(\alpha_{wq}^{GW})\sqrt{-2j}\sin(\frac{\gamma-\alpha_{wq}^{GW}}{2})}) \tag{2.122}$$

$$\delta^2 = 2k_{tq}\rho_t \sin^2(\frac{\gamma-\alpha_{wq}^{GW}}{2}) \tag{2.123}$$
$$\alpha_{wq}^{GW} : \alpha_{pq}^{FW} \text{ or } \alpha_{iq}^{SW/LW}$$

Then, the diffracted field can be expressed as

$$\bar{E}_q^d = \sum_q e^{-jk_{yq}y} I_s(\Omega) \tag{2.124}$$

CHAPTER 3

AN ANALYTICAL SOLUTION FOR EXCITATION COEFFICIENT OF SURFACE WAVES LAUNCHED FROM THE EDGE OF A SEMI-INFINITE ARRAY OF DIPOLES

The existence of an array guided surface wave (AGSW) on a periodic planar finite array of dipoles in free space has been demonstrated in [1], [7-9] based on numerical solutions. The conditions under which surface waves can exist on a finite array, strength of the excited surface waves, and the surface wave effects on the far-zone pattern have been investigated.

In this chapter, derivation of an analytical expression for the excitation coefficient of an AGSW launched from the edge of a semi-infinite array of dipoles in free space is given.

3.1. Array Guided Surface Waves [8-9]

In the context of periodic arrays, the term surface wave most typically arises in relation with an array embedded in a dielectric slab. For these types of surface waves, a grating lobe radiated by the array excites one of the wave guide modes of the dielectric [6]. On the other hand, the surface waves studied here exist on an array of perfectly conducting dipoles. These two types of surface waves can be distinguished by the terms “dielectric slab guided” surface waves and “array guided” surface waves [18].

In order to examine the conditions under which AGSW may arise, the scan impedance of the infinite array is studied at all scan angles. For some scan angle below a certain cutoff frequency, the scan impedance can go to zero. At such frequencies, surface waves can exist in the corresponding truncated array.

The propagation constant of surface waves can be found by setting the scan impedance equal to zero. The phase progression associated with the surface wave currents indicates slow waves, i.e. waves with phase velocity less than the speed of light.

As illustrated at Figure 3.1, considering a finite × infinite array of dipoles, infinite at the y direction and finite at the x direction, the scan impedance can be observed for two conditions. The scan impedance formula is given in Chapter 2. Setting $s_y = 0$, the self impedance $Z_{11}(s_x)$ can be observed for the scan in the H-plane.

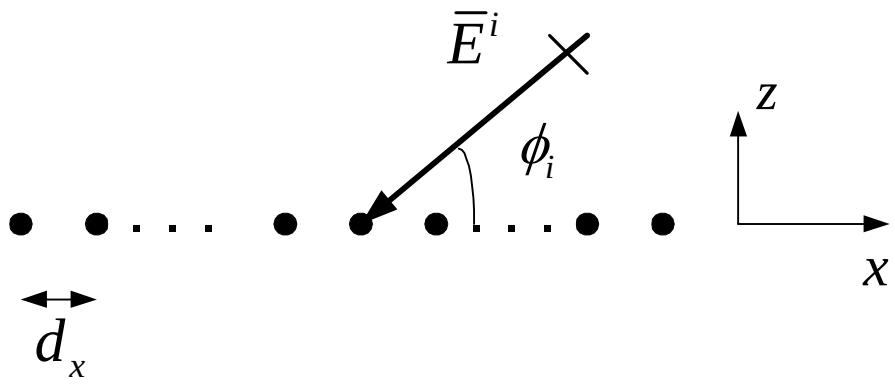

Figure 3.1. Finite × Infinite array of dipoles, finite at x direction with spatial period d_x but infinite at y direction.

As it can be seen from Figures 3.2 and 3.3, the scan impedance goes to zero for 8 GHz but does not pass from zero for 10 GHz. This means with these array

parameters at 10 GHz there is not an AGSW, however at 8 GHz an AGSW exists since scan impedance pass through $s_{x0} = 1.44$. The zeroes of the scan impedance gives the natural waveguide modes of the array of perfectly conducting dipoles. The propagation constant of the surface wave is $\beta = (2\pi/\lambda) \times (s_{x0})$. In the absence of loss, a surface wave propagates along the uniform array with a phase velocity $\upsilon = (c / s_{x0})$ where c is the speed of light. When an edge is encountered this surface wave partially reflected in the opposite direction and partially radiated.

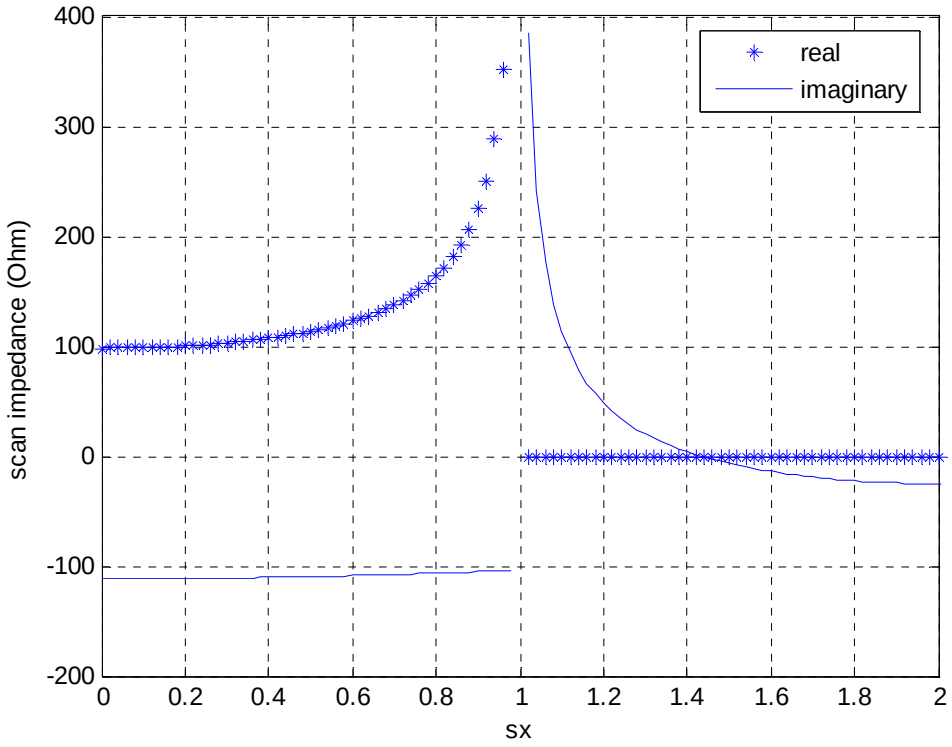

Figure 3.2. Scan impedance for f = 8 GHz, $d_x = 0.9$ cm, $d_z = 1.6$ cm, $2l = 1.5$ cm (wire length), $w_r = 0.0225$ cm (wire radius).

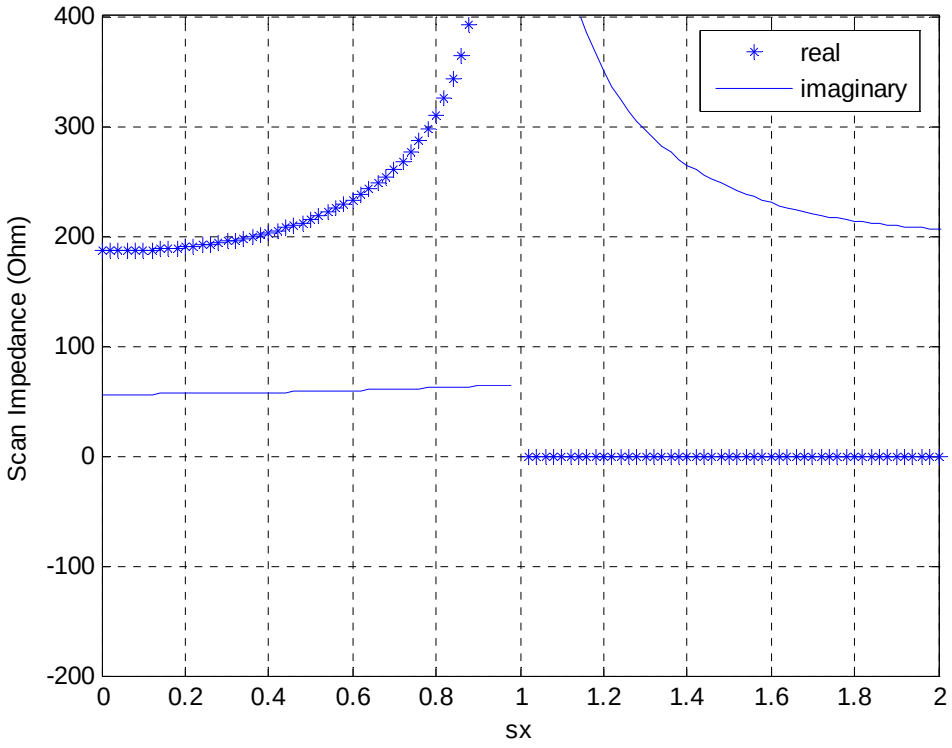

Figure 3.3. Scan impedance for f = 10 GHz, d_x = 0.9 cm, d_z = 1.6 cm, 2l = 1.5 cm (wire length), w_r = 0.0225 cm (wire radius).

One necessary condition for the existence of surface waves is that the interelement spacing along the direction of propagation must be less than one-half wavelength. If this is not the case there will always be a propagating Floquet mode and scan impedance will always a positive real part.

In order to examine array guided surface wave propagation and excitation, a method is given in [8-9] based on numerical methods. A surface wave is excited at the edge of an array with launching coefficient $C(f, \varphi^i)$. This coefficient depends on frequency and angle of incidence, but assumed to be independent of the size of the array. A surface wave propagates along the array without loss until it encounters an edge, at which point it is reflected in the opposite direction with reflection

coefficient Γ(f). Γ(f) is assumed to be independent of array size and angle of incidence. The propagation constant of the surface waves can be found from the zeroes of the scan impedance as stated before.

3.2. Scattering of an EM Field Incident on a Planar Semi-Infinite Array of Dipoles in Free Space

In Figure 3.4 the problem of scattering of an electromagnetic wave incident on a planar semi-infinite array of dipoles in the z = 0 plane in free space is illustrated. The incident field is generated by a distant, uniform electric line source of density J_i and known strength I at (ρ_i, φ_i). Assume that the conditions of the existence of the surface wave are satisfied.

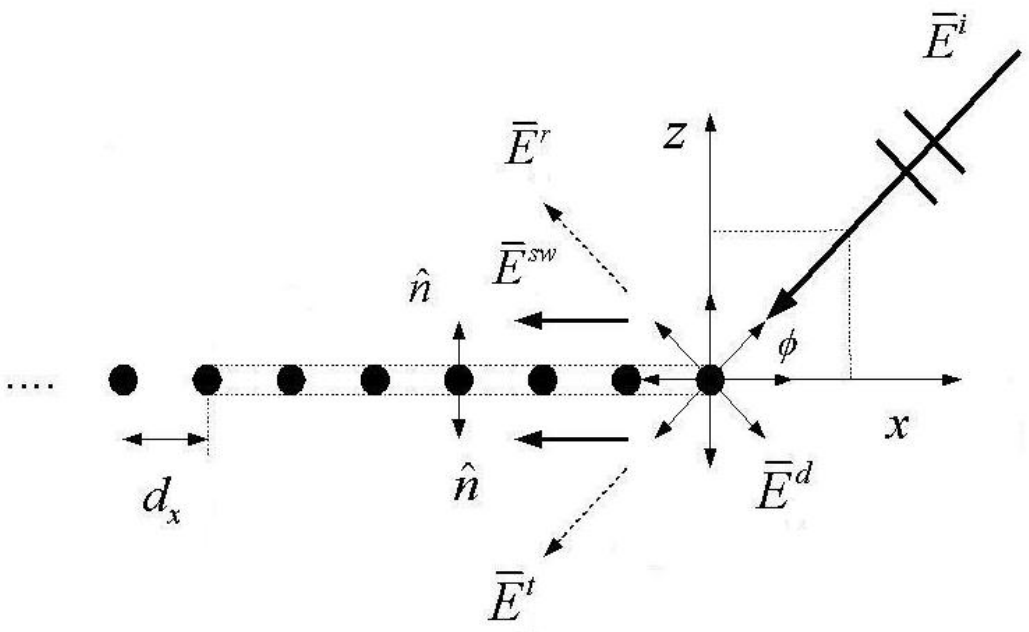

Figure 3.4. Plane wave incident on a semi-infinite array of dipoles in free space and related field components. The array is infinite at y direction with spatial period d_y and semi-infinite in x direction with period d_x.

Once launched, a surface wave propagates in the $-\hat{x}$ direction along the array face and attenuating at the directions normal to the array face. The electric field of the surface wave is denoted by $\bar{E}^{sw}$. Also, adding the asymptotic high frequency electric fields pertaining to the Floquet modal transmitted, reflected and diffracted fields, denoted by $\bar{E}^{t}$, $\bar{E}^{r}$ and $\bar{E}^{d}$ respectively, the total field can be written as

$$\bar{E} = \bar{E}^{i} + \bar{E}^{sw} + \bar{E}^{r,t} + \bar{E}^{d} \tag{3.1}$$

The corresponding magnetic fields are denoted by $\bar{H}^{t}$, $\bar{H}^{r}$, $\bar{H}^{d}$ and $\bar{H}^{sw}$.

The fields scattered by the array in Figure 3.4 are produced by the current density $\bar{J}(n,m)$ on each (n, m)th dipole element which is assumed to be open circuited.

$$\begin{aligned} &\bar{J}(n,m) = \hat{y} I(n,m) f_m(y) \delta(x - nd_x) \delta(z) \\ &n = 0, -1, -2, \ldots \\ &m = 0, \pm 1, \pm 2, \ldots \end{aligned} \tag{3.2}$$

The current distribution function $f_m(y)$ in (3.2) is assumed to be a piecewise sinusoid. As it is noted in Chapter 2, this distribution function is commonly employed for a short, thin dipole element.

On the terminal of an element, two current components responsible for Floquet waves and surface waves exist. The current elements are denoted by I^{FW} and I^{SW}. The diffraction currents can be ignored. If this total current is written in the radiation integral, then the asymptotic evaluation of this integral gives the field components in (3.1). The Floquet current component can be written as shown in Chapter 2.

I^{SW} component of this terminal current launches the surface wave $\bar{E}^{sw}$ on the semi-infinite array $x < 0$ region as illustrated in Figure 3.4. The surface wave current can be expressed as

$$I^{sw}(n,m) = Ce^{j\beta n d_x} \tag{3.3}$$

In Equation (3.3), β represents the surface wave propagation constant, and as said before it can be found from scan impedance of the infinite array. The amplitude in (3.3) is an unknown and it is the launching coefficient of the surface wave component.

Following the steps explained in Chapter 2, the electric field expression for surface waves can be obtained with the current given in (3.3) as

$$\begin{aligned}\bar{E}^{sw}(\bar{r}) = \frac{Z}{4\pi k d_y}\sum_{q=-\infty}^{\infty}\int_{-\infty}^{\infty} C\tilde{f}(k_{yq})\frac{\left\{\hat{x}(k_x k_{yq}) + \hat{y}(k_{yq}^2 - k^2) + \hat{z}(k_{zq}k_{yq})\right\}}{1-e^{-jd_x(\beta+k_x)}} \\ \times \frac{e^{-jk_x x}e^{-jk_{yq}y}e^{-jk_{zq}z}}{k_{zq}}\,dk_x\end{aligned} \tag{3.4}$$

The spectral integral in Equation (3.4) can be evaluated with steepest descent methods. The field expression for the surface wave for x < 0 region can be written as

$$\begin{aligned}\bar{E}^{sw} = \sum_{p=-\infty}^{\infty}\sum_{q=-\infty}^{\infty}\frac{\omega\mu}{2k^2 d_x d_y}\,C\,\tilde{f}(k_{yq})e^{j\beta x}e^{j\frac{2\pi px}{d_x}}e^{-jk_{yq}y}e^{-jk_{zpq}^{sw}|z|} \\ \times\left\{\frac{\hat{x}(-k_{xp})k_{yq} + \hat{y}(k_{yq}^2 - k^2) + \hat{z}(k_{zpq}^{sw})k_{yq}}{k_{zpq}^{sw}}\right\}\end{aligned} \tag{3.5}$$

where

$$k_{xp} = \beta + \frac{2\pi p}{d_x} \quad ; \text{p=0,}\pm1,... \tag{3.6}$$

$$k_{yq} = \frac{2\pi q}{d_y} \quad ; \text{q=0,}\pm1,... \tag{3.7}$$

$$k_{zpq}^{sw} = \sqrt{k^2 - k_{xp}^2 - k_{yq}^2} = -j\alpha_{pq}$$
$$\alpha_{pq} = \sqrt{k_{xp}^2 + k_{yq}^2 - k^2} \tag{3.8}$$

In Equation (3.8), an attenuation constant α_{pq} is defined; since the wave attenuates in directions normal to the array face.

The Fourier transform of the current distribution function f(y) can be evaluated as

$$\tilde{f}(k_{yq}) = \int_{-L/2}^{L/2} \frac{\sin k(\frac{L}{2} - |y|)}{\sin(k\frac{L}{2})} \exp\{jk_{yq}\} dy \tag{3.9}$$

The incident field is generated by a distant, uniform electric line source, of known strength I and density $\overline{J}_i$, at (ρ_i, ϕ_i) which can be expressed as

$$\overline{J}_i = \hat{y} I \frac{\delta(\rho - \rho_i)\delta(\phi - \phi_i)}{\rho} \tag{3.10}$$

This line source is y-directed and sufficiently far from the edge of the array. The field expression for electric field for the incident field can be written as

$$\begin{aligned} E_y^i &= -j\omega\mu \frac{I}{2\sqrt{2\pi j}} \frac{\exp\{-jk\rho_i\}}{\sqrt{k\rho_i}} \\ &= \left(\frac{-\omega\mu}{4}\right) I \frac{\sqrt{2j}}{\sqrt{\pi k}} \frac{\exp\{-jk\rho_i\}}{\sqrt{\rho_i}} \end{aligned} \tag{3.11}$$

3.3. Reciprocal Surface Wave Problems

In Equation (3.5), in order to determine the surface wave field, the unknown C has to be found. It may not be directly possible to find C in a convenient fashion. In order to find the unknown excitation coefficient C, a reciprocal problem to the

surface wave excitation problem is introduced [17]. By the Kirchhoff approximation the reciprocal problem can be solved approximately.

In Figure 3.5, the reciprocal problem is illustrated and is named as second problem. The first problem is the excitation of surface wave problem from the edge of the array as illustrated in Figure 3.4. After solving the second problem, two reciprocal problems are combined with a reciprocity integral formulation and the unknown C is determined in Section 3.4.

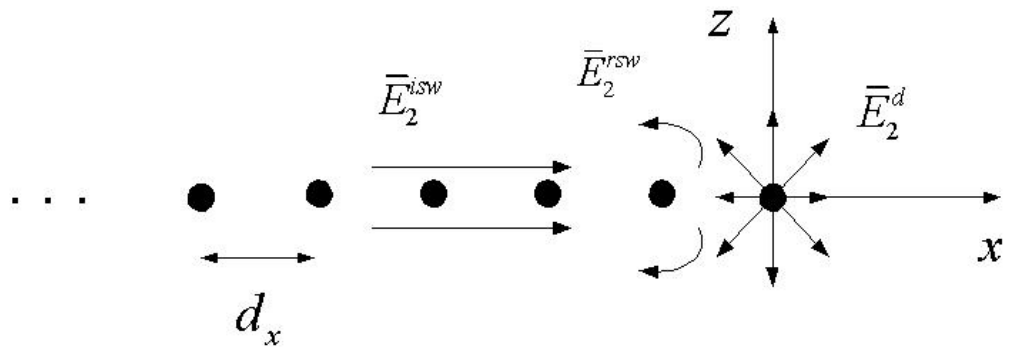

Figure 3.5. The side view of second problem: incident surface wave field is reflected in the opposite direction and diffracted at the edge of the array.

The excitation of the reciprocal configuration is the incident surface wave current $I_2^{isw}(n,m)$ at the terminals of any (n,m)th dipole, which is assumed to exist as if the array was infinite in extent. Therefore, this current can be written as

$$I_2^{isw}(n,m) = I_0 e^{-j\beta n d_x} \tag{3.12}$$

This current gives rise to the incident surface wave field $\bar{E}_2^{isw}$. This incident surface wave field undergoes reflection in the opposite side and diffraction at the edge of the array; therefore, at the edge $\bar{E}_2^{rsw}$ and $\bar{E}_2^{d}$ are produced respectively.

Therefore, the (n, m)th dipole terminal current can be decomposed as

$$I(n,m) = I_2^{isw}(n,m) + I_2^{rsw}(n,m) + I_2^{d}(n,m) \tag{3.13}$$

The reflected current can be expressed as

$$I_2^{rsw}(n,m) = \Gamma I_0 e^{+j\beta n d_x} \tag{3.14}$$

where Γ is surface wave reflection coefficient, for which the numerical values can be found in [8-9]. I_2^{rsw} produces the reflected surface wave $\bar{E}_2^{rsw}$.

In the Kirchhoff approximation for $I_2(n,m)$ it is customary to ignore I_2^{rsw} and I_2^{d} in (3.13). However, in this analysis I_2^{rsw} is included and it constitutes a modified Kirchhoff approximation while only the weaker I_2^{d} is ignored. Therefore, (3.13) can be approximated by

$$I_2(n,m) \approx I_2^{isw}(n,m) + I_2^{rsw}(n,m) \tag{3.15}$$

It can be said that the inclusion of the reflection coefficient (Γ) yields a more accurate result for the excitation coefficient (C).

In order to find the expressions for the incident surface wave, the reflected surface wave and the diffracted surface wave the current can be written as

$$\bar{J}_2(\bar{r}\,') = \hat{y}\, f(y' - md_y)\delta(x' - nd_x)\delta(z')\left(I_0 e^{-j\beta n d_x} + \Gamma I_0 e^{j\beta n d_x}\right) \tag{3.16}$$

Following the same procedure given in Section 3.2, the magnetic vector potential expression can be written as

$$A_{2y} = \frac{1}{4\pi j d_y} \sum_{q=-\infty}^{\infty} \int_{-\infty}^{\infty} I_0 \left(\frac{1}{1-e^{j(\beta-k_x)d_x}} + \Gamma \frac{1}{1-e^{-j(\beta+k_x)d_x}} \right) \times \tilde{f}(k_{yq}) \left[\frac{e^{-jk_x x} e^{-jk_y y} e^{-jk_z z}}{k_z} \right] dk_x \tag{3.17}$$

The electric field expression can be written as

$$\bar{E}_2(\bar{r}) = \frac{Z}{4\pi k d_y} \sum_{q=-\infty}^{\infty} \int_{-\infty}^{\infty} I_0 \left(\frac{1}{1-e^{j(\beta-k_x)d_x}} + \Gamma \frac{1}{1-e^{-j(\beta+k_x)d_x}} \right) \times \left\{ \hat{x}(k_x k_{yq}) + \hat{y}(k_{yq}^2 - k^2) + \hat{z}(k_{zq} k_{yq}) \right\} \tilde{f}(k_{yq}) \times \left[\frac{e^{-jk_x x} e^{-jk_{yq} y} e^{-jk_{zq}^{sw} z}}{k_{zq}^{sw}} \right] dk_x \tag{3.18}$$

The integral in (3.18) can be evaluated by using asymptotic high frequency methods (Appendix A). After evaluation of this integral, and writing the pole and saddle point contributions; the incident, reflected and diffracted surface wave field expressions can be obtained.

The incident surface wave for x < 0 can be written as

$$\bar{E}_2^{isw}(\bar{r}) = \sum_{p=-\infty}^{\infty} \sum_{q=-\infty}^{\infty} \frac{\omega\mu}{2k^2 d_x d_y} I_0 \, \tilde{f}(k_{yq}) e^{-j\beta x} e^{-j\frac{2\pi p}{d_x} x} e^{-jk_{yq} y} e^{-jk_{zpq}^{sw}|z|} \times \left\{ \frac{\hat{x}(k_{xp}) k_{yq} + \hat{y}(k_{yq}^2 - k^2) + \hat{z}(k_{zpq}^{sw}) k_{yq}}{k_{zpq}^{sw}} \right\} \tag{3.19}$$

The reflected surface wave for x < 0 can be expressed as

$$\bar{E}_2^{rsw}(\bar{r}) = \sum_{p=-\infty}^{\infty} \sum_{q=-\infty}^{\infty} \frac{\omega\mu}{2k^2 d_x d_y} \Gamma I_0 \, \tilde{f}(k_{yq}) e^{j\beta x} e^{j\frac{2\pi p}{d_x} x} e^{-jk_{yq} y} e^{-jk_{zpq}^{sw}|z|} \times \left\{ \frac{\hat{x}(-k_{xp}) k_{yq} + \hat{y}(k_{yq}^2 - k^2) + \hat{z}(k_{zpq}^{sw}) k_{yq}}{k_{zpq}^{sw}} \right\} \tag{3.20}$$

Considering the Equation (3.17) and the far-field approximation for electric field given in (3.21), one can obtain an expression for diffracted field valid sufficiently far from the edge as in Equation (3.22). This diffracted field is evaluated for an observation point (ρ,ϕ) measured from the edge of the array as illustrated in Figure 3.5.

$$\hat{y}.\bar{E}_2^d(\bar{r}) = E_{2y}^d(\bar{r}) \sim -j\omega\mu A_{2y}(\bar{r}) \tag{3.21}$$

$$\begin{aligned} E_{2y}^d \sim \sum_q \left(\frac{-\omega\mu}{4}\right) I_0 \frac{\tilde{f}(k_{yq})}{d_y} e^{-jk_{yq}y} \sqrt{\frac{2j}{\pi\sqrt{k^2-k_{yq}^2}}} \frac{e^{-j\sqrt{k^2-k_{yq}^2}\rho}}{\sqrt{\rho}} \frac{1}{2} \\ \times \left\{ \begin{array}{l} \left(1 + j\cot\left[\frac{1}{2}(\beta - \sqrt{k^2-k_{yq}^2}\cos\phi)\right]\right) \\ +\Gamma\left(1 - j\cot\left[\frac{1}{2}(\beta + \sqrt{k^2-k_{yq}^2}\cos\phi)\right]\right) \end{array} \right\} \end{aligned} \tag{3.22}$$

3.4. Application of Reciprocity Theorem to Find Excitation Coefficient

The reciprocity theorem can be used to relate the fields of the original problem to those in the reciprocal problem. The original problem is the excitation of the surface wave from the edge of the array, while the reciprocal problem is the problem formulated in the Section 3.3. The details of the reciprocity theorem is given in Appendix D.

Two reciprocal problems are related in an appropriate volume V, bounded by a closed surface S. The original problem geometry is shown in Figures 3.6 and 3.7, while the reciprocal problem is illustrated in Figure 3.5. The fields of the original problem is denoted by $(\bar{E}_1, \bar{H}_1)$, whereas the fields of the reciprocal problem is denoted by $(\bar{E}_2, \bar{H}_2)$.

The reciprocity integral can be written as

$$\oint_S \left(\bar{E}_1 \times \bar{H}_2 - \bar{E}_2 \times \bar{H}_1\right) \bullet \hat{n} dS = \int_V \bar{E}_2 \bullet \bar{J}_i dV \tag{3.23}$$

where the fields of the first problem (original problem) is given in Equation (3.5), and the fields of the second problem (reciprocal problem) is given in Equations (3.19), (3.20), (3.22). Also, the volume V and closed surface S is illustrated in Figures 3.6 and 3.7. The closed surface can be written as $S = \sum_{i=1}^{9} S_i$.

The right hand side of the Equation (3.23) is a volume integral and the source term is given in Equation (3.10). The source is sufficiently far from the edge of the array; therefore, the field term in the right hand side of the Equation (3.23) can be written as $\bar{E}_2 \sim \bar{E}_2^d$.

The volume integral in (3.23) can be expressed as

$$\int_V \bar{E}_2^d . \bar{J}_i dV = \iiint_{V(\rho,\phi,y)} \left(\hat{y} E_{2y}^d\right) . \left(\hat{y} I \frac{\delta(\rho - \rho_i)\delta(\phi - \phi_i)}{\rho} \right) \rho d\rho d\phi dy \tag{3.24}$$

Due to property of impulse function and taking the integral for y variable as $y : -\infty \to \infty$ and using a Fourier relation for impulse function, the expression for the right hand side of (3.23) can be obtained as in Equation (3.25).

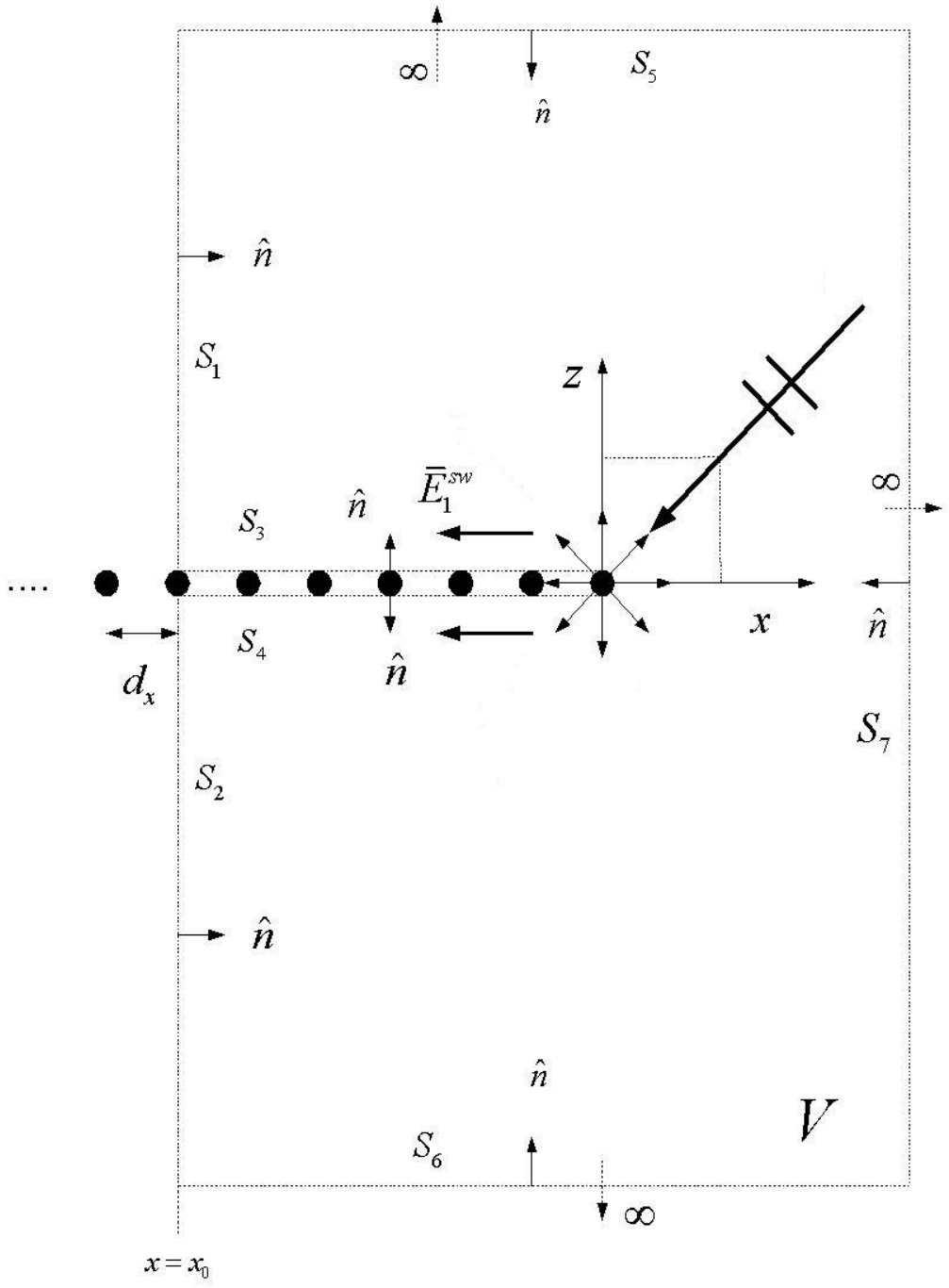

Figure 3.6. Side view of the original problem configuration: the array is excited by an EM field created by a distant line source, and surface wave is launched from the edge.

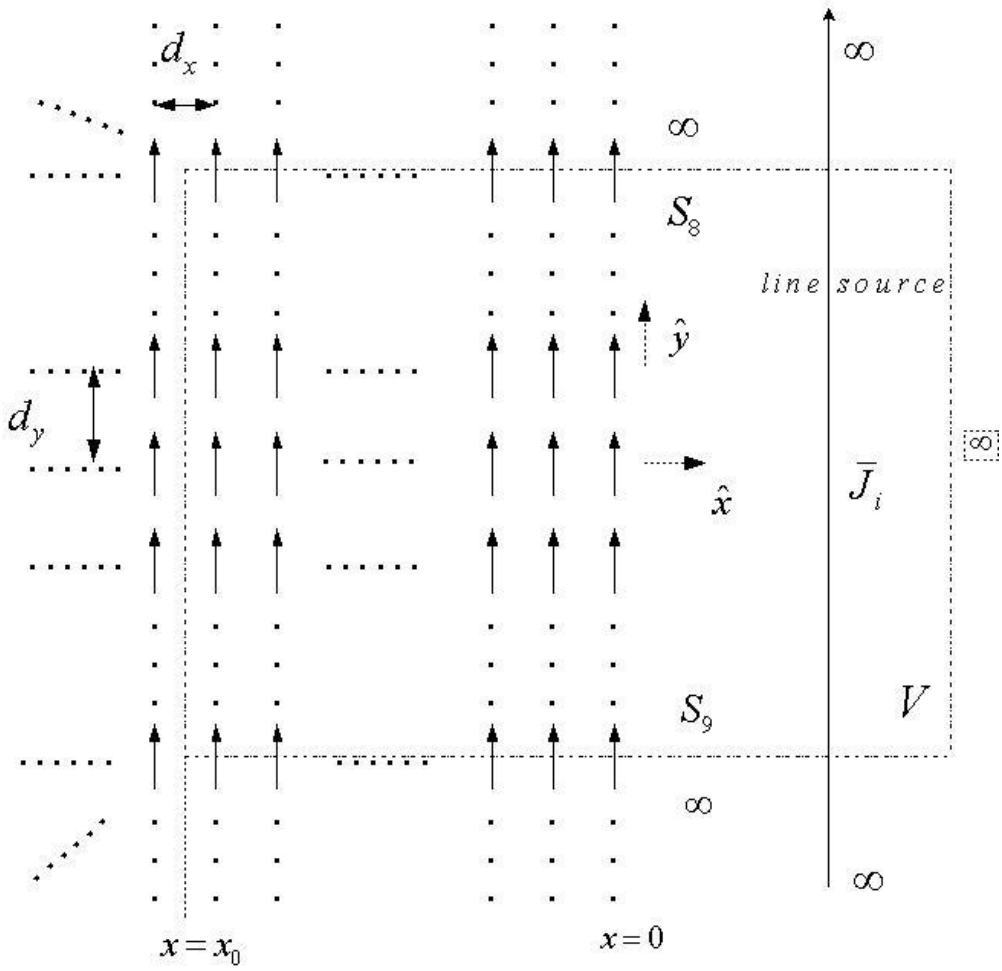

Figure 3.7. Top view of the original problem configuration.

$$\int_V \bar{E}_2^d \bullet \bar{J}_i dV = (2\pi)\left(\frac{-\omega\mu}{4}\right) I_0 I \frac{\tilde{f}(0)}{d_y}\sqrt{\frac{2j}{\pi k}}\frac{e^{-jk\rho}}{\sqrt{\rho}}\frac{1}{2} \times \left\{\begin{array}{l}\left(1+ j\cot\left[\frac{1}{2}(\beta - k\cos\phi)\right]\right) \\ +\Gamma\left(1- j\cot\left[\frac{1}{2}(\beta + k\cos\phi)\right]\right)\end{array}\right\} \tag{3.25}$$

In terms of incident wave expression, Equation (3.25) can be rearranged as

$$\int_V \bar{E}_2^d \bullet \bar{J}_i dV = \left(\bar{E}^i(0)\bullet\hat{y}\right)(2\pi) I_0 \frac{\tilde{f}(0)}{d_y}\frac{1}{2} \times \left\{\begin{array}{l}\left(1+ j\cot\left[\frac{1}{2}(\beta - k\cos\phi)\right]\right) \\ +\Gamma\left(1- j\cot\left[\frac{1}{2}(\beta + k\cos\phi)\right]\right)\end{array}\right\} \tag{3.26}$$

The left hand side of the reciprocity integral is evaluated over the surfaces illustrated in Figures 3.6 and 3.7. The integral over the surfaces at infinity are zero due to the radiation condition. Therefore, for these surfaces, surface integral can be written as

$$\int_{S\infty} \left(\bar{E}_1 \times \bar{H}_2 - \bar{E}_2 \times \bar{H}_1\right)\bullet\hat{n}dS = 0 \tag{3.27}$$

where $S_\infty = \sum_{i=5}^{9} S_i$ represents the surfaces at infinity.

The integrals over the surfaces S_3 and S_4 have symmetric forms with respect to z axis; therefore, the S_3 integral for $z > 0$ is equal to the S_4 integral for $z < 0$. Thus, evaluating the S_3 integral and multiplying the result by two gives the contribution of S_3 and S_4 integrals, i.e. normal integrals which are totally denoted by S_N.

The surface integral S_3, for z > 0 and taking the normal direction as the positive z direction can be expressed as

$$\int_{S_3}\left(\bar{E}_1\times\bar{H}_2-\bar{E}_2\times\bar{H}_1\right)\bullet\hat{z}dxdy=-\int_x\int_y\left(E_{1y}H_{2x}-E_{2y}H_{1x}\right)dydx \tag{3.28}$$

The fields $(\bar{E}_1^{sw};\bar{H}_2^{isw},\bar{H}_2^{rsw},\bar{H}_2^{d})$ and $(\bar{E}_2^{isw},\bar{E}_2^{rsw},\bar{E}_2^{d};\bar{H}_1^{sw})$ can be related by reciprocity theorem. For instance, for $(\bar{E}_1^{sw};\bar{H}_2^{isw})$ and $(\bar{E}_2^{isw};\bar{H}_1^{sw})$ pair, one can write (3.28) as

$$\begin{aligned}
&\left(\frac{-1}{\omega\mu}\right)(-1)\int_x\int_y[(\sum_{p=-\infty}^{\infty}\sum_{q=-\infty}^{\infty}\frac{\omega\mu}{2k^2d_xd_y}\,C\,\tilde{f}(k_{yq})\left\{\frac{(k_{yq}^2-k^2)}{k_{zpq}^{sw}}\right\}\\
&\times e^{j\beta x}e^{j\frac{2\pi px}{d_x}}e^{-jk_{yq}y}e^{-jk_{zpq}^{sw}\Delta z}\\
&\times\sum_{n=-\infty}^{\infty}\sum_{m=-\infty}^{\infty}\frac{\omega\mu}{2k^2d_xd_y}\,\mathrm{I}_0\,\tilde{f}(k_{ym})\left\{\frac{-k_{znm}^{sw}k^2}{k_{znm}^{sw}}\right\}\\
&\times e^{-j\beta x}e^{-j\frac{2\pi nx}{d_x}}e^{-jk_{ym}y}e^{-jk_{znm}^{sw}\Delta z})-\\
&(\sum_{n=-\infty}^{\infty}\sum_{m=-\infty}^{\infty}\frac{\omega\mu}{2k^2d_xd_y}\,\mathrm{I}_0\,\tilde{f}(k_{ym})\left\{\frac{(k_{ym}^2-k^2)}{k_{znm}^{sw}}\right\}\\
&\times e^{-j\beta x}e^{-j\frac{2\pi nx}{d_x}}e^{-jk_{ym}y}e^{-jk_{znm}^{sw}\Delta z}\\
&\times\sum_{p=-\infty}^{\infty}\sum_{q=-\infty}^{\infty}\frac{\omega\mu}{2k^2d_xd_y}\,\mathrm{C}\,\tilde{f}(k_{ym})\left\{\frac{-k_{zpq}^{sw}k^2}{k_{zpq}^{sw}}\right\}\\
&\times e^{j\beta x}e^{j\frac{2\pi px}{d_x}}e^{-jk_{yq}y}e^{-jk_{zpq}^{sw}\Delta z})]dxdy
\end{aligned} \tag{3.29}$$

The integral equation in (3.29) is written for z = Δz plane for z > 0, and the wavenumbers are defined before. For infinitesimally small point sources, Δz→0 can be written.

From the Equation (3.29) it can be seen that the integrand is zero. In a similar manner, the cross-flux of the fields $(\bar{E}_1^{sw},\bar{H}_2^{isw};\bar{E}_2^{isw},\bar{H}_1^{sw})$ and $(\bar{E}_1^{sw},\bar{H}_2^{d};\bar{E}_2^{d},\bar{H}_1^{sw})$ is

zero, since the integrand is zero also for these fields. Therefore, the contributions of the integrals over S_3 and S_4 equal to zero in the reciprocity integral formulation.

As a result, the contributions to the surface integral in the left hand side of the reciprocity integral comes only from the integrals over surfaces S_1 and S_2, which are named as transverse surfaces.

The transverse integral for the surface S_1 for $z > 0$ is equal to the transverse integral for the surface S_2 for $z < 0$ due to the symmetry. Therefore, after evaluating the transverse integral over the surface S_1 and multiplying it by two, one can obtain the left hand side of the reciprocity integral formulation.

The surface integral S_1, for $z > 0$ and taking the transverse direction as the positive x direction can be expressed as

$$\int_{S_1} \left(\bar{E}_1 \times \bar{H}_2 - \bar{E}_2 \times \bar{H}_1 \right) \bullet \hat{x} dydz = \int_z \int_y \left(E_{1y}^{sw} H_{2x} - E_{2y} H_{1x}^{sw} \right) dydz \tag{3.30}$$

where

$$\begin{aligned} E_{2y} &= E_{2y}^{isw} + E_{2y}^{rsw} + E_{2y}^{d} \\ H_{2x} &= H_{2x}^{isw} + H_{2x}^{rsw} + H_{2x}^{d} \end{aligned} \tag{3.31}$$

For the transverse integral, $x = x_0$ is arbitrary as illustrated in Figure 3.6. While $x_0 \to -\infty$, for the second field only the incident surface wave field is considered. The transverse integral contribution (S_T) to the reciprocity integral can be expressed as

$$S_T = 2 \int_z \int_y \left(E_{1y}^{sw} H_{2x}^{isw} - E_{2y}^{isw} H_{1x}^{sw} \right) dydz \tag{3.32}$$

which is equal to the left hand side of the reciprocity integral.

The integral in Equation (3.32) can be expressed as

$$\left(\frac{-1}{\omega\mu}\right)(2)\int_{y=-\infty}^{\infty}\int_{z=0}^{\infty}[(\sum_{p=-\infty}^{\infty}\sum_{q=-\infty}^{\infty}\frac{\omega\mu}{2k^2 d_x d_y}\,C\,\tilde{f}(k_{yq})\left\{\frac{(k_{yq}^2-k^2)}{k_{zpq}^{sw}}\right\}$$
$$\times e^{j\beta x_0}e^{j\frac{2\pi p x_0}{d_x}}e^{-jk_{yq}y}e^{-jk_{zpq}^{sw}z}$$
$$\times\sum_{n=-\infty}^{\infty}\sum_{m=-\infty}^{\infty}\frac{\omega\mu}{2k^2 d_x d_y}\,\mathrm{I}_0\,\tilde{f}(k_{ym})\left\{\frac{k_{xn}k^2}{k_{znm}^{sw}}\right\}$$
$$\times e^{-j\beta x_0}e^{-j\frac{2\pi n x_0}{d_x}}e^{-jk_{ym}y}e^{-jk_{znm}^{sw}z})-$$
$$(\sum_{n=-\infty}^{\infty}\sum_{m=-\infty}^{\infty}\frac{\omega\mu}{2k^2 d_x d_y}\,\mathrm{I}_0\,\tilde{f}(k_{ym})\left\{\frac{(k_{ym}^2-k^2)}{k_{znm}^{sw}}\right\}$$
$$\times e^{-j\beta x_0}e^{-j\frac{2\pi n x_0}{d_x}}e^{-jk_{ym}y}e^{-jk_{znm}^{sw}z}$$
$$\times\sum_{p=-\infty}^{\infty}\sum_{q=-\infty}^{\infty}\frac{\omega\mu}{2k^2 d_x d_y}\,\mathrm{C}\,\tilde{f}(k_{ym})\left\{\frac{-k_{xp}k^2}{k_{zpq}^{sw}}\right\}$$
$$\times e^{j\beta x_0}e^{j\frac{2\pi p x_0}{d_x}}e^{-jk_{yq}y}e^{-jk_{zpq}^{sw}z})]dydz \qquad (3.33)$$

and the replacements $k_{zpq}^{sw}\to -j\alpha_{pq}$ or $k_{znm}^{sw}\to -j\alpha_{nm}$ can be performed. The integration on z parameter can be easily evaluated as $1/(2\alpha_{pq})$. The equating the result of (3.33), which is the left hand side of reciprocity integral, to the the right hand side of reciprocity integral, one can obtain Equation (3.34). From (3.34), after some algebra, the expression for the surface wave excitation coefficient C can be obtained as in (3.35). By using the excitation coefficient expression, one can write surface wave expression as in Equation (3.5). This excitation coefficient expression is valid only for normal incidence case.

$$\sum_p (-\frac{1}{\omega\mu}) \frac{(2\pi)4k^4 I_0 \left[\tilde{f}(0)\right]^2 Ck_{xp}}{-2\alpha_{p0}^3} \frac{\omega^2\mu^2}{4k^4 d_x^2 d_y^2}$$

$$= \int_V \bar{E}_2^d \bullet \bar{J}_i dV = \left(\bar{E}^i(0) \bullet \hat{y}\right)(2\pi) I_0 \frac{\tilde{f}(0)}{d_y} \frac{1}{2} \tag{3.34}$$

$$\times \left\{ \begin{array}{l} \left(1 + j\cot\left[\frac{1}{2}(\beta - k\cos\phi)\right]\right) \\ +\Gamma\left(1 - j\cot\left[\frac{1}{2}(\beta + k\cos\phi)\right]\right) \end{array} \right\}$$

$$C = \left(\frac{d_x^2 d_y}{\omega\mu\tilde{f}(0)}\right) \frac{1}{\sum_p \left(\frac{k_{xp}}{\alpha_{p0}^3}\right)} \left(\bar{E}^i(0) \bullet \hat{y}\right) \times \left\{ \begin{array}{l} \left(1 + j\cot\left[\frac{1}{2}(\beta - k\cos\phi)\right]\right) \\ +\Gamma\left(1 - j\cot\left[\frac{1}{2}(\beta + k\cos\phi)\right]\right) \end{array} \right\} \tag{3.35}$$

Some example plots are given in Figures 3.8 and 3.9, and the analytically found excitation coefficient is compared with numerically found excitation coefficient taken from [9]. The incident wave is assumed to be E^i = 1 V/m.

In order to improve the modified Kirchhoff approximation after 90^0 the analytically found excitation coefficient is multiplied by (1+cos(φ)), because when the angle of incidence approaches 180^0 the excitation coefficient should be zero.

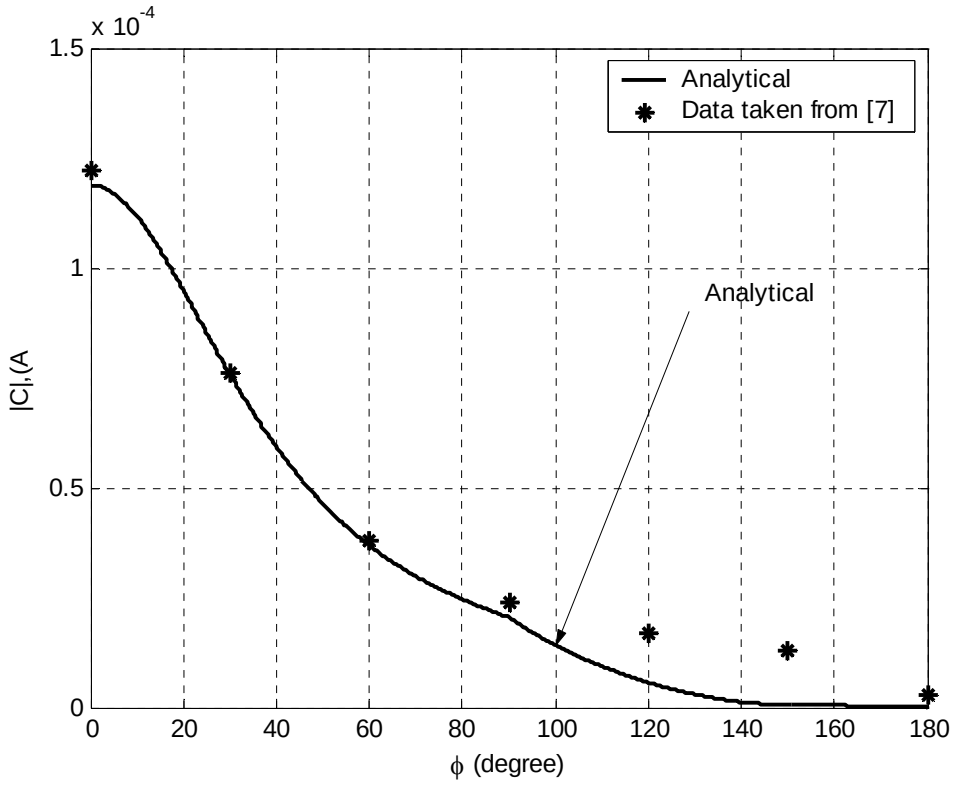

Figure 3.8. Comparison of the corrected analytical expression in Equation (3.35) with the excitation coefficient data given in [7-9] for f = 7.7 GHz, dx = 0.9 cm, dy = 1.6 cm, dipole length (2l) = 1.5 cm.

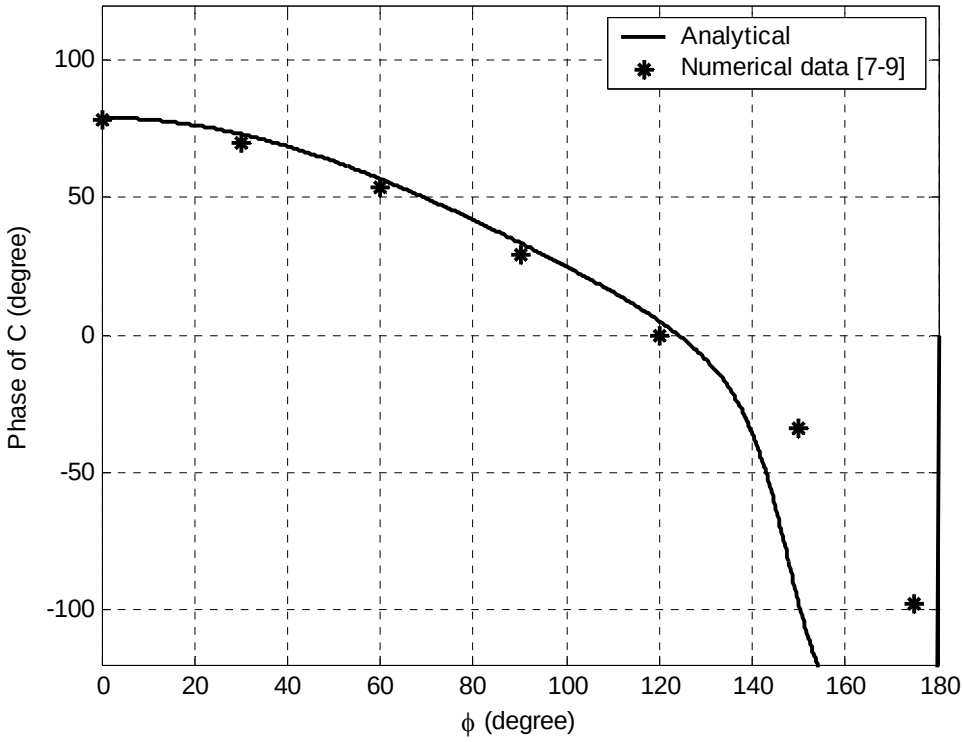

Figure 3.9. Comparison of the phase of the corrected analytical expression in Equation (3.35) with the excitation coefficient phase data given in [7-9].

If the reflected waves does not taken into consideration, i.e. if Kirchhoff approximation is used, the expression in Equation (3.35) does not include reflection coefficient. The comparison of modified Kirchhoff and Kirchhoff approximations are given in Figures 3.10 and 3.11.

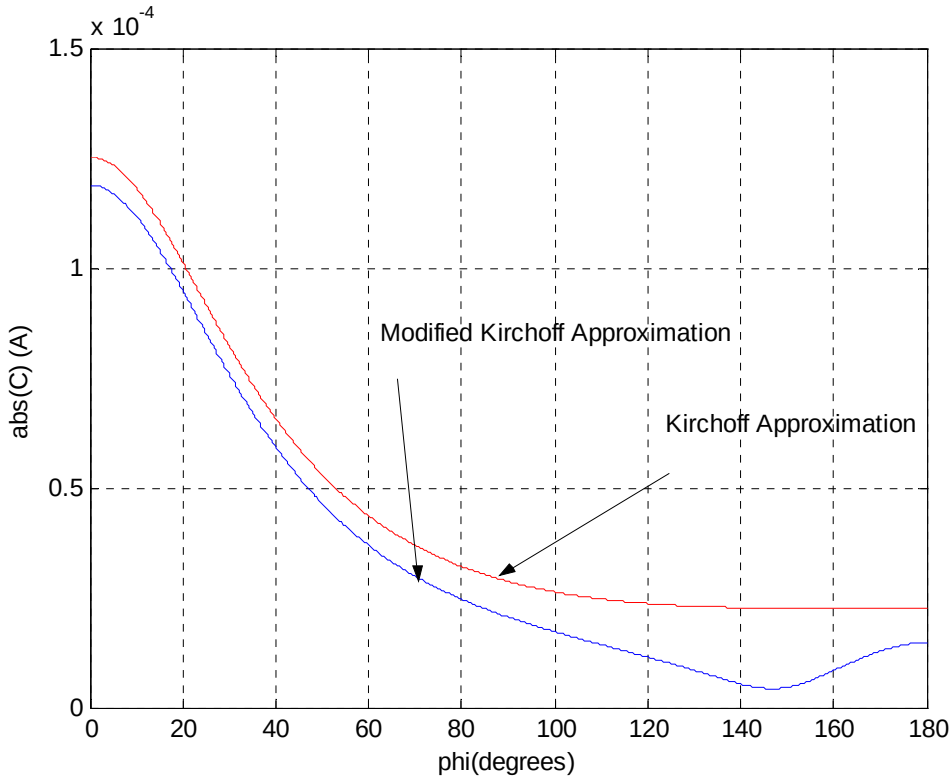

Figure 3.10. Absolute value of the excitation coefficient for modified Kirchhoff and Kirchhoff approximations.

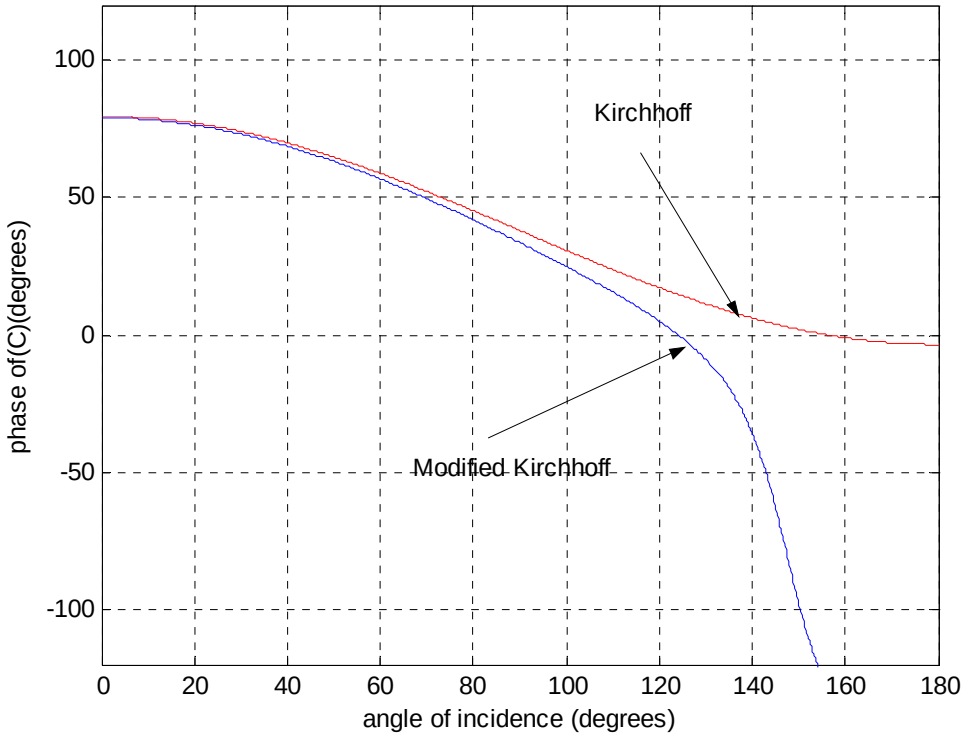

Figure 3.11. Phase of the excitation coefficient for modified Kirchhoff and Kirchhoff approximations.

3.5. An Interpretation of Far-Field Effects of Surface Waves on Finite × Infinite Array of Dipoles in Free Space Based on Approximate Solutions

As it has been demonstrated in Chapter 2, the total far-field of a Floquet excited finite × infinite array (i.e. strip array) can be constructed via edge diffracted Floquet waves in an asymptotic manner.

In the previous section, a near-field interpretation of the surface waves on a semi-infinite array is given. Actually, the excited surface wave creates a modal field and this field is effective close to the array. However, this modal field decay far from the array due to the exponential decay nature normal to the array.

For a finite × infinite array of dipoles in free space, once a surface wave excited from one edge, it travels on the array. When it encounters an edge, then the surface wave is diffracted and partially reflected back. Then the reflected wave again travels to the other edge and diffracted at that edge. This process goes in infinite bounce and reflect modes ([8], [9]). However, for a first order approximation the reflected waves may be ignored. In order to have satisfactory results, for a second order approximation only the first reflected waves together with excited waves can be considered.

When the certain existence conditions for the array guided surface waves are satisfied, i.e. the element sizes are less than λ/2 and the spacing between dipoles is less than λ/2, the far-field of a strip array can be constructed as superposition of Floquet edge diffracted fields and edge diffracted array guided surface waves.

Consider a scattering problem which is illustrated in the Figure 3.12. The phase reference is chosen as the edge of the array. The array is a finite × infinite array of dipoles in free space.

As it is illustrated in Figure 3.13, from the first edge (e1) of the array, a left-traveling array guided surface wave is excited. This surface wave travels on the array surface and when it encounters the second edge (e2) it is diffracted at that edge and partially reflected back. Then the reflected surface wave travels to the first edge again and diffracted at this edge. This process goes on like this; however, to the first order approximation the reflected currents can be ignored. If one wants to more accurate results, then for a second order approximation, only the first edge reflected waves can be considered. It is obvious that inclusion of the all bounce and reflect modes give best result.

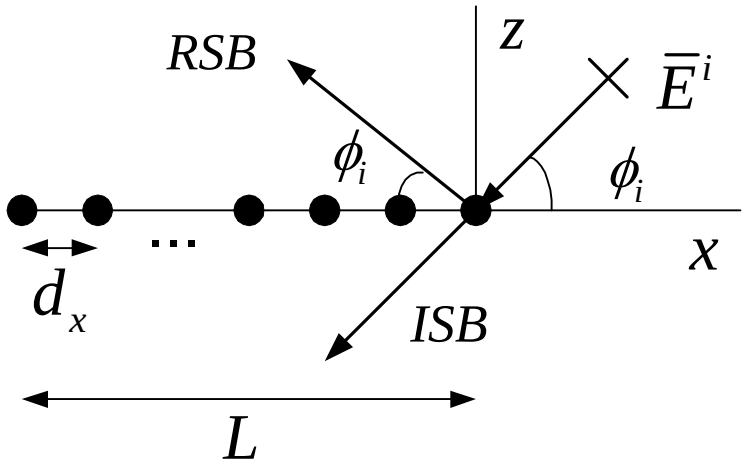

Figure 3.12. A plane wave normally incident on the edge of a strip array of length L, RSB : Reflection Shadow Boundary, ISB : Incident Shadow Boundary, ϕ_i : incidence angle, d_x : interelement period along x-direction

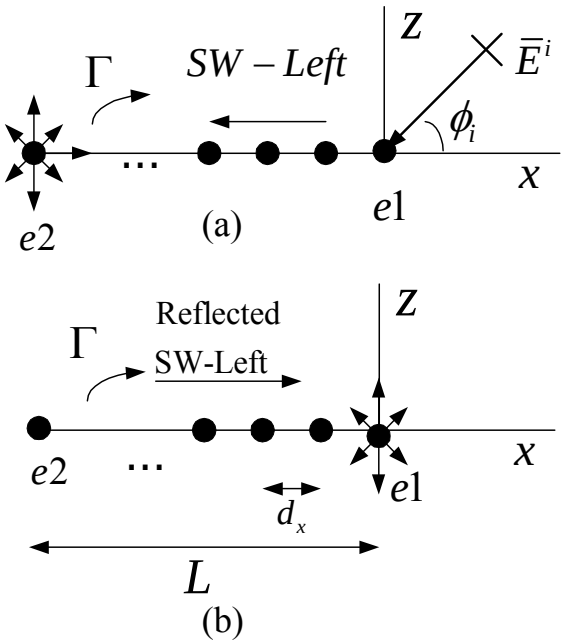

Figure 3.13. (a) Surface wave excited from the first edge (e1) of the array travels to the second edge (e2) and it is diffracted and partially reflected at that edge. (b) Then, reflected AGSW is diffracted at the first edge.

As it is illustrated in Figure 3.14, when the plane wave is incident on the array, not only a left-traveling surface wave is excited but a right-traveling surface wave is excited from the second edge (e2). Then, the right traveling surface waves comes to the first edge on the array surface and it is diffracted and partially reflected back. The reflected right-traveling wave again travels on the surface of the array and comes to the second edge again. Then, it is diffracted at the second edge.

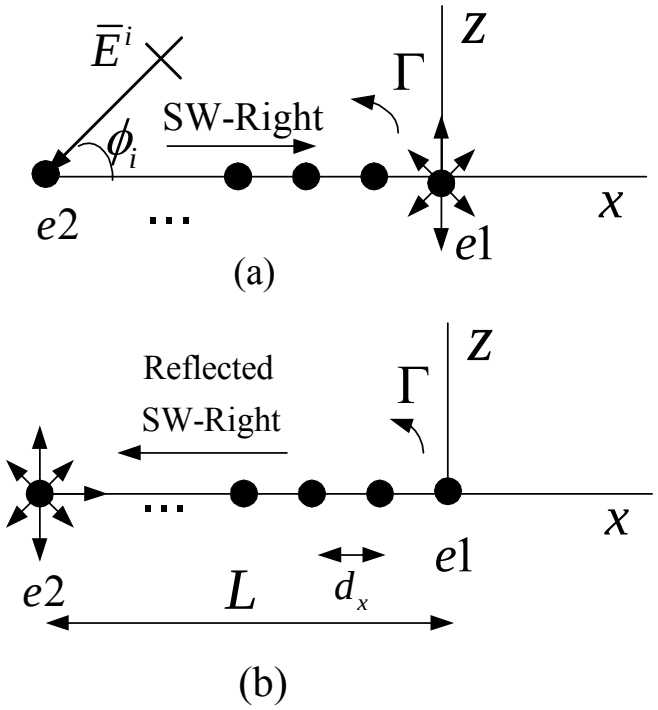

Figure 3.14. (a) Surface wave excited from the second edge (e2) of the array travels to the first edge (e1) and it is diffracted and partially reflected at that edge. (b) Then, reflected AGSW is diffracted at the second edge.

Therefore, in the first order approximation, the total far field of this strip array can be written as

$$\begin{aligned}
&\bar{E}^{farField} = \bar{E}^{d,sw,e2}_{left} + \bar{E}^{d,sw,e1}_{right} + \bar{E}^{d,FW,e1} + \bar{E}^{d,FW,e2} \\
&\bar{E}^{d,sw,e2}_{left} : \textit{Left traveling SW diffracted at edge2} \\
&\bar{E}^{d,sw,e1}_{right} : \textit{Right traveling SW diffracted at edge1} \\
&\bar{E}^{d,FW,e1} : \textit{Floquet Wave diffracted at edge1} \\
&\bar{E}^{d,FW,e2} : \textit{Floquet Wave diffracted at edge2}
\end{aligned} \tag{3.36}$$

For the second order approximation, the first reflected waves are included. Then, the total far field of this strip array can be approximated as

$$\begin{aligned}
&\bar{E}^{farField} = \bar{E}^{d,sw,e2}_{left} + \bar{E}^{d,sw,e1}_{ref,left} + \bar{E}^{d,sw,e1}_{right} + \bar{E}^{d,sw,e2}_{ref,right} + \bar{E}^{d,FW,e1} + \bar{E}^{d,FW,e2} \\
&\bar{E}^{d,sw,e1}_{ref,left} : \textit{reflected left travelling wave diffracted at edge1} \\
&\bar{E}^{d,sw,e2}_{ref,right} : \textit{reflected right travelling wave diffracted at edge2}
\end{aligned} \tag{3.37}$$

The diffracted surface waves can be evaluated using Equation 3.22. In the example given in Figure 3.15, using the first order approximation, the effects of the surface waves on the far field pattern of the array can be observed. Then, for the second order approximation, Figure 3.16 is given.

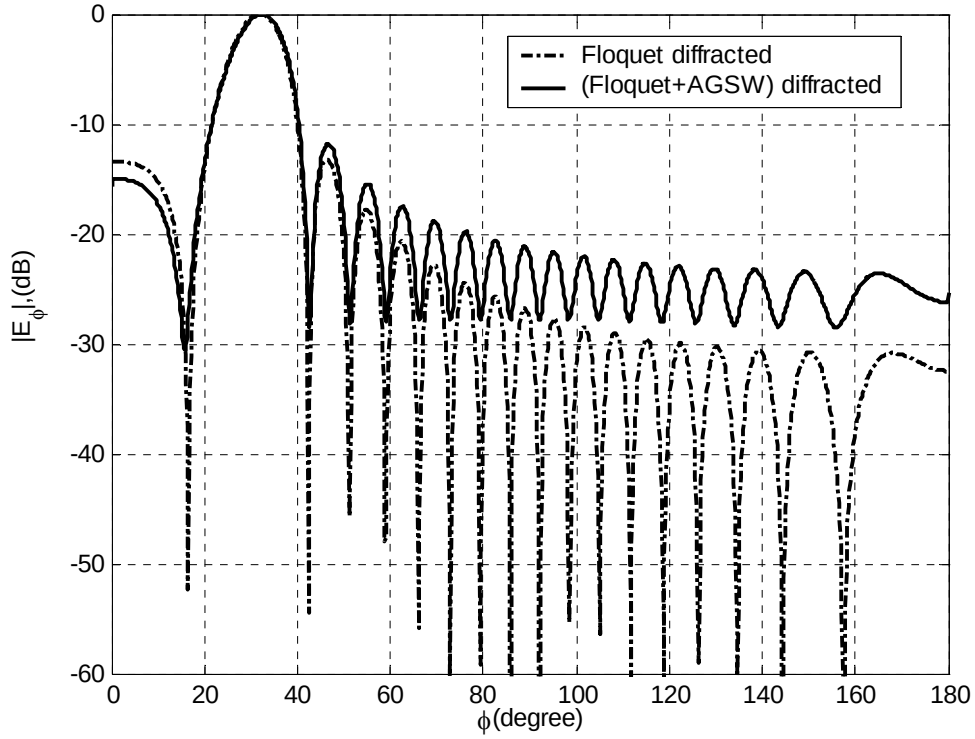

Figure 3.15. Scattered field from strip array (first order approximation); N = 35, dx = 0.9 cm, dy = 1.6cm, wr = 0.0225 cm, dipole length = 1.5 cm, f = 8.6 GHz, incidence angle = 32^0.

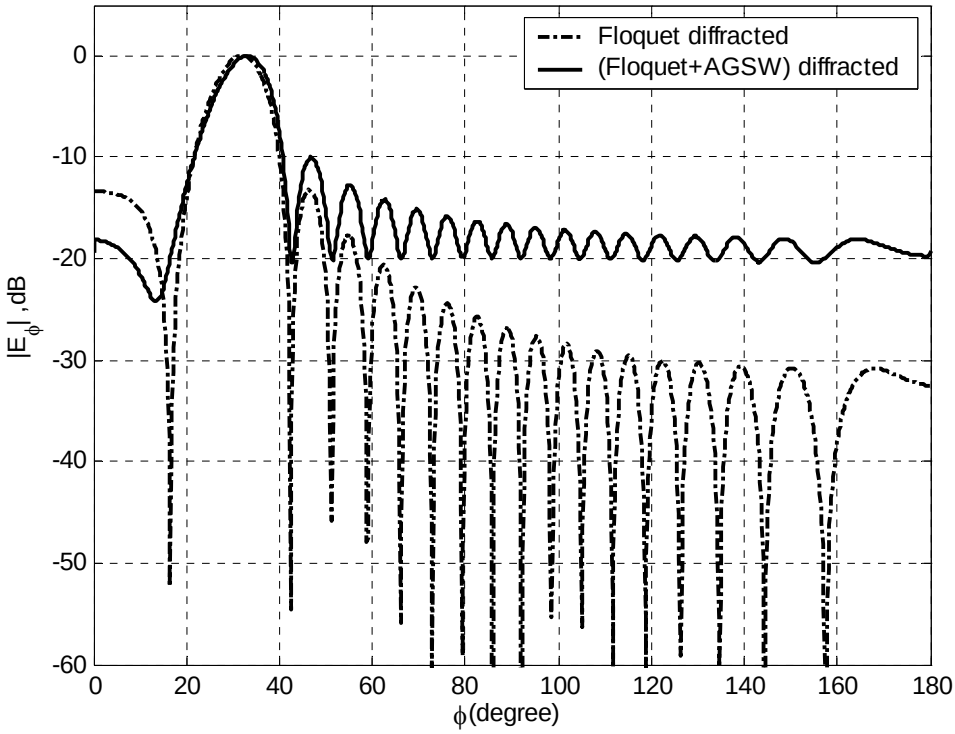

Figure 3.16. Scattered field from strip array (second order approximation); N = 35, dx = 0.9 cm, dy = 1.6cm, wr = 0.0225 cm, dipole length = 1.5 cm, f = 8.6 GHz, incidence angle = 32^0.

This array is same with the one given in [18, pp. 2249, Fig. 5(a)]. In Figure 3.17, Floquet + AGSW diffracted field is plotted on the same graph with Floquet diffracted field and the actual fields [18]. The results are not exactly the same; because, the approximate asymptotic solution does not include all the bounce and reflect modes of the surface waves.

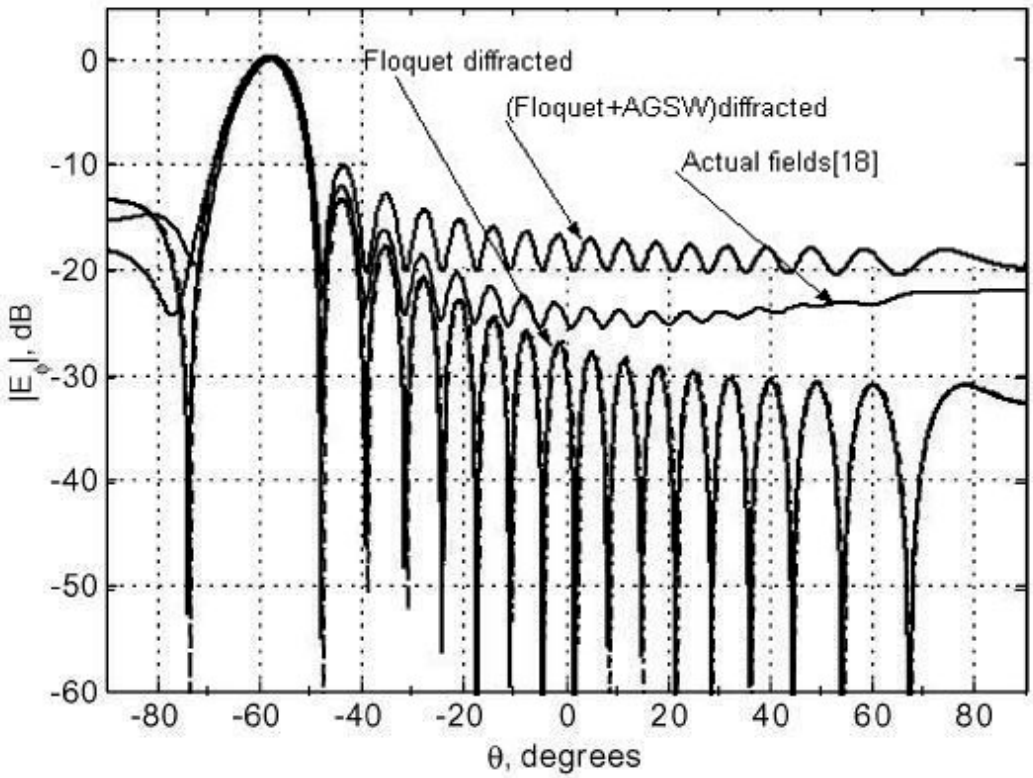

Figure 3.17. Comparison with the results given in [18]. Floquet diffracted and (Floquet + AGSW) diffracted fields are analytically found fields.

From the Figures 3.15 and 3.16, it can be seen that, due to the surface waves, the main beam of the array is not affected so much; however, in far side lobes there are serious differences between Floquet excited and Floquet + Surface Wave excited array patterns. These conclusions are consistent with the comments given in [18].

3.6. An Asymptotic Field Expression for AGSW Excited at the Edge of a Semi-Infinite Array of Dipoles on Infinite Grounded Dielectric Slab

When the certain existence conditions are satisfied, like in the free space case, array guided surface waves are excited [18] on the array of dipoles on infinite grounded

dielectric slab. Following the same procedure in previous sections for the free space case, the surface wave expression can be obtained.

In the Figure 3.18, an array guided surface wave $\bar{E}^{sw}$ is excited from the edge of the array. In the derivations same coordinate system parameters with Floquet excited case are defined.

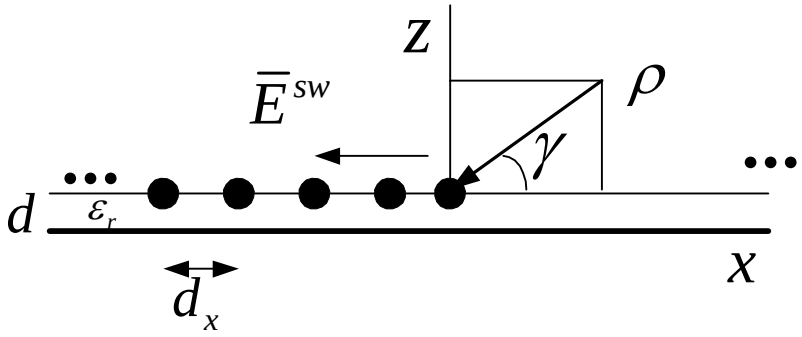

Figure 3.18. A surface wave launched from the edge of a semi-infinite array of dipoles on infinite grounded dielectric slab, which is illuminated by a plane wave.

Again, by using the same procedure as given in Section 2.9, the following expression for the excited surface wave can be obtained by assuming the current has the form $I^{sw} = C\exp\{j\beta n d_x\}$, where C is the excitation coefficient and β is the surface wave propagation constant.

$$\bar{E}^{sw} = 2\pi j \sum_p \sum_q \frac{C\tilde{f}(k_{yq})\bar{D}_q(\alpha_{pq}^{SW})}{jk_{tq}d_x \sin\alpha_{pq}^{FW}} e^{-j(-k_{xp}x + k_{yq}y + k_{zpq}z)} \tag{3.38}$$

where

$$
\begin{aligned}
k_{xp} &= \beta + \frac{2\pi p}{d_x};\ p = 0, \pm 1, \pm 2, \ldots \\
k_{yq} &= \frac{2\pi q}{d_y};\ q = 0, \pm 1, \pm 2, \ldots \\
k_{zpq} &= -js_{pq} \\
s_{pq} &= \sqrt{k_{xp} + k_{yq} - k^2}
\end{aligned}
\tag{3.39}
$$

CHAPTER 4

CONCLUSION

In this work, the field expressions of a semi-infinite array of dipoles in free space are derived by asymptotic high frequency methods. In the evaluation of asymptotic integrals saddle point techniques are used. After obtaining electric field integral expression, saddle point techniques are used to deform the original integration path through the steepest descent path, and the integrals are evaluated as pole and saddle point contributions. By this way, asymptotic field mechanisms are obtained and discussed.

The validity of the derived asymptotic field expressions are checked with a reference solution based on the element-by-element summation of the field contributions of the individual dipole elements. The evaluation of the the asymptotic expressions is very fast in comparison to element-by-element summation. It has been shown that when the field point is far from the edge of the array by 0.2λ or more, asymptotic expressions give accurate results.

The far-field expressions are obtained for a finite × infinite array of dipoles in free space with the classical antenna array theory. Then the equivalence of this expression and the asymptotic field expressions of the edge diffracted fields are demonstrated.

The asymptotic high frequency expressions for the array guided surface waves as well as Floquet waves are derived. Because the array guided surface waves are very

important in order to predict correct radiation characteristics of an array antenna with spacing less than $\lambda/2$, the problem of the excitation of this type of surface waves from the edge of a semi-infinite array of dipoles is studied. An analytical array guided surface wave excitation coefficient formula is derived by using reciprocity theorem. The effects of the array guided surface waves reflected from the edges of the array are included by modifying the Kirchhoff approximation. The derived result is compared with numerical results given in literature.

The formulation techniques used in this work can be used to describe the radiation and scattering of EM waves from fully truncated arrays.

APPENDIX A

SUMMARY OF ASYMPTOTIC METHODS

This appendix summarizes the asymptotic techniques for evaluating integrals in this research. The detailed discussion on these techniques can be found in [30-31], [33-37].

A.1. Asymptotic Approximation of an Integral Containing an Isolated First Order Saddle Point

The method of steepest descents for evaluating the integral of which integrand containing an isolated first order saddle point is summarized in this section. According to the steepest descent algorithm, if the complex integration path does not go through a steepest descent path (SDP), it is assumed that it can be deformed to do so.

Consider an integral I(Ω) of the form

$$I(\Omega) = \int_C f(z)\, e^{\Omega g(z)} dz \tag{A.1}$$

where the complex functions of z, f(z) and g(z) are analytic, so that the path C can be deformed if necessary. C denotes the integration path in the complex z plane which extends to the infinity. Ω is real, positive, and large. It is assumed that g(z) has a first order saddle point z_s,where $g'(z_s) = 0$ and $g''(z_s) \neq 0$.

Since the integrand is an analytical function, one can deform the integration path C into SDP which passes through saddle point z_s, yielding the result

$$I(\Omega) = \int_C f(z)\, e^{\Omega g(z)} dz = \int_{SDP} f(z)\, e^{\Omega g(z)} dz \tag{A.2}$$

The steepest descent path is the path along which $\mathrm{Im}\{g(z)\} = \mathrm{Im}\{g(z_s)\}$ and $\mathrm{Re}\{g(z)\} \leq \mathrm{Re}\{g(z_s)\}$.

By introducing the transformation

$$g(z) = g(z_s) - s^2 \tag{A.3}$$

the integral in (A.2) can be written as

$$I(\Omega) = \int_{-\infty}^{\infty} G(s)\, \mathrm{e}^{\Omega g(z_s)} e^{-\Omega s^2} ds \tag{A.4}$$

where

$$G(s) = f(z)\frac{dz}{ds} \tag{A.5}$$

$$\frac{dz}{ds} = \frac{-2s}{g'(z)} \tag{A.6}$$

Since $\mathrm{Im}\{g(z)\} = \mathrm{Im}\{g(z_s)\}$ and $\mathrm{Re}\{g(z)\} \leq \mathrm{Re}\{g(z_s)\}$ along the SDP, $s^2 \geq 0$ according to the transformation in (A.3) is real. Thus, s is also real along that path. Therefore,the SDP in the z plane is mapped to the real axis in the s plane and the saddle point z_s in the z plane is mapped to s = 0 in the s plane.

By taking the derivative with respect to s on (A.3) two times and using the fact that $g'(z_s) = 0$, (A.7) can be obtained.

$$
\begin{aligned}
&-s^2 = g(z) - g(z_s) \Rightarrow \\
&-2s\left(\frac{ds}{dz}\right) = g'(z) \Rightarrow -2\left(\frac{ds}{dz}\right)\left(\frac{ds}{dz}\right) - 2s\frac{d^2s}{dz^2} = g''(z) \\
&z = z_s \rightarrow s = 0 \\
&\left(\frac{ds}{dz}\right)_{z=z_s} = \left(\frac{g''(z_s)}{-2}\right)^{1/2} \Rightarrow \\
&\left(\frac{dz}{ds}\right)_{s=0} = \sqrt{\frac{-2}{g''(z_s)}}
\end{aligned}
\tag{A.7}
$$

Since G(s) is analytic, it can be expressed in terms of Taylor series as

$$
G(s) = \sum_{n=0}^{\infty}\left[\frac{d^n G(s)}{ds^n}\right]_{s=0}\frac{s^n}{n!} \tag{A.8}
$$

Using (A.8) in (A.4) yields

$$
\begin{aligned}
I(\Omega) &= e^{\Omega g(z_s)}\int_{-\infty}^{\infty}\sum_{n=0}^{\infty}\left[\frac{d^n G(s)}{ds^n}\right]_{s=0}\frac{s^n}{n!}\ \mathrm{e}^{-\Omega s^2}\ ds \\
&= e^{\Omega g(z_s)}\sum_{n=0}^{\infty}\left[\frac{d^n G(s)}{ds^n}\right]_{s=0}\frac{1}{n!}\int_{-\infty}^{\infty} s^n e^{-\Omega s^2} ds
\end{aligned}
\tag{A.9}
$$

where

$$
\int_{-\infty}^{\infty} s^n e^{-\Omega s^2} ds = \left\{\begin{array}{ll} \dfrac{\Gamma(\frac{n+1}{2})}{\Omega^{\left(\frac{n+1}{2}\right)}} & \text{; if n is even} \\ 0 & \text{; if n is odd} \end{array}\right\} \tag{A.10}
$$

$$
\Gamma(m+1) = \int_0^{\infty} x^m e^{-x} dx \tag{A.11}
$$

By using (A.10) in (A.9), one obtains

$$I(\Omega) = e^{\Omega g(z_s)} \sum_{m=0}^{\infty} \left[\frac{d^{(2m)} G(s)}{ds^{(2m)}} \right]_{s=0} \frac{1}{(2m)!} \frac{\Gamma(m+\frac{1}{2})}{\Omega^{m+\frac{1}{2}}} \tag{A.12}$$

For the first order approximation, for a large value of Ω, only the leading term m = 0 in (A.12) can be retained. For the first order approximation, the integral is approximated by

$$I(\Omega) = e^{\Omega g(z_s)} G(0) \frac{\Gamma(\frac{1}{2})}{\Omega^{\frac{1}{2}}} + O(\frac{1}{\Omega^{\frac{3}{2}}}) \tag{A.13}$$

where

$$\begin{aligned} G(0) &= f(z_s) \left[\frac{dz}{ds} \right]_{\substack{s=0 \\ (z=z_s)}} = f(z_s) \sqrt{\frac{-2}{g''(z_s)}} \\ \Gamma(\frac{1}{2}) &= \sqrt{\pi} \end{aligned} \tag{A.14}$$

Using (A.14) in (A.13) yields

$$I(\Omega) \sim e^{\Omega g(z_s)} f(z_s) \sqrt{\frac{-2\pi}{\Omega g''(z_s)}} + O(\frac{1}{\Omega^{\frac{3}{2}}}) \tag{A.15}$$

A.2. Asymptotic Approximation of an Integral Containing a First Order Saddle Point and Many Nearby Simple Poles

A uniform asymptotic expansion of an integral with a first order saddle point and many nearby simple poles is presented in this section [31], [34]. This method is introduced by Van der Waerden (VdW); in literature this method is known as Van der Waerden method.

Consider an integral I(Ω) of the form

$$I(\Omega) = \int_C f(z)\, e^{\Omega g(z)} dz \qquad \text{(A.16)}$$

where Ω is real, positive, and large. The functions f(z) and g(z) are complex functions. The contour is in the complex z plane and extends to the infinity. It is assumed that f(z) has M simle poles at z_i (i= 1, 2, …, M) and g(z) has a first order saddle point at z_s where $g'(z_s) = 0$ and $g''(z_s) \neq 0$. It is assumed that the poles close to the saddle point.

By deforming the contour C into the steepest descent path (SDP) which passes through the saddle point z_s, one obtains

$$I(\Omega) = \int_C f(z)\, e^{\Omega g(z)} dz = \int_{SDP} f(z)\, e^{\Omega g(z)} dz + 2\pi j \sum_{i=1}^{M} \varepsilon_i r_i e^{\Omega g(z_i)} U_{pi} \qquad \text{(A.17)}$$

where r_i is the residue of f(z) at the pole z_i, given by

$$r_i = \lim_{z \to z_i} f(z)(z - z_i) \qquad \text{(A.18)}$$

and $\varepsilon_i = +1$ if the pole z_i is enclosed by the contour deformation in the counter clockwise sense whereas $\varepsilon_i = -1$ for the clockwise enclosure of pole.

U_{pi} represents the unit step function defined by

$$U_{pi} = \begin{cases} 1 & ;\ if\ z_i\ is\ captured \\ 0 & ;\ otherwise \end{cases} \qquad \text{(A.19)}$$

Consider the integral along the SDP

$$I_s(\Omega) = \int_{SDP} f(z)\, e^{\Omega g(z)} dz \qquad \text{(A.20)}$$

By employing the transformation

$$g(z) = g(z_s) - s^2 \tag{A.21}$$

The integral in (A.20) can be written as

$$I(\Omega) = \int_{-\infty}^{\infty} G(s)\, \mathrm{e}^{\Omega g(z_s)} e^{-\Omega s^2}\, ds \tag{A.22}$$

where

$$G(s) = f(z)\frac{dz}{ds} \tag{A.23}$$

$$\frac{dz}{ds} = \frac{-2s}{g'(z)} \tag{A.24}$$

The saddle point z_s and the poles z_i in the z plane are mapped to s = 0 and s =s_i in the s plane, respectively. The pole s_i in the s plane is defined by

$$s_i^2 = g(z_s) - g(z_i) \equiv -ja_i = -j(js_i^2) \tag{A.25}$$

where a_i is the measure of the distance between z_i and z_s. Also, from the first section, one has

$$\left(\frac{dz}{ds}\right)_{s=0} = \sqrt{\frac{-2}{g''(z_s)}} \tag{A.26}$$

Since G(s) is a function containing M simple poles {s_i}, it can be expressed in the form

$$G(s) = P(s) + \sum_{i=1}^{M} \frac{R_i}{s - s_i} \tag{A.27}$$

where P(s) is an analytic function and R_i is the residue of G(s) at the pole s = s_i, given by

$$R_i = \lim_{s \to s_i} G(s)(s - s_i) \tag{A.28}$$

The analytic function P(s) can be written in terms of a Taylor series expansion around s = 0 as

$$P(s) = \sum_{n=0}^{\infty} \frac{P^{(n)}(0)}{n!} s^n \tag{A.29}$$

By using (A.29) in (A.27), one can write

$$G(s) = \sum_{n=0}^{\infty} \frac{P^{(n)}(0)}{n!} s^n + \sum_{i=1}^{M} \frac{R_i}{s - s_i} \tag{A.30}$$

Substituting (A.30) into (A.22) yields

$$\begin{aligned} I_s(\Omega) &= \int_{-\infty}^{\infty} \left\{ \sum_{n=0}^{\infty} \frac{P^{(n)}(0)}{n!} s^n + \sum_{i=1}^{M} \frac{R_i}{s - s_i} \right\} \mathrm{e}^{\Omega g(z_s)} e^{-\Omega s^2} \, ds \\ &= e^{\Omega g(z_s)} \left\{ \sum_{n=0}^{\infty} \frac{P^{(n)}(0)}{n!} \int_{-\infty}^{\infty} s^n e^{-\Omega s^2} ds + \sum_{i=1}^{M} R_i \int_{-\infty}^{\infty} \frac{e^{-\Omega s^2}}{s - s_i} ds \right\} \end{aligned} \tag{A.31}$$

The first integral in (A.31) can be evaluated employing (A.10) and (A.11). For the second integral the result in (A.32) can be used.

$$\begin{aligned} \int_{-\infty}^{\infty} \frac{e^{-\Omega s^2}}{s - s_i} ds &= 2 s_i \sqrt{\frac{\pi}{a_i}} e^{j\Omega a_i} \int_{\sqrt{\Omega a_i}}^{\infty} e^{-j\tau^2} \, d\tau \\ &= -\frac{1}{s_i} \sqrt{\frac{\pi}{\Omega}} F\left[j\Omega s_i^2 \right] \end{aligned} \tag{A.32}$$

where F[.] is the Fresnel transition function. Fresnel transition function is defined as

$$F(x) = 2j\sqrt{x} \exp\{jx\} \int_{\sqrt{x}}^{\infty} e^{-j\tau^2} \, d\tau \tag{A.33}$$

The proper branch of $\sqrt{a} = \sqrt{js_p^2}$, defined by $\frac{-3\pi}{4} < \arg(\sqrt{a}) < \frac{\pi}{4}$, must be chosen to satisfy the radiation condition corresponding to $e^{j\omega t}$ time convention. For large values of its argument, Fresnel transition function tends to unity as

$$if\ \delta \gg 1 \Rightarrow F(\delta^2) \to 1 \tag{A.34}$$

By using (A.31) and (A.32) the saddle point contribution can be written as

$$I_s(\Omega) = e^{\Omega g(z_s)} \left\{ \sum_{m=0}^{\infty} \frac{P^{(2m)}(0)}{(2m)!} \frac{\Gamma(m+\frac{1}{2})}{\Omega^{m+\frac{1}{2}}} - \sum_{i=1}^{M} \frac{R_i}{s_i} \sqrt{\frac{\pi}{\Omega}} F[j\Omega s_i^2] \right\} \tag{A.35}$$

From (A.27) it can be shown that

$$P^{(2m)}(0) = G^{(2m)}(0) + (2m)! \sum_{i=1}^{M} \frac{R_i}{s_i^{2m+1}} \tag{A.36}$$

By using (A.36) one can write

$$I_s(\Omega) = e^{\Omega g(z_s)} \sqrt{\frac{\pi}{\Omega}} \times \left\{ G(0) + \sum_{i=1}^{M} \frac{R_i}{s_i} \left(1 - F[j\Omega s_i^2]\right) + \frac{1}{\sqrt{\pi}} \sum_{m=0}^{\infty} \frac{P^{(2m)}(0)}{(2m)!} \frac{\Gamma(m+\frac{1}{2})}{\Omega^m} \right\} \tag{A.37}$$

As a first order approximation, only the m = 0 term can be evaluated for a large value of Ω, then saddle point contribution can be expressed as

$$I_s(\Omega) = e^{\Omega g(z_s)} \sqrt{\frac{\pi}{\Omega}} \left\{ G(0) + \sum_{i=1}^{M} \frac{R_i}{s_i} \left(1 - F[j\Omega s_i^2]\right) + O(\frac{1}{\Omega}) \right\} \tag{A.38}$$

This method can be used whether the pole crosses the SDP at saddle point or the pole is far from the saddle point.

Fresnel transition function is plotted in Figure A.1 for a real argument x. It can be seen that the F→1 for large arguments.

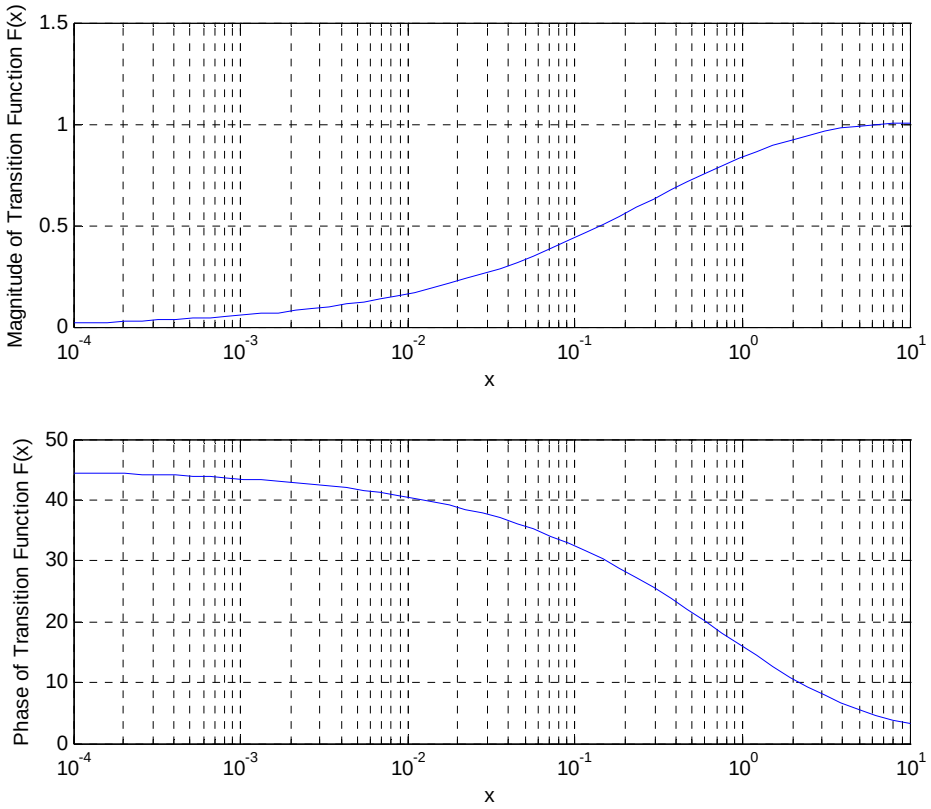

Figure A.1. The behaviour of Fresnel transition function F(x), where x is the real argument.

APPENDIX B

FLOQUET'S THEOREM

Periodic structures may be characterized by periodic boundary conditions or a periodically varied dielectric constant. Considering a wave propagating in a periodic structure as in Figure B.1, Floquet's theorem can be described. The fields at a point z in an infinite periodic structure differ from the fields one period L away by a complex constant. This is obviously true because in an infinite periodic structure, there should be no difference between the fields at z and at z + L except for the constant attenuation and phase shift. A wave u(z) at z and a wave u(z + L) at z + L are related in the same manner as a wave u(z + L) at z + L and a wave u(z + 2L) at z + 2L.

Mathematically, the following equation can be written:

$$\frac{u(z+L)}{u(z)} = \frac{u(z+2L)}{u(z+L)} = \frac{u(z+mL)}{u(z+(m-1)L)} = C = \text{constant} \tag{B.1}$$

From this the equation given below can be written:

$$u(z+mL) = C^m u(z) \tag{B.2}$$

The constant C is in general complex,

$$C = e^{-j\beta L},\ \beta : complex \tag{B.3}$$

In Equation B.3, β represents the propagation constant. Considering a function:

$$R(z) = e^{j\beta z} u(z) \tag{B.4}$$

Then, the following equation can be written:

$$R(z+L) = e^{j\beta(z+L)} u(z+L) = R(z) \tag{B.5}$$

Therefore, R(z) is a periodic function of z with period L, and thus can be represented in a Fourier series.

$$R(z) = \sum_{n=-\infty}^{\infty} A_n e^{-j(2n\pi/L)z} \tag{B.6}$$

Using (B.4) a general expression for a wave in a periodic structure with the period L can be written as:

$$\begin{aligned} u(z) &= \sum_{n=-\infty}^{\infty} A_n e^{-j(\beta+2n\pi/L)z} = \sum_{n=-\infty}^{\infty} A_n e^{-j\beta_n z} \\ &where,\ \beta_n = \beta + 2n\pi / L \end{aligned} \tag{B.7}$$

In general, the wave consists of both positive-going and negative-going waves. Then, the following equation can be written:

$$u(z) = \left\{ \sum_{n=-\infty}^{\infty} A_n e^{-j\beta_n z} \right\} + \left\{ \sum_{n=-\infty}^{\infty} B_n e^{+j\beta_n z} \right\} \tag{B.8}$$

This is a representation of a wave in periodic structures in a form of an infinite series. The n^{th} term in (B.7) is called the n^{th} space harmonic or Hartree harmonic. Equation (B.8) is a mathematical representation of Floquet's theorem.

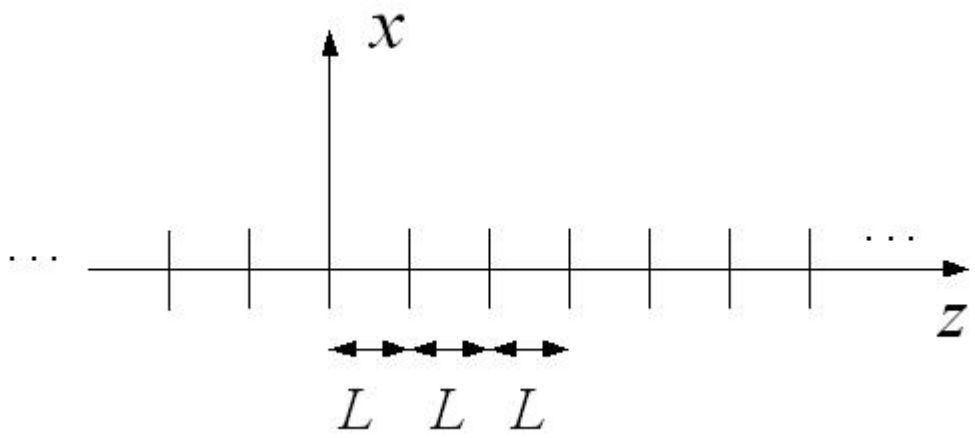

Figure B.1. Periodic structure along z axis with period L.

APPENDIX C

SCAN IMPEDANCE

The current in the reference element of an infinite planar array is related to the induced voltage by

$$V^i = Z_{11} I_0^F \tag{C.1}$$

where Z_{11} is the self impedance of the planar array, V^i is induced voltage and I_0 is the current in the reference element. When the impedance matrix formulation is written, (1,1) element is the self impedance of the array [9]. That's why the notation is like that.

The currents of the elements on infinite dimensions are related to reference element current by Floquet's theorem.

Considering a method of moments (MoM) impedance matrix formulation, the self-impedance is found by reacting the fields of the array onto test filament placed along the centerline of the reference element [1]. From (C.1) the self impedance can be written as in Equation (C.2) where E_{pq} represents the total array array field.

$$Z_{11} = -\frac{V_0}{I(0)^2} = -\frac{\int_{-L/2}^{L/2} f(y)(\bar{E}_{pq}.\hat{y})dy}{I(0)^2} \tag{C.2}$$

APPENDIX D

RECIPROCITY THEOREM

The reciprocity theorem [19], [23], [38] is useful in formulating problems as well as checking final answers. In this section Lorentz relation, which is used in this research, is given.

For a volume V, its boundary is a closed surface S. Considering two fields F_a and F_b produced by sources A and B, respectively, the Lorentz relation can be written as

$$< F_a SF_b >=< AVF_b > - < BVF_a > \tag{D.1}$$

where reaction between source A and a field F_b and source B and field F_a are defined by

$$\begin{aligned} < AVF_b >&= \int_V (\bar{J}_a.\bar{E}_b - \bar{M}_a.\bar{H}_b)dV \\ < BVF_a >&= \int_V (\bar{J}_b.\bar{E}_a - \bar{M}_b.\bar{H}_a)dV \end{aligned} \tag{D.2}$$

In (D.2), J represents the electric sources and M represents the magnetic sources, while E represents electric field, H represents the magnetic field.

Through a surface of S (not necessarily closed) the cross-flux of two fields F_a and F_b is defined by

$$< F_a SF_b >= \int_S (\bar{E}_a \times \bar{H}_b - \bar{E}_b \times \bar{H}_a) \,.\, \hat{n}ds \tag{D.3}$$

The Lorentz reciprocity integral formula can be written more explicitly as

$$\int_S (\bar{E}_a \times \bar{H}_b - \bar{E}_b \times \bar{H}_a) \cdot \hat{n} ds = \int_V (\bar{J}_a . \bar{E}_b - \bar{M}_a . \bar{H}_b) dV - \int_V (\bar{J}_b . \bar{E}_a - \bar{M}_b . \bar{H}_a) dV \quad \text{(D.4)}$$

The relation in (D.4) holds under rather general conditions, namely:

- Sources A and/or B may be inside or outside V.
- Fields F_a and F_b may be produced in different media provided that these two media coincide in V.
- The media are isotropic, but may be inhomogenous with scatterers presented.

In Figure (D.1), two reciprocal problems are demonstrated. The blocks (1, 2, 3) are scatterers and the medium in (a) is identical with the medium in (b) only inside V, not necessarily outside.

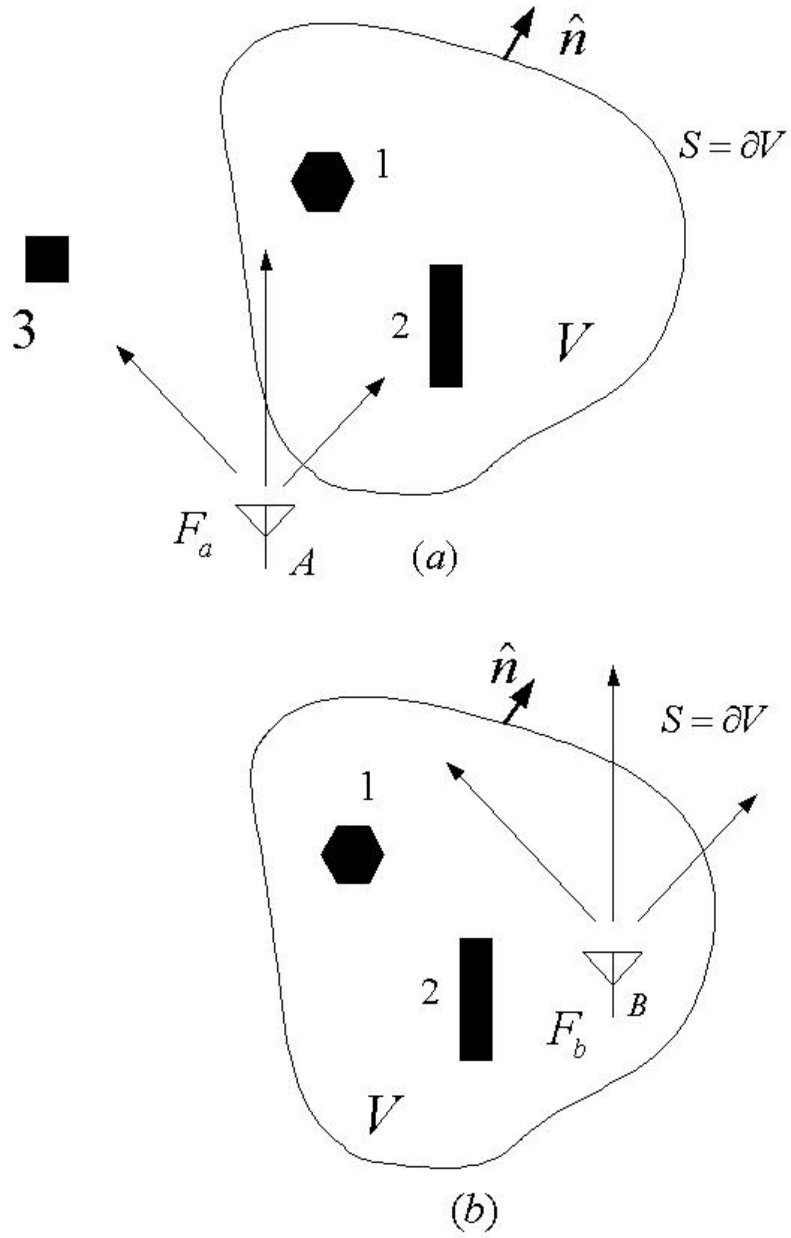

Figure D. 1. (a) Field produced by A (b) Field produced by B (Adopted from [38]).

REFERENCES

[1] B. Munk, *Frequency Selective Surfaces: Theory and Design*. New York: Wiley, 2000.

[2] R. Hansen, *Phased Array Antennas*. New York: Wiley, 1998.

[3] R. J. Mailloux, “Phased Array Theory and Technology,” Proc. IEEE, vol. 70, pp. 246-291, March 1982.

[4] T. Wu, *Frequency Selective Surface and Grid Array*. New York: Wiley, 1995.

[5] J. D. Kraus, *Antennas*. McGraw-Hill, Inc., 1998.

[6] D. M. Pozar and D. H. Schaubert, “Scan blindness in infinite phased array of printed dipoles,” IEEE Trans. Antennas and Propagat., vol. AP-32, no. 6, pp. 602-610, June 1984.

[7] B.A. Munk, D.S. Janning, J.B. Pryor and R.J. Marhefka, “Scattering from Surface Waves on Finite FSS”, IEEE Trans. Antennas Propagat., vol.49, no.12, pp.1782-1793, Dec. 2001.

[8] D.S. Janning and B.A. Munk, “Effects of surface Waves on the Currents of Truncated Periodic Arrays”, IEEE Trans. Antennas Propagat., vol.50, no.9, pp.1254-1265, Sept. 2002.

[9] D. Janning, ‘Surface Waves In Arrays of Finite Extent’, PhD Thesis, The Ohio State University, 2000.

[10] D.M. Pozar, “Analysis of finite phased arrays of printed dipoles”, IEEE Trans. Antennas Propagat., vol.-33, no.10, pp.1045-1053, Oct.1985.

[11] K. Skrivervik and J. R. Mosig, “Analysis of Finite Phase Arrays of MicrostripPatches," IEEE Trans. Antennas Propagat., vol. 41, No. 8, pp. 1105-1114, August 1993.

[12] W. L. Ko and R. Mittra, “Scattering by a truncated periodic array,” IEEE Trans. Antennas Propagat., vol. 36, pp. 496–503, Apr. 1988.

[13] Ishimaru, R. J. Coe, G. E. Miller, and W. P. Geren, “Finite Periodic Structure Approach to Large Scanning Array Problems," IEEE Trans. Antennas Propagat., vol. AP-33, No. 11, pp. 1213-1220, November 1985.

[14] F. Capolino, M. Albani, S. Maci and L. Felsen, “Frequency domain Green’s function for a planar periodic phased array, Parts I and II”, IEEE Trans. Antennas Propagat., no.1, pp.67-85, Jan. 2000.

[15] Ö.A. Çivi, P.H. Pathak, H.T. Chou, and P. Nepa, “A Hybrid UTD-MoM for efficient analysis of EM radiation/scattering from large finite planar arrays”, Radio Science, vol.35, no.2, pp.607-620, March-April 2000.

[16] A. Allam and E. Parker, “Application of Pocklington’s equation to analysis of dipole frequency selective surfaces of finite size”, IEE Proc., Pt.H, vol.134, pp.521-526, Dec. 1987.

[17] P.H. Pathak, P.Janpugdee, and D.S. Janning, “Analytical expressions for the launching and diffraction of a surface wave by the edge of a semi-infinite periodic array of dipoles in free space”, ICEA 2001 Proceedings, Turin Italy.

[18] Ö. A. Çivi, P. H. Pathak, “Array Guided Surface Waves on a finite planar array of dipoles with or without a grounded substrate,”, IEEE Trans. Antennas Propagat., vol. 54, no.8, pp.2244-2252, Agu. 2006.

[19] R. F. Harrington, *Time Harmonic Electromagnetic Fields*. McGraw-Hill, Inc., 1961.

[20] A. Polemi, A. Toccafondi, and S. Maci, “High-frequency Green's function for a semi-infinite array of electric dipoles on a grounded slab I. formulation”, IEEE Trans. Antennas Propagat., no.12, pp.1667-1677, Dec. 2001.

[21] P. Janpugdee, ‘An efficient discrete Fourier Transform based ray analysis of large finite planar phased arrays’, MSc Thesis, The Ohio State University, 2002.

[22] P.Janpugdee and P.H.Pathak, “A DFT based UTD Ray Analysis of Large Finite Phased Arrays on a Grounded Substrate”, IEEE Trans. on Antennas and Propagat. vol. 54, no. 4, April 2006.

[23] R.E. Collin, *Field Theory of Guided Waves*, 2nd Edition. New York: IEEE Press, 1991.

[24] D. Sengupta, “On the phase velocity of wave propagation along an infinite Yagi structure”, IRE Trans. Antennas Propagat., vol.AP-7, pp.234-239, July 1959.

[25] L. Shen, “Characteristics of propagating waves on Yagi-Uda structures”, IEEE Trans. Microwave Theory Tech., vol.MTT-19, pp.536-542, June 1971.

[26] R. J. Mailloux, “Excitation of a Surface Wave Along an Infinite Yagi-Uda Array”, IEEE Trans. Antennas Propagat., Vol. AP-13, pp. 719-724, Sept. 1965.

[27] R. J. Mailloux, “The Long Yagi-Uda Array,” IEEE Trans. Antennas Propagat, Vol. AP-14, pp.128-137, March 1966.

[28] J.Richmond and R. Garbaez, “Surface waves on periodic arrays of imperfectly conducting vertical dipoles over the flat earth”, IEEE Trans. Antennas Propagat., vol.AP-27, pp.783-787, Nov.1979.

[29] F. Serracchioli and C. A. Levis, “The Calculated Phase Velocity of Long End-Fire Uniform Dipole Arrays,” IEEE Trans. Antennas Propagat., Vol. AP-7, no.5, pp. S424-S434, Dec. 1959.

[30] A. Ishimaru, *Electromagnetic Wave Propagation, Radiation, and Scattering*. New Jersey: Prentica-Hall, 1991.

[31] L. B. Felsen and N. Marcuvitz, *Radiation and Scattering of Waves*. New York: Prentice-Hall/IEEE Press, 1994.

[32] Ö. A. Çivi, P. H. Pathak, and H.-T. Chou, “On the Poisson Sum Formula for the Analysis of Wave Radiation and Scattering from Large Finite Arrays," IEEE Trans. Antennas Propagat., vol. 47(5), pp. 958-959, May 1999.

[33] M. J. Ablowitz and A. S. Fokas, *Complex Variables: Introduction and Applications.* Cambridge, United Kingdom: Cambridge University Press, 1997.

[34] R. E. Colin and F. J. Zucker, *Antenna Theory, Part 2.* McGraw-Hill Book Company, New York, 1969.

[35] R. G. Rojas, “Comparison Between Two Asymptotic Methods," IEEE Trans. Antennas Propagat., vol. AP-35, No. 12, pp. 1489-1492, December 1987.

[36] F.B. Hildebrand, *Advanced Calculus For Applications*, 2nd Edition, Prentice-Hall, Inc., 1976

[37] J. L. Volakis and M. I. Herman, “A Uniform Asymptotic Evaluation of Integrals," IEEE Trans. Antennas Propagat., vol. 74, No. 7, pp. 1043-1044, July 1986.

[38] Y. T. Lo and S. W. Lee, *Antenna Handbook, Volume I,* New York: Van Nostrand Reinhold, 1993.